

# Physiological vessel on chip model with integrated flow and oxygen control for *in vitro* small pulmonary artery studies

***By: Janet Huisman, BSc.***

Thesis submitted in partial fulfilment of the requirements for the Degrees of  
*Master of Biomedical Engineering and Master of Nanotechnology*

Department of Applied Stem Cell Technologies

Faculty of Science and Technology

University of Twente

Enschede, The Netherlands



**UNIVERSITY  
OF TWENTE.**

Supervisory committee:

Chairman:	Prof. Dr. Robert Passier
Head supervisor:	Dr. Andries van der Meer
Daily supervisor:	Laura de Heus, MSc.
External Supervisor:	Prof. Dr. Ir. Jurriaan Huskens

Date: 22-09-2021

# ABSTRACT

---

## **English**

Oxygen tension and shear stress are believed to play a crucial role in the development of various vascular diseases such as pulmonary arterial hypertension. Since no physiological *in vitro* model yet exists to study the effect of these stimuli on the behaviour of patient-specific vascular cells, the aim of this research was to develop a three dimensional (3D) small pulmonary artery on chip (sPAoC) model with integrated flow and oxygen control. The proposed design consists of an oxygen impermeable microfluidic chip in which oxygen tension and flow rate can be controlled to mimic both the small pulmonary artery and the surrounding alveoli. The vessel is formed via displacement of collagen by a less viscous fluid (viscous finger patterning) to obtain a perfusable 3D collagen lumen in which human induced pluripotent stem cell (hiPSC) derived endothelial cells (ECs), smooth muscle cells and fibroblasts can be cultured. Although earlier characterization of these hiPSC-ECs revealed an immature arterial/venous phenotype, their response to hypoxia was found to be similar to primary pulmonary arterial ECs, providing previously unknown information about the current phenotype of the hiPSC-ECs. Additionally, a concept version of the chip system was fabricated without the alveolar compartment and imaging confirmed successful formation of cylindrical lumens in these chips with an average diameter of  $313 \pm 34 \mu\text{m}$  and a success rate of 90%. Finally, oxygen sensor spots and unidirectional flow were successfully integrated in this chip system. Together these initial results demonstrate the possibilities of the proposed sPAoC model for analysis of the vascular behaviour in response to stimuli such as (patho)physiological oxygen tensions and shear stresses.

## **Nederlands**

Zuurstofspanning en schuifspanning spelen vermoedelijk een cruciale rol in de ontwikkeling van verscheidene vaatziektes zoals pulmonaire arteriële hypertensie. Aangezien er nog geen fysiologisch *in vitro* model bestaat om het effect van deze stimuli op het gedrag van patiënt-specifieke vaatcellen te bestuderen was het doel van dit onderzoek om een driedimensionale (3D) kleine longslagader op chip (sPAoC) te ontwikkelen met geïntegreerde controle van de vloeistofstroming en zuurstofspanning. Het voorgestelde ontwerp bestaat uit een zuurstof impermeabele microfluidische chip waarin de zuurstofconcentratie en stroomsnelheid kunnen worden gecontroleerd om zowel de kleine longslagader als de omliggende longblaasjes na te bootsen. Het bloedvat is gevormd via verplaatsing van collageen door een minder viskeuze vloeistof (viscous finger patterning) om een 3D lumen te verkrijgen waarin menselijke geïnduceerde pluripotente stamcel (hiPSC) afgeleide endotheelcellen (ECs), gladde spiercellen en fibroblasten kunnen worden gekweekt. Alhoewel eerdere karakterisering van deze hiPSC-ECs een onvolwassen arterieel/veneus fenotype onthulde is de reactie op hypoxie vergelijkbaar met primaire longslagader ECs, wat voorheen onbekende informatie verschaft over het huidige fenotype van de hiPSC-ECs. Verder is een conceptversie van het chip systeem gefabriceerd zonder het longblaasjescompartiment en beeldvorming bevestigde succesvolle formatie van cilindrische lumens in deze chips met een gemiddelde diameter van  $313 \pm 34 \mu\text{m}$  en een slagingspercentage van 90%. Ten slotte zijn zuurstofsensoren en unidirectionele stroming succesvol geïntegreerd in het chip system. Samen tonen deze initiële resultaten de mogelijkheden van het voorgestelde sPAoC model voor analyse van het vasculaire gedrag als reactie op stimuli zoals (patho)fysiologische zuurstofspanningen en schuifspanningen.

## **Key words:**

*vascular diseases, pulmonary arterial hypertension, small pulmonary artery, organ on chip, vessel on chip, oxygen tension, hypoxia, shear stress, flow, human induced pluripotent stem cells, endothelial cells, microfluidic chip, PMMA, viscous finger patterning, collagen lumen*

## **ACKNOWLEDGEMENTS**

---

The work that was performed during this project would not have been possible without the support of various others. First of all, I would like to thank my daily supervisor Laura de Heus for her guidance in and outside of the lab. Our many fruitful discussions taught me a lot and brought my work to a higher level. Secondly, I wish to thank Dr. Andries van der Meer and Prof. Dr. Robert Passier for giving me the opportunity to pursue this project and for their valuable feedback. Additional thanks to all other members of the Applied Stem Cell Technologies group at the University of Twente, in particular to Tarek Gensheimer for his help with the chip fabrication and oxygen sensing, Aisen de sa Vivas for helping me with the fluidics and Jim Koldenhof for sharing his viscous finger patterning method. Furthermore, I would like to thank Elsbeth Bossink of the BIOS group for her help with the chloroform polishing and finally Prof. Dr. Ir. Jurriaan Huskens for being my external supervisor.

## LIST OF ACRONYMS

---

2D	two dimensional
3D	three dimensional
ACTB	$\beta$ -Actin
actin- $\alpha$ 2	alpha smooth muscle actin
APS	ammonium persulfate
APTES	(3-aminopropyl)triethoxy silane
AST	applied stem cell technologies
BMPR2	bone morphogenetic protein receptor type II
BSA	bovine serum albumin
CD31	cluster of differentiation 31
CNC milling	computer numerical controlled milling
CO <sub>2</sub>	carbon dioxide
COC	cyclic olefin copolymer
COP	cyclic olefin polymer
COUP-TFII	chicken ovalbumin upstream promoter transcription factor 2
DAPI	4',6-diamidino-2-phenylindole
ECM	extracellular matrix
ECs	endothelial cells
EGM-2	endothelial cell growth medium 2
ELISA	enzyme-linked immunosorbent assay
eNOS	endothelial nitric oxide synthase
ET-1	endothelin 1
ETFE	ethylene tetrafluoroethylene
FBS	foetal bovine serum
FEP	fluorinated ethylene-propylene
FITC	fluorescein isothiocyanate
FLIM	fluorescence life-time imaging microscopy
GA	glutaraldehyde
GAPDH	glyceraldehyde 3-phosphate dehydrogenase
GSL	griffonia simplicifolia lectin I
HIF-1 $\alpha$	hypoxia-inducible factor 1 alpha
HIF-2 $\alpha$	hypoxia-inducible factor 2 alpha
hiPSC	human induced pluripotent stem cells
hiPSC-ECs	human induced pluripotent stem cell derived endothelial cells
hMVECs	human microvascular endothelial cells
HPA	helix pomatia agglutinin lectin
hPAECs	human pulmonary arterial endothelial cells
HRP	horseradish peroxidase
HUVECs	human umbilical vein endothelial cells
myosin SM-1/2	smooth muscle myosin
NO	nitric oxide
O <sub>2</sub>	oxygen
OCT	optical coherence tomography
OoC	organ on chip
PAH	pulmonary arterial hypertension
PBB	permeabilization and blocking buffer solution
PBS	phosphate buffered saline
PC	polycarbonate
PDA	polydopamine
PDMS	polydimethylsiloxane
PEEK	polyether ether ketone
PFA	perfluoro alkoxy
PLIM	phosphorescence life-time imaging microscopy
PMMA	poly(methyl methacrylate)
PP	polypropylene
PS	polystyrene
PTFE/Teflon™	polytetrafluoroethylene
PVDC	polyvinylidene chloride
PVDF	polyvinylidene fluoride
qPCR	quantitative polymerase chain reaction
ROS	reactive oxygen species
SDS	sodium dodecyl sulphate
SDS-PAGE	sodium dodecyl sulphate polyacrylamide gel electrophoresis
SMCs	smooth muscle cells

sPAoC	small pulmonary artery on chip model
sPAs	small pulmonary arteries
TBST	tris-buffered saline solution with Tween 20
TNF- $\alpha$	tumor necrosis factor alpha
TRIS	tris(hydroxymethyl)aminomethane
VE-cadherin	vascular endothelial cadherin
VEGF	vascular endothelial growth factor
VFP	viscous finger patterning
VoC	vessel on chip
WB	western blotting
WSS	wall shear stress

# TABLE OF CONTENTS

---

1	Introduction .....	8
1.1	The Importance of Blood Vessels .....	8
1.2	Vascular Dysfunction .....	8
1.3	Relevant Factors in Vascular (dys)function .....	8
1.4	Models to Study Vascular (dys)function .....	10
1.5	Research Question .....	11
1.6	Thesis Structure .....	13
2	Background.....	14
2.1	Physiology of the pulmonary arteries .....	14
2.1.1	Blood vessel structure .....	14
2.1.2	Vascular Cell Types.....	15
2.1.3	Types of Vasculature .....	16
2.1.4	(Patho)physiological Oxygen Tensions.....	19
2.1.5	(Patho)physiological Shear Stresses .....	20
2.2	Organ on a chip systems .....	21
2.2.1	Materials .....	21
2.2.2	Fabrication Techniques .....	23
2.2.3	Integration of Cells.....	24
2.2.4	Readout Methods .....	25
2.3	Oxygen Control and Sensing .....	26
2.3.1	Oxygen Tension Definitions .....	26
2.3.2	Oxygen Control Systems.....	27
2.3.3	Oxygen Sensing .....	28
2.4	Flow Control and Sensing .....	31
2.4.1	Fluid and Flow Definitions.....	31
2.4.2	Flow Control and Sensing.....	31
3	Proposed Solution.....	33
3.1	System Requirements.....	33
3.1.1	Microfluidic Device.....	33
3.1.2	Cell Culture .....	33
3.1.3	Oxygen sensing.....	34
3.1.4	Fluidic Interface .....	34
3.2	Existing Solutions.....	35
3.3	Proposed Ideal Setup.....	35
3.4	Timeline and Planning.....	36
4	Computational Modelling.....	38
4.1	Modelling of Flow Control.....	38
4.2	Modelling of Oxygen Control.....	40
4.3	Discussion.....	42
5	Experimental Progress.....	44
5.1	Characterization of Cellular Behaviour.....	44

5.1.1	Materials and Methods .....	44
5.1.2	Results and Discussion .....	46
5.1.3	Conclusions and Recommendations .....	50
5.2	Chip Fabrication with Oxygen and Flow Control .....	51
5.2.1	Materials and Methods .....	51
5.2.2	Results and Discussion .....	54
5.2.3	Conclusions and Recommendations .....	62
6	Discussion.....	64
7	Conclusions .....	66
8	References.....	67

# 1 INTRODUCTION

---

## 1.1 THE IMPORTANCE OF BLOOD VESSELS

Blood is essential for life. It transports oxygen and nutrients to all cells throughout the body, and at the same time carries waste products away from the cells. Furthermore, it helps regulate body temperature, pH, water balance and hormone homeostasis. And last but not least, blood plays an important role in the immune system by destroying pathogens and minimizes blood loss via coagulation. To enable the blood to carry out all these functions, a vast network of blood vessels provides a pathway through which the blood can travel. Many different types of blood vessels are present, each with their own function and physiological environment. Arteries carry the blood from the heart to each organ and tissue while veins carry the blood back to the heart. Capillaries are the smallest blood vessels, connecting the arteries and veins with each other and allowing for exchange of gas and other substances with all tissues. [3]

## 1.2 VASCULAR DYSFUNCTION

A healthy vascular system is fundamental for proper functioning of the body. However, many people suffer from problems with their vasculature, causing pain, disability or even death. In fact, cardiovascular diseases are the number one cause of death worldwide [23]. There are many different types of vascular problems, most of them caused by atherosclerosis (a buildup of plaque inside the vessel), vasculitis (inflammation of the blood vessel wall) or aneurisms (bulges in the blood vessels). These problems often cause stenosis (narrowing of the blood vessels), hypertension (high blood pressure) and an increased risk of thrombosis (blood clotting) and embolisms, such as in peripheral artery disease, coronary artery disease, carotid artery disease or cerebrovascular disease (stroke). Each of these conditions can lead to a reduced blood supply to the tissues (ischemia) and eventually organ failure. [24] [25]

Another, less common vascular disease is pulmonary arterial hypertension, or PAH for short. This rare, progressive disorder is characterized by a high blood pressure in the arteries of the lungs, mainly affecting the smaller pulmonary arteries (sPAs) with a size ranging in diameter from 500  $\mu\text{m}$  down to 70  $\mu\text{m}$  [26]. These sPAs carry deoxygenated blood from the right ventricle of the heart to and through the lungs, where the blood becomes oxygenated and is transported throughout the body. When these vessels become constricted for some reason, the blood pressure increases. This makes it harder for the heart to pump blood to the lungs. As a result, the right side of the heart increases in size to accommodate for the increased pressure in the sPAs. However, this happens at the expense of the left side of the heart, decreasing its ability to efficiently pump blood to the rest of the body [27] [28] [29]. Currently there is no cure for this disease, although several types of FDA approved medication exist to promote vasodilation, reduce coagulation and decrease blood pressure to delay right heart failure.

## 1.3 RELEVANT FACTORS IN VASCULAR (DYS)FUNCTION

Various factors play an important role in the maintenance of a healthy vascular function, such as genetics, lifestyle and the immune system. Many of these factors can also be assigned as a possible cause for PAH, although the exact mechanism for disease development is still unclear. Currently, it is believed that the constriction of sPAs of PAH patients is caused by some kind of injury to the endothelial cells (ECs) that line the small blood vessels of the lung, as well as changes in the smooth muscle cells (SMCs) (see **Figure 1**). This provokes increased proliferation of these cells, inducing remodelling and thickening of the vessel wall leading to constriction and increased blood pressure. [27] [29]

It is also thought that the vessels of patients with PAH are particularly sensitive to certain internal and/or external factors that cause injury to the ECs and result in constriction of the pulmonary vessels. For example, it is known that 15-20% of patients with PAH have a genetic

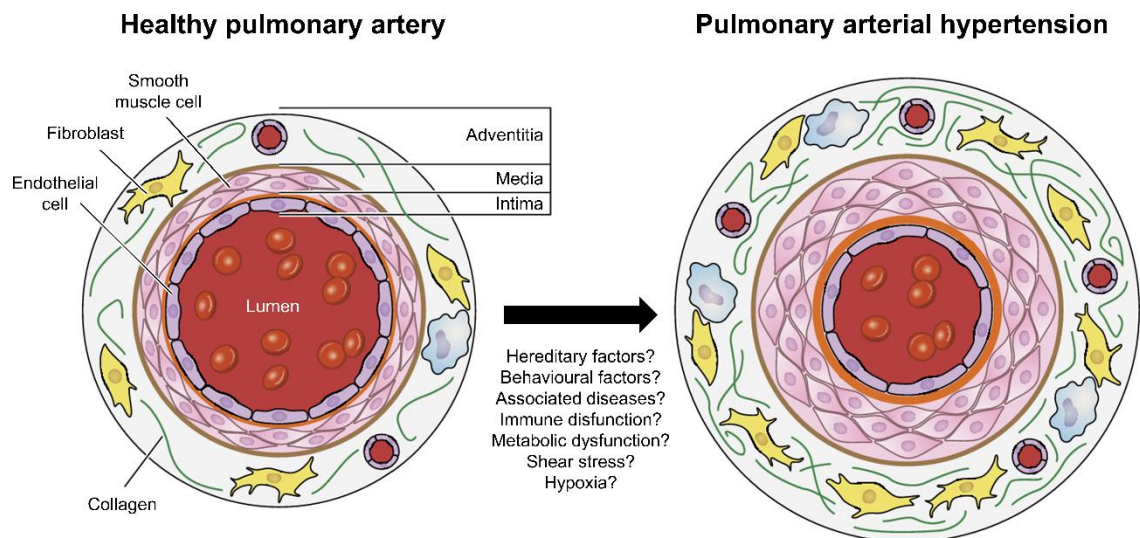


**Figure 1** Schematic representation of vascular remodelling as observed in patients with PAH and possible factors that might initiate or aggravate this remodelling. Adapted from [2].

mutation, most commonly in the bone morphogenetic protein receptor type 2 (BMPR2) gene or genes that are closely linked to BMPR2 [29]. BMPR2 is a transmembrane protein that plays a role in regulating the growth and differentiation of numerous types of cells, and a mutation in this gene could promote cell proliferation and/or prevent cell death, resulting in an overgrowth of cells in the sPAs and constriction of these arteries [30]. However, approximately 80% of individuals with a mutated BMPR2 gene will not develop PAH. It is therefore expected that other genes and/or environmental triggers also play a role in the development of PAH, referred to as the multiple-hit hypothesis. [29] [31] [32]

These other possible factors that could trigger PAH development include behavioural factors, associated diseases, inflammatory responses and metabolic factors. For example, it is found that PAH mostly affects females between the ages of 30 and 60 [29]. Sex hormones such as oestrogen and testosterone are therefore regarded as possible triggers for dysfunction of the cells in the vascular wall [33]. Furthermore, inflammatory cytokines such as tumour necrosis factor  $\alpha$  (TNF- $\alpha$ ) are found to be present in higher concentrations in the blood of PAH patients compared to a control group and TNF- $\alpha$  is also known to suppresses BMPR2 receptors. [34] [35] [36] [37]

It is also thought that abnormal oxygen tensions might cause injury to the ECs lining the sPAs. Oxygen is a major player in the regulation of the lumen size through which the blood is able to flow, a process which is mainly coordinated by the ECs lining the vessel walls. When the oxygen concentration in a specific artery is too low or too high, the ECs excrete various substances that activate the SMCs in the arteries to either open up (vasodilation) or constrict (vasoconstriction), thereby maintaining a healthy oxygen tension and blood pressure throughout the body. However, in patients with PAH this process might be dysregulated, as the vasoconstrictor molecule endothelin-1 (ET-1) has been reported to be increased in the lungs of PAH patients [38] and both protein and mRNA levels of hypoxia-inducible factor 1 $\alpha$  (HIF-1 $\alpha$ ) and hypoxia-inducible factor 2 $\alpha$  (HIF-2 $\alpha$ ) were significantly elevated in patients with PAH [39] [40]. Additionally, it is observed that living at a high altitude where the oxygen tension is much lower is a risk factor for the development of PAH [29] [41].

Finally, abnormal shear stresses caused by the flow of blood could be a trigger for PAH. Shear stress has been shown to influence the transcription of growth factors, adhesion molecules and molecules involved in vascular tone such as ET-1 and nitric oxide (NO) and affect the rate of EC proliferation, permeability of the vessel wall and migration of ECs [8] [42]. Furthermore, the wall shear stress of sPAs was found to be significantly lower in patients with severe PAH compared to healthy controls [43].

## 1.4 MODELS TO STUDY VASCULAR (DYS)FUNCTION

Various models exist to study the effects of these factors on vascular (dys)function (see **Figure 2**), but none fully recapitulate the human vascular behaviour *in vivo*. Two dimensional (2D) *in vitro* models are often used in the first stages of research, since they are relatively cheap and allow for a large number of experiments to be performed simultaneously in a controlled environment. By using human derived cells, the effect of a certain mechanical or chemical factor on these cells can be studied. However, these *in vitro* models often fail to mimic the complexity of human biology in patients. With these models it is for example not possible to determine the effect of a particular factor on the entire body, since only one or a few cell type(s) can be studied at the same time with no genetic variation. Furthermore, they do not replicate the three dimensional (3D) organisation found in the human body and certain mechanical factors such as flow cannot be incorporated. Although more advanced models such as Transwell and dynamic systems can be used to improve on some of these limitations, these 2D models remain a simplification of reality. [44] [45]

Another possible method to research the human vasculature are animal models. Rats and mice are often used for this purpose, since they exhibit considerable similarities in structure and function in biology with humans. The main advantage of using these animal models is that they do allow for studying the effect of a chemical or mechanical factor on the entire body and not just on the target cells as is done in *in vitro* studies. On top of that, it can be investigated which role the immune system plays in the treatment. Nevertheless, the physiology and genetic background of these animals are significantly different from those of humans, making them less than ideal models for research into vascular (dys)function in humans. Additionally, animal testing allows for less control of the microenvironment, is more expensive and time consuming and there is a big social and ethical push to reduce animal testing as much as possible. In some cases, it is possible to study the effect of certain factors on the vasculature in humans, either in healthy or diseased subjects. But even these studies are not fully representative, since usually limited subjects are available which do not represent the worldwide variation in genetic and behavioural background. Furthermore, these studies are often very expensive, time-consuming and require approval by a medical ethics committee. [44] [45]

As an alternative to wet-lab experiments, various computer models are being developed that could be used to predict the outcome of a certain treatment based on current knowledge of human physiology and pathology. These *in silico* models have many advantages, since they are cheap and large data sets can be generated in a short period of time. However, the knowledge of the human physiology and pathology is far from complete, making this method

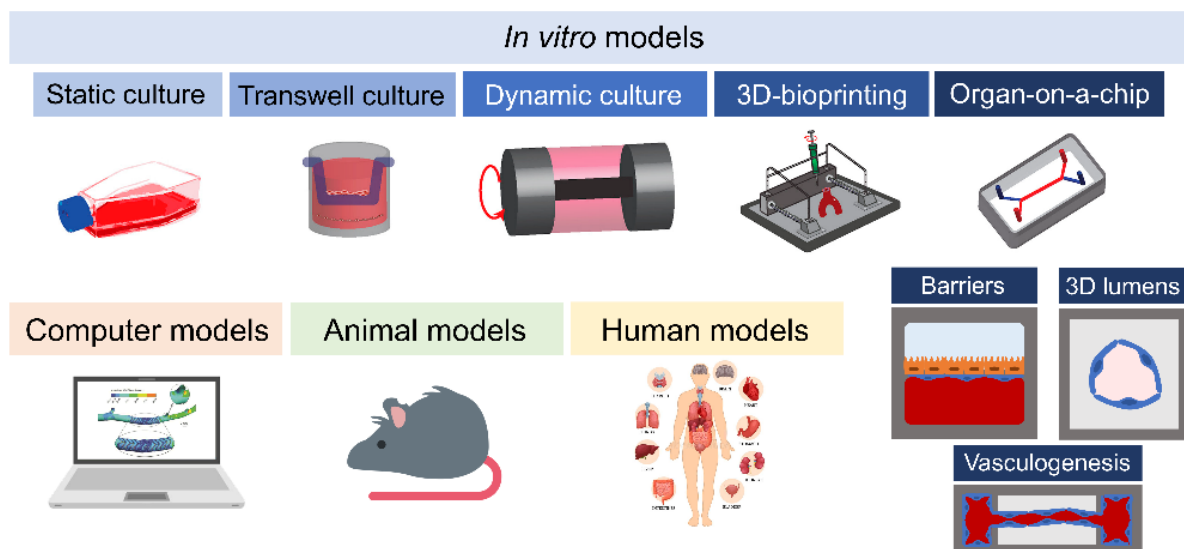


**Figure 2** Various models to study vascular (dys)function, including *in vitro* models like static culture and OoC systems, as well as computer, animal and human models. Adapted from [14].

less reliable and advanced compared to previously mentioned models. Besides, wet-lab experiments will still be required for validation and optimization of the model. [44] [45]

To overcome most of the limitations of each of the aforementioned methods, advanced *in vitro* models such as organ on chip (OoC) systems have been developed. In these models, a specific organ or set of organs is mimicked in a microfluidic device. This allows for 3D structures to be created, which better mimic the human organs than 2D *in vitro* models. Additionally, mechanical forces such as flow and electrical stimulation can be applied, which is mostly not possible with regular *in vitro* models. By using human derived (stem)cells, an advanced *in vitro* model can be created of a specific individual, allowing for personalized medicine and diagnostics. This could overcome some of the problems faced with animal models, which have a distinctly different physiology and genetic background than humans. Nevertheless, OoC systems also know some limitations. Currently, significant research and development is still required before such a system could be applied in a clinical setting. Additionally, some factors like lifestyle and aging are difficult to incorporate in these models. [44] [45]

When looking specifically at vascular OoC models, several different systems have been developed so far. Most of these models are used to study vascular barrier and exchange functions, such as the exchange of gasses between the alveoli and the lung capillaries [46], the blood brain barrier [47] or the absorption of nutrients in the gut [48]. For these purposes, a 2D barrier might deliver sufficient information about the mechanisms behind these exchange functions. However, for vascular studies into processes like perfusion, vasoconstriction, stenosis and angiogenesis, 3D geometries are preferred or even required. One way this can be achieved is by creating microfluidic chips with either rectangular or circular geometries and lining them with ECs and additional cell types to emulate the organisation of blood vessels *in vivo*. Coatings and/or matrices can also be applied in these chips to incorporate extracellular matrix (ECM) proteins and/or create 3D lumens inside rectangular channels [13]. For models of capillaries and vasculogenesis, rows of micropillars and/or patterned 3D matrices are often employed to create an environment in which the ECs can form a microvascular network. [13] [44] [49] [50]

## 1.5 RESEARCH QUESTION

As demonstrated in the previous sections, a lot is still unknown about vascular functioning and the development of diseases such as PAH. All the while, no suitable model yet exists to obtain this knowledge, which is required for the evolution of novel therapeutics. Nonetheless, several advances in the OoC field do have the potential to aid in this process, including a 3D hydrogel based vessel on chip (VoC) system first published by Bischel *et al.* [51] [52] and further developed by Andries van der Meer and others within the Applied Stem Cell Technologies (AST) group at the University of Twente [13] [17] (see **Figure 3**). This system consist of a polydimethylsiloxane (PDMS) microfluidic chip with a rectangular channel, in which a 3D collagen lumen is fabricated using a technique called viscous finger patterning (VFP). Vascular cells are then cultured inside this lumen to create a 3D VoC which can be used to successfully mimic various types of vascular dysfunction.

Given the genetic nature of some pulmonary vascular diseases like PAH, it would be advantageous to use patient specific human induced pluripotent stem cell (hiPSC) derived cells in such a model. However, it is unknown whether vascular cells derived from hiPSCs currently have the characteristic behaviour of cells found in the sPAs. It is however hypothesized that by culturing hiPSC-derived vascular cells in a microenvironment that mimics the environment as found in the sPAs, a phenotype can be induced that is more representative of the sPA physiology. Thus, to further improve on this VoC system and better mimic the sPA microenvironment *in vivo*, some of the previously indicated factors that play an important role in the maintenance of vascular (dys)function should be regarded and incorporated in this model.

In this research, the focus will be on incorporating control of both oxygen tension and shear stress in this existing VoC system, since these factors are regarded as “key modulators of

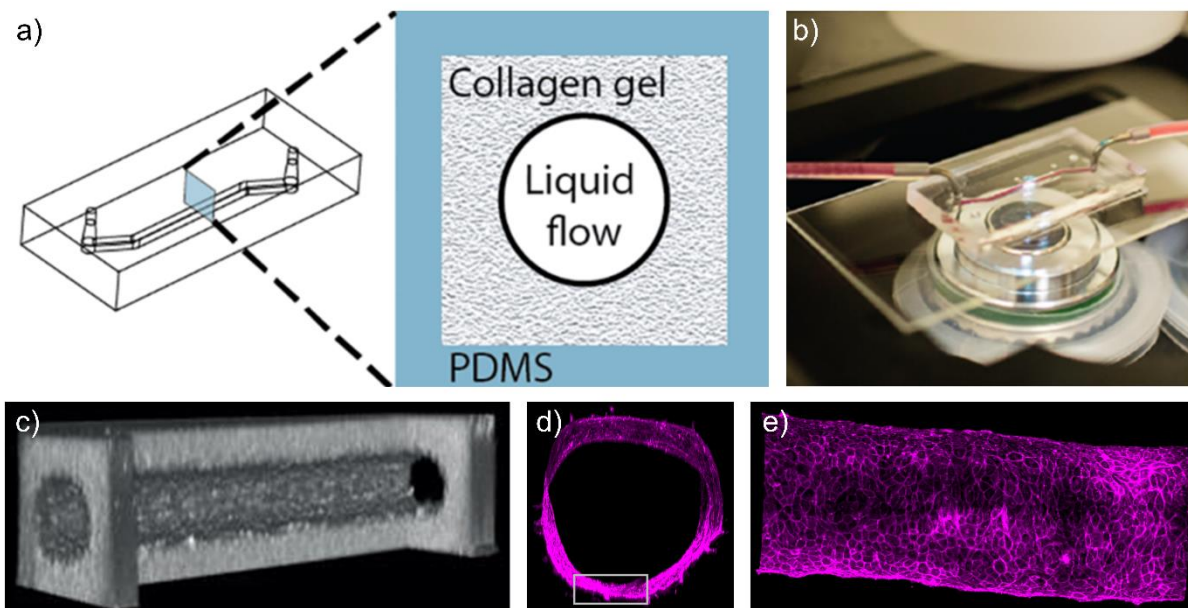


**Figure 3** a) Schematic diagram of the PDMS chip used to generate the 3D VoC system. b) Photograph of the 3D VoC system. c) 3D cut-out reconstruction of a 2-photon second harmonic generation image showing the collagen lumen. d-e) Fluorescence confocal micrographs of the engineered vessel made up of ECs viewed in cross-section (d) and from the top (e). From [13] and [17].

endothelial structure and function and initiate and perpetuate pulmonary vascular remodelling associated with PAH”, as stated by Humbert *et al.* [26], and “a better understanding of the molecular mechanisms underlying endothelial adaptation to high shear stress and chronic hypoxia will greatly enhance our understanding of the pathogenesis of PAH, and may aid in identifying new therapeutic strategies” [26]. Additionally, when regarding the multiple-hit hypothesis, neither hereditary factors such as mutations in the BMPR2 receptor, atypical shear stresses nor hypoxia alone seem to be sufficient to structurally induce pulmonary vascular remodelling, while a combination of these factors could be the trigger for vascular remodelling as observed in patients with PAH [31]. This hypothesis is supported by the research as summarized by Pugliese *et al.* [2], who states that the current scientific knowledge suggest that “hypoxia acts as an inflammatory stimulus in combination with changes in flow and pulsatility to initiate and perpetuate pulmonary vascular remodeling”.

However, before the influence of these factors on the behaviour of vascular cells can be studied, an improved 3D vascular model needs to be developed that specifically mimics the sPA in regard to oxygen tension, shear stress and cellular phenotype. The research question that will be addressed in this research can therefore be formulated as follows:

***How can the influence of oxygen tension and shear stress on the behaviour of vascular cells be studied in a 3D small pulmonary artery on chip model?***

To be able to answer this research question in the best possible way, it can be split up into several sub-questions, which will be discussed in further detail in the remainder of this section.

***How can the cellular behaviour of vascular cells be characterized?***

Before it is possible to study the influence of factors like oxygen tension and flow rate on the behaviour of the hiPSC derived vascular cells, it is required to establish what “cellular behaviour” is, how this differs between different types of vascular cells and which markers and readout methods can be used to characterize this behaviour. Since PAH mainly affects the sPAs, but not the larger pulmonary arteries, systemic arteries or veins [26], it is important to formulate the main similarities and differences in cellular behaviour between the cell types that

reside in each of these tissues. This information can then be used to create a VoC system that specifically mimics the sPA microenvironment. For this purpose, markers should be identified that can be used to distinguish between these different cell types. Additionally, markers might be identified that can be used to characterize the phenotype as observed in PAH.

Once these markers are established, compatible read-out methods need to be selected that can be used for both 2D and 3D characterization of the cellular behaviour. In this way, the differences in cellular behaviour can be characterized in both 2D cell culture and in the 3D VoC system. Additionally, it is important to determine the natural cellular behaviour of these different cell types in response to various oxygen tensions and flow rates to be able to validate whether the developed VoC system behaves similar to the *in vivo* situation and whether these factors aid in the differentiation and maturation of the hiPSCs towards sPA specific cells. This also makes it possible to demonstrate whether certain oxygen tensions and/or flow rates stimulate healthy cellular behaviour or pathological behaviour as observed in patients suffering from PAH.

### ***How can the oxygen tension be controlled in a 3D small pulmonary artery on chip system?***

Once the cellular behaviour can be characterized and it is understood which cellular behaviour can be expected in different situations, the cells can be exposed to different oxygen tensions to determine its influence on the cellular behaviour. In order to achieve this, an oxygen control systems needs to be incorporated in the 3D small pulmonary artery on chip (sPAoC) model. Different methods of oxygen control need to be researched and material choices need to be made before the most promising method can be fabricated and experimentally validated. Towards this end, oxygen sensors might need to be incorporated in the design to allow for spatial and temporal control of the oxygen tension that is perceived by the cells.

### ***How can the flow rate be controlled in a 3D small pulmonary artery on chip system?***

Similarly, a flow control systems needs to be designed and fabricated that allows for exposure of the cells to a predetermined shear stress in the 3D sPAoC. This will require a pumping system, tubing, connections and a method to confirm that the aspired shear stresses are actually experienced by the cells. Using this flow control system, it should then be possible to study the effect of different flow rates and shear stresses on the cellular behaviour. Once this is achieved, experimental validation of the combined effect of oxygen tension and shear stress on the cellular behaviour can be determined. For this purpose, it is crucial that the flow control system is compatible with the oxygen control system.

## **1.6 THESIS STRUCTURE**

In the remainder of this thesis, it is attempted to answer these questions and to demonstrate successful design, fabrication and experimental validation of a 3D sPAoC which allows for control of both oxygen tension and flow rate. First of all, background information from a literature study will be disclosed on the physiology of healthy and diseased sPAs and the characteristics of the various cell types that need to be considered, allowing for the selection of markers that can be used to distinguish these different cell types *in vitro*. Then, different possible methods for controlling oxygen and flow rate within a VoC system will be discussed. Next, a design is presented which allows for control of both oxygen tension and flow rate in a sPAoC. Finally, experimental progress on characterization of the cellular behaviour, chip fabrication and control of oxygen and flow is shown and discussed.

## 2 BACKGROUND

### 2.1 PHYSIOLOGY OF THE PULMONARY ARTERIES

For the development of a sPAoC, it is important to understand the physiology of the sPAs *in vivo*, in both healthy and diseased conditions. In this section, detailed information will be provided regarding the blood vessels structure, vascular cells and the different types of blood vessels. Using this information, markers are identified that can be used to distinguish between these different cell types in order to characterize the cellular behaviour of the cells in 2D and 3D sPAoC models. Additionally, (patho)physiological oxygen tensions and shear stresses are defined which need to be mimicked in the sPAoC. Additional background information can be found in Supplementary Material S1.

#### 2.1.1 Blood vessel structure

As mentioned earlier, blood vessels are important circulatory passageways that function as a transport system for nutrients, gasses and many other substances through the body. This blood vessel system can be divided into a pulmonary circulation, which carries oxygen-poor blood from the heart to the lungs and oxygen-rich blood back to the heart, and a systemic circulation, which carries oxygen-rich blood from the heart to all other organs and oxygen-poor blood back to the heart. [3]

Blood vessels can further be divided into three main types: arteries, vein and capillaries. The arterial and venous vessel walls all consist of three layers: the tunica intima, the tunica media and the tunica adventitia (see **Figure 4**). The tunica intima is the innermost layer of the vessel wall and consist of a thin layer of ECs. The middle layer (tunica media) mainly contains

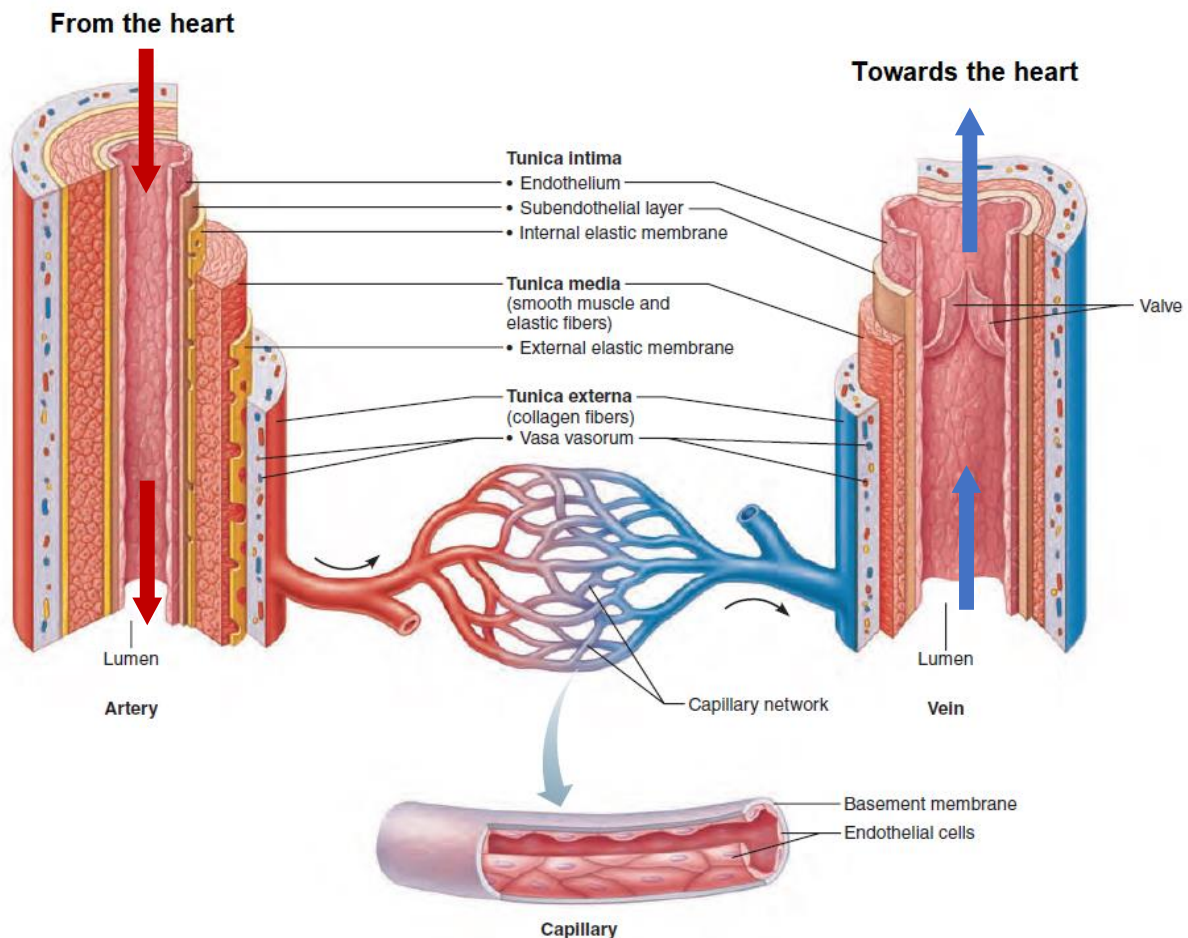


**Figure 4** Generalized structure of arteries, veins, and capillaries and their wall structure. From [3].

circularly arranged SMCs and sheets of elastin. This middle layer plays an important role in vasoconstriction and vasodilation in response to neural, chemical and other signals and it is generally much thicker in arteries than in veins. The outermost layer of the arterial and venous vessel walls (tunica adventitia) accommodates fibroblasts that secrete collagen and elastin fibres to provide stability and flexibility to the blood vessels. The tunica adventitia is usually thicker in veins compared to arteries. Capillary walls do not have this three layered structure, but only consist of a single layer of ECs that can be enveloped by pericytes. [3]

### 2.1.2 Vascular Cell Types

The main cell types that reside in the vascular walls are ECs, SMCs and fibroblasts. Each of these cell types interact with each other on various levels to maintain a proper vascular function. The layering of these cell types is visualised in **Figure 5**. [3]

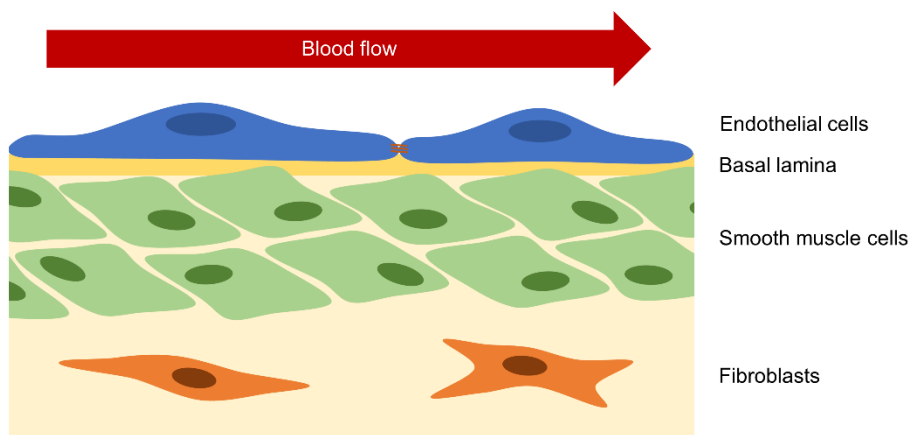


**Figure 5** Schematic representation of various cell types residing in the vascular wall. Vascular ECs lining the lumen are separated from the SMCs by a basal lamina. Fibroblasts in the tunica adventitia are responsible for the production of ECM proteins.

#### 2.1.2.1 Endothelial Cells

Vascular ECs line the inner wall of the blood vessels. They are polarized because of direct exposure to the blood flow on the apical side and anchoring onto a basal lamina on the basolateral side. Their shape varies depending on their location in the body, but in general they are thin and slightly elongated. They can grow to be approximately 30-50  $\mu\text{m}$  in length, 10-30  $\mu\text{m}$  in width and have an average thickness of 0.1-10  $\mu\text{m}$  [53]. An EC monolayer *in vitro* shows a characteristic cobble-stone pattern and the ECs are aligned in the direction of the blood flow to minimize the shear stress they experience due to the flowing blood (see **Figure 6**). Because of tight cell-cell junctions, permeability of blood through the vessel wall is very low in arteries and veins. In capillaries however, the permeability of the vessel wall is higher to allow exchange of substances with the surrounding tissue. [53]

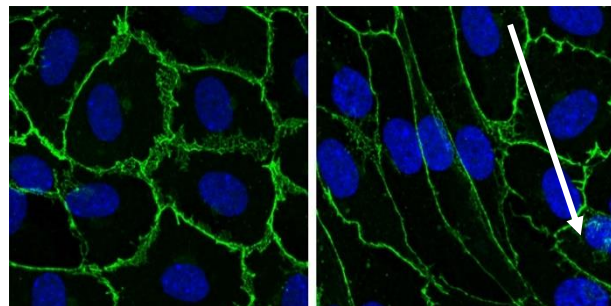


**Figure 6** Fluorescent images of ECs where nuclei are labelled in blue and VE-cadherin molecules are labelled in green. On the right, the cells are elongated and aligned due to unidirectional flow in the direction as indicated by the arrow. From [12].

Since ECs are in direct contact with the blood, they play a crucial role in many physiological processes including vasoconstriction and vasodilation and the permeability of fluids, cells and other substances in the blood. They have mechanoreceptors that allow them to sense the shear stress due to flow of blood over their surface and are able to detect changes in the oxygen tension of the blood. By signalling this information to the surrounding cells (such as SMCs), they enable the blood vessel to adapt its diameter and wall thickness to suit the blood

flow. For this purpose, they are able to synthesize and release various factors to modulate the blood flow rate, including NO and ET-1. Additionally, ECs also sense and act upon factors that are secreted by other cells. Dysregulation in any of these signalling pathways can lead to vascular dysfunction. In the case of PAH, endothelial-to-mesenchymal transition is often observed, which is a process in which ECs lose polarity and cell-to-cell contacts and undergo a dramatic remodeling of the cytoskeleton. [53] [54] [55] [56]

Various biomarkers can be used to identify whether a cell exhibits an endothelial phenotype. Some of these endothelial-specific biomarkers are vascular endothelial cadherin (VE-cadherin), which is an endothelial adhesion molecule located at the junctions between ECs, platelet endothelial cell adhesion molecule 1 (CD31) and the endothelial nitric oxide synthase enzyme (eNOS) [57] [58].

### **2.1.2.2 Smooth Muscle Cells**

Vascular SMCs are the most common cells in the tunica media of the vessel wall. In larger vessels, there can be up to 40-60 layers of SMCs around a single layer of ECs. In the sPAs, this smooth muscle layer can have a thickness of tens to hundreds of micrometers [3]. SMCs play important roles in the physiological functioning of blood vessels, since they allow blood vessels to contract and relax. In healthy blood vessels, the SMCs contain many contractile fibres with SMC-specific contractile proteins, such as alpha smooth muscle actin (actin- $\alpha$ 2) and smooth muscle myosin (myosin SM-1/2). The contraction of these fibres can be mediated via various pathways and substances such as NO and ET-1 as are produced by the ECs for vasodilation and vasoconstriction respectively. [59]

At the onset and development of most vascular diseases, including PAH, the SMCs undergo phenotypic modulation, characterized by a loss of contractile filaments and associated molecules. The SMCs will start to grow and migrate, causing thickening of the blood vessel wall. It has also been observed that reactive oxygen species (ROS) can cause damage to the SMCs, causing this phenotypic modulation. To classify cells as SMCs and distinguish them from ECs, several biomarker molecules can be used including actin- $\alpha$ 2 and myosin SM-1/2 [60].

### **2.1.2.3 Fibroblasts**

Fibroblasts can mainly be found in the tunica adventitia of larger blood vessels. For a long time, it was thought that these cells were merely present for structural support of the blood vessel, but it is now realized that these supporting cells also play an important role in mediation of vascular remodelling and repair, as well as in the deposition of the ECM proteins such as collagen, laminin and fibronectin. For example, it has been demonstrated that both vasoconstriction and vasodilatation can be dependent on fibroblasts in the tunica adventitia and that these fibroblasts are able to contract after stimulation with ET-1, similarly to SMCs. At the same time, fibroblasts are also able to produce ET-1 themselves. This expression can be mediated by the environmental oxygen tension and oxidative stress. In addition, NO derived from adventitial inducible nitric oxide synthase can also regulate SMC function. [61]

When looking at the pathology of PAH, the fibroblasts in the adventitial layer are activated and start to proliferate and transform into myofibroblasts, as indicated by the expression actin- $\alpha$ 2 and myosin SM-1/2. Additionally, interstitial collagen as produced and degraded by the fibroblasts starts to accumulate, which is also associated with vascular disease development. Lastly, fibroblasts are able to generate ROS via the NADPH oxidase pathway, which could have a paracrine effect on vascular hypertrophy as seen in the onset of PAH. Since not many fibroblast-specific biomarkers exist, the easiest way to classify fibroblasts is by elimination of other cell types using biomarkers for ECs and SMCs. [61] [62] [63]

## **2.1.3 Types of Vasculature**

Now that it is clear which layers and cell types are present in the blood vessel structure, it is possible to look into the different types of vascular structures that exist throughout the human body. In this thesis, a distinction will be made between the ECs found in macrovascular and microvascular blood vessel structures, between arteries and veins and between pulmonary

and systemic vessels. It is important to note however that these are not the only cells and types of vasculature present and that many different distinctions can be made, even within each of these categories. The reason why characterization was mainly focussed on the ECs and not on the SMCs or fibroblasts, is because these will be the first cells to be incorporated in the 3D sPAoC system. ECs are also the first cells that will come into contact with a change in oxygen tension or flow rate of the blood. Additionally, the main reason why these specific categories were chosen is because it is intended to develop a model for vascular diseases such as PAH, which mainly affect the sPAs. [26]. Thus, it needs to be established that the fabricated vessel is indeed small (70-500  $\mu\text{m}$ ), pulmonary and arterial.

### 2.1.3.1 Macrovasculature versus Microvasculature

Based on their anatomy, it is relatively easy to distinguish macrovasculature (arteries and veins) from microvasculature (arterioles, venules and capillaries). Most importantly, arteries and veins are larger than arterioles and venules and contain a much thicker tunica media. In general, arterioles are defined to have a diameter of 10-100  $\mu\text{m}$ , whereas arteries are larger and capillaries are smaller than this range [64]. However, large variations still exist within each of these categories due to differences in size and microenvironmental factors such as shear stress and oxygen tension. And when only looking on a cellular level, this distinction between macrovasculature and microvasculature is even harder to make.

Nevertheless, several genes have been identified that are expressed differently between ECs of macro- and microvasculature. For example, larger vessels generally express more fibronectin and collagen 5 $\alpha$ , likely related to their thicker vascular wall, while microvasculature has a higher expression of basement membrane proteins such laminin and collagen 4 $\alpha$  [65]. Furthermore, many genes associated with angiogenesis are expressed in microvascular ECs (hMVECs) but not in ECs from larger vessels, since microvascular networks are the main sites for angiogenesis in adults [65]. However, these differences are very general while especially for ECs gene expression considerably depends on the organ of origin.

Research focusing specifically on the pulmonary macro- and microvascular is scarce. Nevertheless, it has been established that there is a difference in the lectin binding pattern between hMVECs and pulmonary arterial ECs (hPAECs). Specifically, it seems that *Helix pomatia* agglutinin lectin (HPA) binds to hPAECs but not to hMVECs, while *Griffonia Simplicifolia* Lectin I (GSL) binds to hMVECs but not to hPAECs (see **Figure 7**) [2] [16] [58]. Here, the transition between microvascular and macrovascular ECs occurs in vessels with a diameter between 40-60  $\mu\text{m}$ , since vessels larger than 60  $\mu\text{m}$  do not bind GSL, while vessels smaller than 40  $\mu\text{m}$  do [66]. Lastly, expression of eNOS and NO can also be used to distinguish between hPAECs and hMVECs [16] [67]

### 2.1.3.2 Arteries versus Veins

Even though both arteries and veins consist of the same three layers, there are many differences that distinguish them from one another. Generally speaking, veins are larger in diameter than arteries but have much thinner walls. Arteries have a thinner tunica adventitia but have a much thicker tunica media and are thus more muscular than veins. This makes that arteries are stronger and more rigid than veins. Veins however have in general a larger lumen

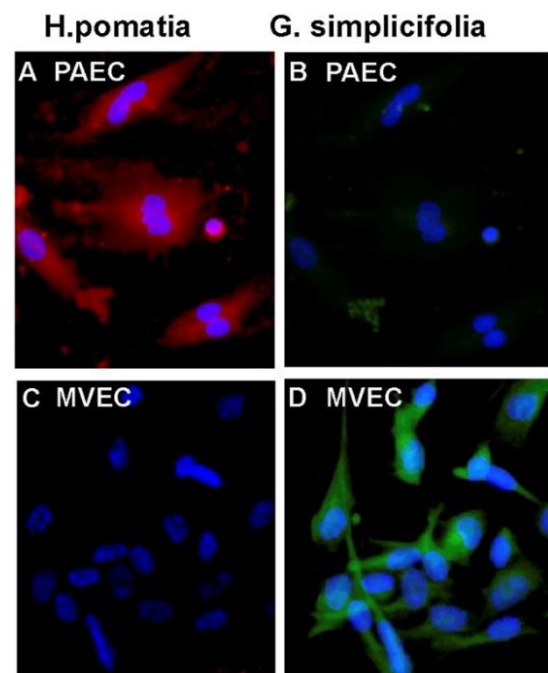


**Figure 7** Binding of lectins to hMVECs and hPAECs in vitro. Immunofluorescent HPA (red) binds hPAECs (A) but not hMVECs (C), while immunofluorescent GSL (green) binds hMVECs (D) but not to hPAECs (B). Cell nuclei are stained with DAPI. From [16].

diameter than their arterial counterpart, resulting in a larger volume of blood residing in the veins compared to the arteries. [68] Another major difference between arteries and veins is blood pressure, which is much higher in the arteries compared to the veins (see **Figure 8**). Since the wall shear stress (WSS) experienced by the ECs in the vessel wall depends on both the blood pressure and the cross-sectional area of the vessels, the blood velocity (and thus also the flow rate and WSS) is lowest in the capillaries and highest in the arteries. This is the case for all systemic vessels except the pulmonary vessels, where the pressure is higher in the veins than in the arteries. Since the blood pressure in the veins is considerably lower than in the arteries, valves are needed to prevent backflow of the blood. In the arteries and the pulmonary veins, no valves are present since the blood pressure is strong enough to ensure unidirectional flow. The concentration of oxygen in the blood can also be used to distinguish between arteries and veins, which is generally higher in the arteries compared to the veins, except for the pulmonary circulation. [3] [68]

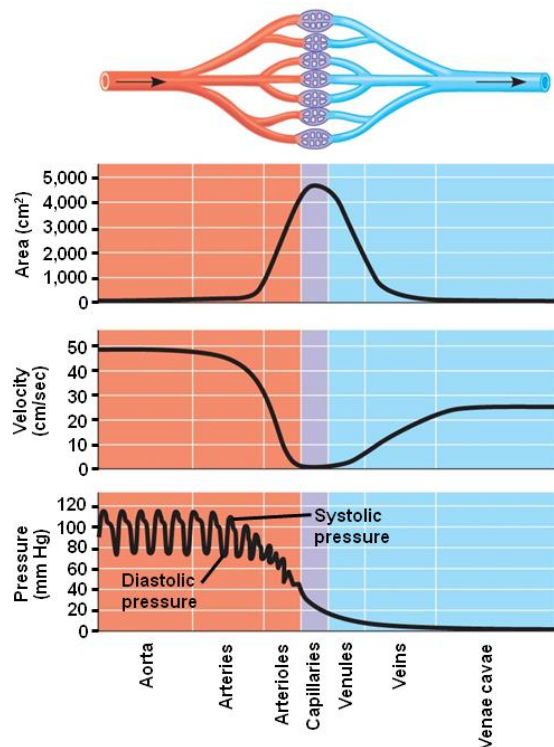
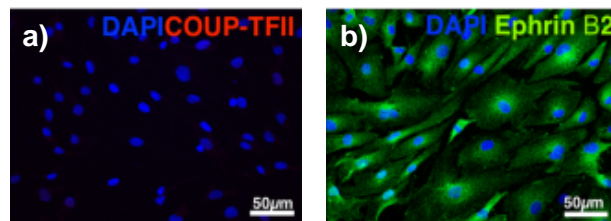


**Figure 8** Schematic overview of a) the cross-sectional area (in  $\text{cm}^2$ ), b) the velocity (in  $\text{cm/sec}$ ) and c) the pressure (in  $\text{mmHg}$ ) in systemic blood vessels of various types and sizes. From [3].

When looking on a cellular level, the ECs lining the vessel walls are slightly different for arteries and veins. While in veins the cells are more round and cobblestone like, they become more elongated and aligned in arteries. This is because the blood pressure and shear stresses are generally higher in arteries, causing the cells to align in the direction of the blood flow. Furthermore, a difference in ECs can be observed regarding the distribution of junction molecules, which varies throughout the vascular tree to comply to the requirements at each location. These junctions, which regulate permeability of the vessel wall, are found to be much tighter in arteries than in veins but are even more relaxed in arterioles, venules and capillaries. [68] Lastly, the expression of biomarkers such as COUP transcription factor 2 (COUP-TFII) and Ephrin B2 can be used to identify venous and arterial ECs respectively (see **Figure 9**). [10] [65] [68]

### Arterial endothelial-like cells



### Venous endothelial-like cells

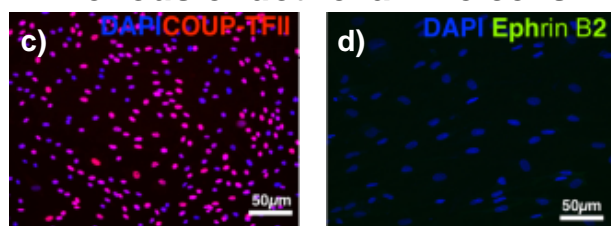


**Figure 9** Arterial endothelial-like cells showing a low expression of COUP-TFII (a) and a high expression of Ephrin B2 (b), while venous endothelial-like cells show a high expression of COUP-TFII (c) and a low expression of Ephrin B2 (d). From [10].

#### 2.1.3.3 Pulmonary versus Systemic Vasculature

The most recognisable distinction between pulmonary and systemic vessels are the blood pressure and shear stresses that can be found in these vessels. While in systemic arteries such as the aorta the blood pressure is high, in the pulmonary arteries the blood pressure is

significantly lower. [3] [69] Additionally, pulmonary arteries have larger diameters and much thinner walls than systemic arteries. Thus, anatomically they are more similar to systemic veins than to systemic arteries. Their larger diameter also gives them a much lower resistance, about one tenth of the resistance as experienced in the aorta. These differences all result in a much lower WSS experienced by the ECs in the pulmonary arteries compared to those in the systemic arteries. [69] [70]

Another major difference between the pulmonary arteries and the systemic arteries are the oxygen levels, as the systemic arteries carry oxygen-rich blood while the pulmonary arteries carry oxygen-poor blood [3]. Besides a difference in absolute oxygen tension, pulmonary and systemic arteries also respond differently to relative changes in oxygen tension. While systemic arteries respond to hypoxia with vasodilation, allowing more oxygen rich blood to flow towards the hypoxic tissues, pulmonary arteries actually constrict in a response to hypoxia, thereby diverting blood to better-oxygenated lung segments and improving systemic oxygen delivery [2] [71].

This behaviour can also be observed on a cellular level. For example, it has been shown that hPAECs in response to hypoxia produce more laminin, fibronectin, and elastin, decrease the production and/or activity of NO and increase the production of ET-1 to achieve vasoconstriction (see **Figure 10**). This is opposite for systemic arterial ECs, which increase NO production and reduce ET-1 secretion to induce vasodilation [1] [2] [72]. This adapted biomarker expression in response to hypoxia can therefore be used to characterize whether ECs behave more like systemic or pulmonary arterial ECs *in vitro*.

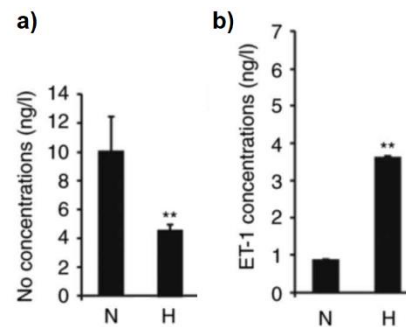


**Figure 10** Expression of a) NO and b) ET-1 in normoxia (N) or hypoxia (H) (5% O<sub>2</sub> for 24h) in hPAECs. Adapted from [1].

### 2.1.4 (Patho)physiological Oxygen Tensions

For the creation of a sPAoC model, it is desired to control the oxygen tension in the chip and study its effect on the cellular behaviour. Towards this end it is important to understand which oxygen tensions should be used to emulate hypoxic, normoxic and hyperoxic conditions. However, these terms are a bit indistinct since the oxygen concentration that needs to be maintained is not the same throughout the body (see **Figure 11**). Thus, it is necessary to know the (patho)physiological oxygen tensions in different parts of the body to discern what a “low” oxygen concentration actually means.

While the air that we breath contains around 21% oxygen (160 mmHg), the oxygen concentration is already reduced to around 14% (100 mmHg) once it reaches the alveoli in the lungs [73]. This oxygen is then exchanged with the blood in the lungs and flows through the pulmonary veins, where the oxygen concentration is around 13%. The oxygen rich blood then quickly flows through the heart and into the aorta,

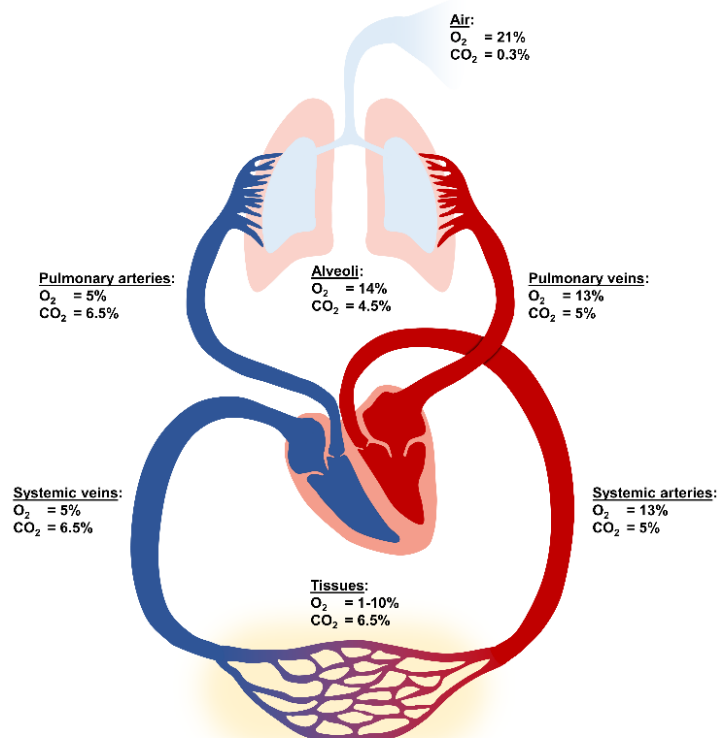


**Figure 11** Physiological oxygen and carbon dioxide concentrations throughout the human body. Adapted from [4].

after which most of the oxygen is delivered to various tissues. The oxygen tension in these tissues can vary from 1% in the skin to almost 10% in the kidneys. The blood then flows back to the heart via the systemic veins, which have an oxygen concentration of only 5% (40 mmHg). Finally, it moves back to the lungs via the pulmonary artery, where the blood still has an average oxygen tension of 5%. Hence, it can be presumed that an oxygen tension below 5% can be regarded as hypoxia for the ECs as found in the sPAs, while for systemic ECs an oxygen tension below 13% might already evoke a cellular response to hypoxia. [74] [75] [76] [77]

Moreover, it has been observed that the cellular response to hypoxia not only depends on the absolute oxygen tension that is regarded as “hypoxia”, but also on the degree of hypoxia, the length of exposure and the type and location of the cells. For example, it seems that both HIF-1 $\alpha$  and HIF-2 $\alpha$  are upregulated in response to acute hypoxia (<24 hours), but only HIF-2 $\alpha$  remains upregulated during chronic hypoxia (>24 hours) [78]. Furthermore, HIF-2 $\alpha$  can already be upregulated when the oxygen tension is slightly decreased, while HIF-1 $\alpha$  expression only increases when the oxygen tension is significantly reduced [78]. Additionally, ECs and SMCs in different parts of the vascular tree respond differently to hypoxia [2]. Lastly, it is important to note that in the lungs not only the oxygen concentration in the blood plays a role in the EC behaviour, but the oxygen concentration in the alveoli also seems to have an effect on the vascular behaviour [71].

### 2.1.5 (Patho)physiological Shear Stresses

Besides oxygen tension, it is also of interest to study the effect of different shear stresses on the cellular behaviour in a sPAoC system. In healthy vasculature, these shear stress values can range from 0.5 to 120 dyn/cm<sup>2</sup> (1 dyn/cm<sup>2</sup> is equal to 0.1 Pa) depending on the vessel type and size of the tissue [79]. While in veins these shear stresses are only 1–5 dynes/cm<sup>2</sup>, they are generally much higher (10-40 dynes/cm<sup>2</sup>) in arteries. In a healthy pulmonary arteries, shear stresses between 10-25 dyn/cm<sup>2</sup> are commonly found. However, patients with vascular disorders such as PAH can have shear stresses in the pulmonary arteries that are either much higher (> 80 dyn/cm<sup>2</sup>) or much lower (5-8 dyn/cm<sup>2</sup>) than this physiological range. It is therefore thought that both increased and decreased flow rates may induce vascular dysfunction [8]. This hypothesis is supported with the research by Li *et al*, who demonstrated that a shear stress of 20-60 dynes/cm<sup>2</sup> promotes vasodilation, as shown by a high expression of nitrite and a low expression of ET-1, while both higher and lower shear stresses promote vasoconstriction in hPAECs (see **Figure 12**). [8] [42]

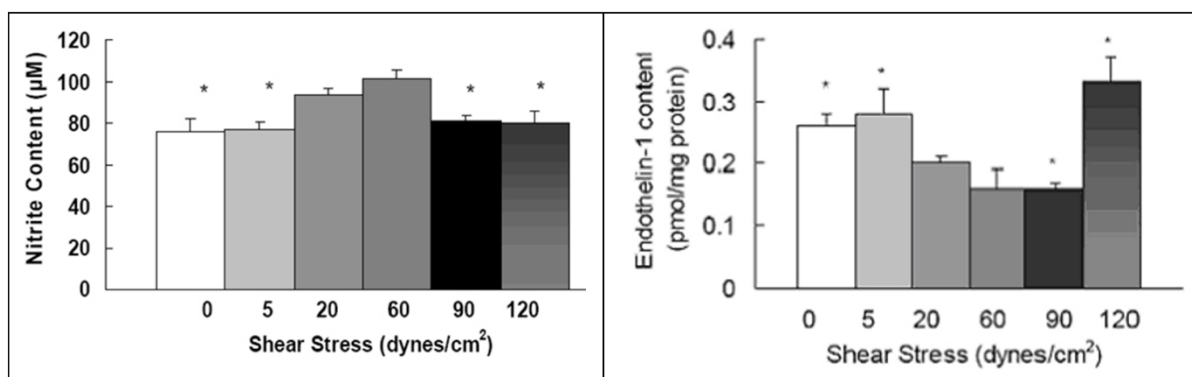


**Figure 12** (a) Nitric oxide release in flow medium as measured by the total content of nitrite. (b) ET-1 content in the flow medium as measured with ELISA. Medium was collected from the flow circulation after cells were exposed to different shear stresses. From [8].

## 2.2 ORGAN ON A CHIP SYSTEMS

The aim of this project is to create a 3D sPAoC in which the influence of oxygen tension and flow rate on the behaviour of vascular cells can be studied. For the development of such a system, it is important to review the state-of-the-art in the field of OoC and VoC technology. The term OoC was first introduced to a wider audience in 2010, when Huh *et al.* demonstrated a lung-on-a-chip system in which the alveolar-capillary interface of the human lung was mimicked, incorporating mechanical forces such as fluid flow and mechanical strain [46]. Quickly after, many other organs were integrated in a microfluidic chip, including the gut, liver, kidney, brain and heart. Already in 2009, van der Meer *et al.* published about the possibility to create vessels and capillaries in microfluidic channels [80], and in 2013 a 3D VoC co-culture of human ECs and embryonic stem cell-derived pericytes was demonstrated [81]. The VoC system that will be used as the basis for this research is the previously described 3D hydrogel based VoC system first published by Bischel *et al.* [51] [52] and further developed by Andries van der Meer and others within the Applied Stem Cell Technologies (AST) group at the University of Twente (see **Figure 3**). [13] [17]

To improve on this existing system and allow for control of oxygen tension and shear stress, the material choices and fabrication methods for this VoC system will be reviewed and alternatives will be considered. Additionally, information will be provided about incorporation of cells and possible readout methods in such a system.

### 2.2.1 Materials

Various different materials are being used for the fabrication of microfluidic chips and OoC systems, each with their own advantages and limitations. In general, the main requirements that need to be considered for their application in OoC systems are a non-toxicity to cells, permeability to gasses such as oxygen and CO<sub>2</sub>, optical transparency required for microscopic visualization and the costs of materials and fabrication processes [82].

Inorganic materials such as silicon and glass were the first materials to be used for microfluidic cell culture devices. However, these materials are not gas permeable, making them unsuitable for long-term cell culture. Additionally, fabrication of silicon or glass chips requires photolithography and etching, which are expensive and time-consuming fabrication methods [83]. To overcome these limitations, people started fabricating OoC devices out of elastomers such as PDMS. These elastic polymers are usually gas permeable, biocompatible and optically transparent, making them perfectly suitable for cell culture. Additionally, elastomers are cheap and easy to fabricate into complex 3D structures. Another advantage of using elastic materials for OoC systems is that they allow for pneumatically controlled deformation, which can be used to mimic pulsatile stresses as found in the lung, gut and larger vasculature. However, elastomers do know some limitations. For example, PDMS is incompatible with some organic solvents, has a high hydrophobicity and shows strong adsorption of biomolecules. [83] [84] [85]

Besides elastomers, other plastic materials can also be used for the fabrication of OoCs, including poly(methyl methacrylate) (PMMA), polycarbonate (PC), polystyrene (PS) and cyclic olefin copolymer (COC). These materials are generally more rigid than elastomers, optically transparent and biocompatible, but less gas-permeable than PDMS and often incompatible with most organic solvents. However, they show a lower adsorption and are more resistant to the permeation of small molecules. Additionally, thermoplastics are suitable for thermomechanical processing methods such as injection moulding, making them more suitable for commercialization and mass production. [83]

To allow for cells to be cultured in OoCs made with any of the aforementioned materials, it is often required to apply a coating that promotes cell adhesion. For this purpose hydrogels are often used, since they are able to mimic the ECM, are highly biocompatible and material properties such as elasticity, porosity, permeability, stiffness and degradability are easily tuneable. Hydrogels can broadly be classified into natural, synthetic, and hybrid hydrogels. Natural hydrogels include collagen, gelatine, alginate, agarose and fibrin, while polyethylene glycol, polylactic acid, poly(lactic-co-glycolic acid) and poly( $\epsilon$ -caprolactone) are examples of

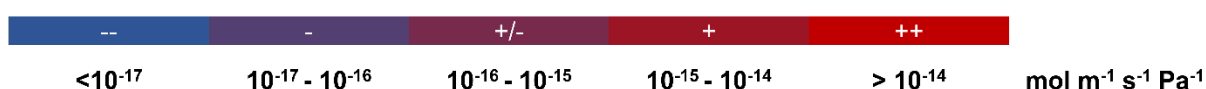
synthetic hydrogels. Natural hydrogels are generally more biocompatible and better promote cell attachment and growth than synthetic hydrogels, but their mechanical properties are less tuneable and they often show limited long-term stability and more variability between batches.

Besides materials for the OoC itself, it is also important to look into materials for fluidic connections between the chip and the outside world. For initial insertion of fluids in the OoC device, it is often sufficient to use standard sized polypropylene (PP) pipette tips which can directly be inserted into the inlets of the chip. However, when a controlled flow through the channels of the OoC is required, it is often desired to introduce a pumping system which is connected to the chip via tubing. Microfluidic tubing exists in many different sizes and materials, but polyether ether ketone (PEEK), polytetrafluoroethylene (PTFE/Teflon™), fluorinated ethylene-propylene (FEP), perfluoro alkoxy (PFA) and ethylene tetrafluoroethylene (ETFE) are often used, either with or without a polyvinylidene chloride (PVDC) or polyvinylidene fluoride (PVDF) coating. [86] [87] [88] [89] Fluidic connectors might be required to interface between the OoC and the tubing. These can be commercially obtained or fabricated in-house and are often made from stainless steel, PEEK, ETFE, PP or PTFE [90] [91].

Since it is desired to be able to control the oxygen tension in the OoC device to determine its effect on the cellular behaviour, oxygen permeability of the chip material is a key parameter that needs to be regarded. In **Table 1**, an overview is given of the oxygen permeability coefficient of some materials often used in OoC systems. This oxygen permeability coefficient

**Table 1** Overview of oxygen permeability of various materials commonly used in OoC systems. Data from [92] [93] [94] [95] [96] [97] [98] [99].

Material		Oxygen permeability coefficient	
		mol m <sup>-1</sup> s <sup>-1</sup> Pa <sup>-1</sup>	Relative permeability
<b>Inorganic materials</b>			
Silicon		0	--
Glass		0	--
Metal		0	--
<b>Elastomers</b>			
Polydimethylsiloxane	PDMS	2.04*10 <sup>-14</sup>	++
<b>Thermoplastics</b>			
Poly(methyl methacrylate)	PMMA	3.16*10 <sup>-17</sup>	-
Polycarbonate	PC	5.00*10 <sup>-16</sup>	+/-
Polystyrene	PS	6.89*10 <sup>-16</sup>	+/-
Cyclic olefin copolymer	COC	1.43*10 <sup>-16</sup>	+/-
<b>Hydrogels</b>			
Water		2.55*10 <sup>-14</sup>	++
<b>Fluidic connections</b>			
Polyether ether ketone	PEEK	3.93*10 <sup>-17</sup>	-
Polytetrafluoroethylene	PTFE	1.53*10 <sup>-15</sup>	+
Fluorinated ethylene-propylene	FEP	1.02*10 <sup>-15</sup>	+
Perfluoro alkoxy alkane	PFA	1.53*10 <sup>-15</sup>	+
Ethylene tetrafluoroethylene	ETFE	1.79*10 <sup>-16</sup>	+/-
Polypropylene	PP	4.85*10 <sup>-16</sup>	+/-
Polyvinylidene chloride	PVDC	1.02*10 <sup>-19</sup>	--
Polyvinylidene fluoride	PVDF	2.81*10 <sup>-17</sup>	-



(expressed in mol m<sup>-1</sup> s<sup>-1</sup> Pa<sup>-1</sup>) is a combination of the oxygen diffusion coefficient ( $D_{O_2}$ ) and Henry's absorption coefficient ( $H_{O_2}$ ). As can be observed, PDMS has a very high oxygen

permeability, while most thermoplastics have a much lower permeability and inorganic materials and metals are (almost) impermeable to oxygen. Of these thermoplastics, PMMA has the lowest oxygen permeability. The oxygen permeability of hydrogels seems to depend largely on the water content and extent of crosslinking within the hydrogel, but it is generally slightly lower than the permeability of oxygen in water. For the fluidic connections, PEEK and ETFE show the lowest oxygen permeability and a PVDC coating could reduce the oxygen permeability of the tubing even more. [92] [93] [94] [95] [96] [97] [98] [99]

## 2.2.2 Fabrication Techniques

A number of fabrication techniques can be used to create OoC devices, depending on the used material and availability of equipment and facilities. For the fabrication of silicon and glass chips, standard lithography and etching methods are often applied in a cleanroom environment. When making microfluidic chips out of elastomers such as PDMS, soft lithography methods are usually employed (see **Figure 13a**). For this technique a mould is created using either standard photolithography with a silicon or glass substrate or using micro milling or 3D printing of thermoplastics such as PMMA, depending on the desired feature size. Once such a mould has been fabricated, a PDMS pre-polymer solution can be casted onto the mould, after which it should be degassed and cured in an oven. When the solution has polymerized, it can easily be peeled off from the mould, which can be reused multiple times. The PDMS chips can then easily be cut into the desired size and inlets can be punched for fluidic connections. Sealing of the chip is usually achieved by bonding the PDMS chips to a glass slide (coated with PDMS if necessary) via oxygen plasma exposure.

For the fabrication of thermoplastic OoC devices, various different methods can be applied depending on the quantity of chips that are required and the desired chip design. For prototyping and low-volume device fabrication, direct fabrication methods such as computer numerical controlled (CNC) milling can be used, in which computerized controls and rotating

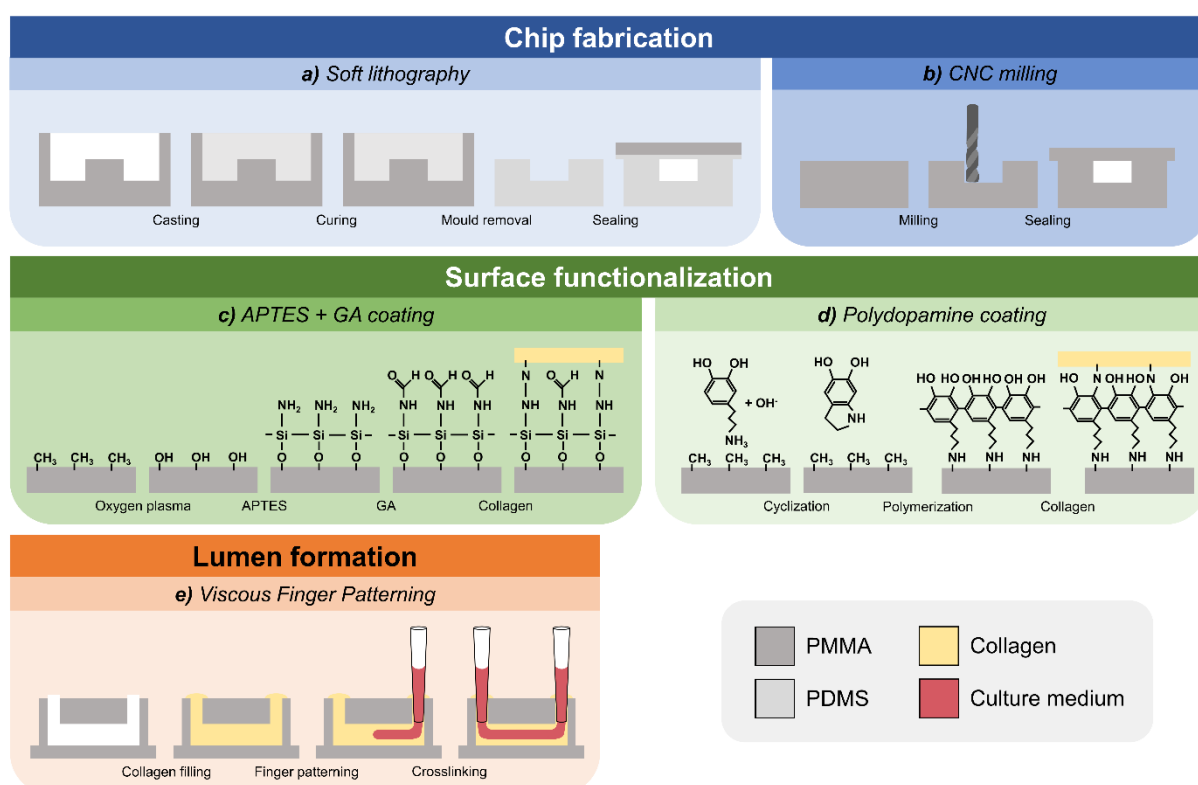


**Figure 13** Schematic overview of fabrication techniques for the creation of OoC devices. Soft lithography can be used for the fabrication of OoCs from elastomeric materials such as PDMS (a) while for thermoplastics such as PMMA, CNC milling is often employed (b). Surface functionalization can be achieved via APTES + GA coating (c) or using a PDA coating (d) to covalently bind hydrogels such as collagen to the OoC surface. Finally, lumens can be formed via VFP (e).

mill and drill bits are used to remove material from the workpiece to produce the desired chip design (see **Figure 13b**). For smaller features, laser ablation or direct lithography can be employed to remove material, and it is also possible to create thermoplastic OoCs by 3D printing. Mass production of thermoplastic chips requires different fabrication techniques such as hot embossing or injection moulding. To seal a chip made from thermoplastic material, several bonding methods can be employed such as sealing with an adhesive film, bonding to another material using double sided tape, thermal bonding, plasma bonding or solvent bonding techniques. [100] [101]

Before integration of hydrogels and cells in elastomeric or thermoplastic chips, additional surface functionalization is usually required. One example of such a coating is a layer-by-layer coating of (3-aminopropyl)triethoxy silane (APTES), glutaraldehyde (GA), and collagen to covalently bind collagen on a PDMS surface (see **Figure 13c**) [102] [103] [104]. Before this method can be applied, the chip surface needs to be treated with oxygen plasma to convert the silane groups (Si-CH<sub>3</sub>) into silanol groups (Si-OH). Next, the chips are incubated with APTES solution, which reacts with the exposed OH groups on the chip surface. After washing, the chips are exposed to GA, which in turn reacts with the amine groups of the APTES. Lastly, collagen can bind to the aldehyde groups of the GA molecules. Alternatively, polydopamine (PDA) coatings can be used to bind collagen to a chips' surface (see **Figure 13d**) [105] [106]. First, dopamine is oxidized in an alkaline environment, after which it cyclizes and polymerizes into PDA. At the same time, the dopamine/PDA molecules bind to the surface to form a PDA film. Finally, the collagen is able to bind to the OH groups of the PDA coating.

After surface functionalization, hydrogel materials can be integrated in the microfluidic chips to promote cell adhesion and better mimic the native ECM. It is for instance possible to coat the walls of the channels in a microfluidic chip with a hydrogel precursor solution such as collagen, which can bind to the channel walls and crosslink to form a collagen coating. This collagen crosslinking can be activated by changing the pH of the collagen solution towards a more alkaline environment and by increasing the temperature. Pre-patterning of the hydrogel to create a 3D hydrogel lumen is also an option, for example using a cylindrical needle which is removed after crosslinking or via VFP. VFP is a technique which makes use of the physical phenomenon where a less viscous fluid will flow through and displace a more viscous fluid, resulting in the formation of finger-like lumens in the viscous fluid, in this case the hydrogel (see **Figure 13e**). This process relies on the balance between viscous forces and the interfacial tension between the collagen solution and the displacing fluid, which in turn depend on many parameters such as the composition and viscosity of the collagen solution, temperature and timing. [44] [51] [83] [107]

### **2.2.3 Integration of Cells**

Once the microfluidic device is fabricated using the desired materials, cells need to be integrated into the system. Many different cell types and sources can be considered, but the best choice of cells largely depends on the final goal of the research and the availability of the desired cells. In general, three main cell sources can be distinguished. Firstly, cell lines can be obtained commercially from companies such as ATCC [108] or AMsBio [109]. These cell lines have extensively been validated and usually show high proliferation, maturity and reproducibility. Additionally, they have clear culture protocols and are generally easy to handle. However, since these cells have been immortalized for the creation of the cell line, their phenotype might be quite different from the primary cell types found *in vivo*. [110]

Secondly, primary cells from human donors can be used, which better mimic the phenotype as found in the mature human body. Furthermore, primary cells are able to model disease pathologies that reflect the actual clinical phenotype. However, due to genetic differences between donors and batches, variability of the cells might be an issue. Besides, primary cells are limitedly available and require specialized culture conditions to retain their phenotype. These primary cells can be obtained directly from a hospital or they can be commercially bought from companies such as Lonza [111] and PromoCell [112].

Lastly, hiPSC derived cells can be used for the 3D culture in an OoC device. Benefits of this cell source are that stem cells are theoretically indefinitely renewable and can be derived

from each individual, healthy or diseased. For OoC purposes, hiPSCs show a large potential since they would allow for personalized organ or even body models that are completely fabricated using the cells from a specific individual. Since hiPSCs can be genetically engineered to create or remove disease-specific mutations, the genetic impact of a disorder can be studied in such a system, which is not possible with the other cell sources. Given the genetic nature of some pulmonary vascular diseases like PAH, hiPSCs as a cell source are therefore of primary interest in this study. Nevertheless, hiPSCs also know several drawbacks. First of all, the creation and differentiation of these hiPSCs is lengthy and expensive compared to the ease of purchase of commercially available cells. Furthermore, hiPSCs exhibit an immature phenotype and might show limited differentiation towards specific tissues due to epigenetic memory. Lastly, differentiation and maturation protocols are not always available and are non-standardized, which could have an effect on the experimental reproducibility.

The creation of hiPSCs by reprogramming adult cells from skin or blood vessels was first demonstrated by Takahasi *et al.* in 2006 [113]. They showed that by using four specific chemical factors it is possible to induce a pluripotent stem cell phenotype in adult cells. After this reprogramming, the hiPSCs can be differentiated into a variety of cell types. For this project, differentiation into ECs, SMCs and fibroblasts is of interest, since these are the main cells residing in the vasculature. Although several different methods are available, the differentiation protocol by Orlova *et al.* [114] [115] has been used in this research to differentiate hiPSCs into ECs. By using similar methods but different chemical factors, the same group has shown to also be able to generate vascular SMCs. [11] [114] [115] [116]

Further maturation of these cells can be achieved with both chemical and mechanical factors. For example, it has been demonstrated that different concentrations of vascular endothelial growth factor (VEGF) can be used to differentiate the hiPSC derived ECs (hiPSC-ECs) into arterial or venous phenotype [10]. Furthermore, factors such as substrate stiffness and a 3D environment are thought to contribute to maturation of hiPSCs [110]. Lastly, environmental factors such as flow and an physiological oxygen tension are hypothesized to induce a phenotype that is more representative of the sPA physiology.

#### **2.2.4 Readout Methods**

After chip fabrication and integration of cells in the device, it is desired to characterize the cellular behaviour before and after applying certain stimuli such as different oxygen tensions and/or flow rates, both in 2D and 3D cell cultures. Earlier in this report, several biomarkers have been identified that can be used to characterize whether cells behave like a certain subpopulation of vascular ECs. The gene or protein expression of these biomarkers can be analysed with various assay, some of which will be discussed shortly below. Before an appropriate assay can be selected however, a few parameters need to be considered. First of all, it is important to establish whether it is desired to look at the expression on the level of DNA, mRNA or proteins. Secondly, it should be determined whether the samples are collected during the experiment, while the cells are alive, or at the end, when the cells can be fixated or lysed. [117]

For measuring at a gene level, quantitative polymerase chain reaction (qPCR) and a reporter cell line are often used. When looking into protein expression on the other hand, several other methods can be considered. For end-point protein detection, Western blotting (WB) or immunostaining can be used. With WB, the cells are lysed and loaded into a gel for electrophoretic separation of the proteins based on size. Next, the proteins are transferred onto a membrane, which is incubated with antibodies that are specific for the protein of interest. Finally, these antibodies are visualized as chemiluminescent or fluorescent bands that can be semi-quantified using image analysis. While WB shows a high sensitivity and specificity, it is an expensive and labour-intensive method. Instead, immunostaining can be used to fixate, permeate and stain the cells with target-specific antibodies that are usually fluorescently labelled. This allows for the visualization of a spatial expression pattern of a protein, which is not possible with WB. However, quantification of the protein expression is more difficult with this method. [117]

Instead of analysing the cells at the end of an experiment, it is also possible to analyse proteins in and on live cells during the experiment. Depending on the localization of the protein and the available antibodies, it is sometimes possible to perform immunostaining with live cells. Furthermore, secretion of proteins or other substances can be measured in the medium using for example a colorimetric assay or an enzyme-linked immunosorbent assay (ELISA). With a colorimetric assay, a certain reagent is added to the sample which undergoes a measurable colour change in the presence of the analyte. This colour change is proportional to the amount of analyte present in the sample, resulting in quantitative data on the secretion of the protein or substance. ELISA makes use of a similar principle, but instead a specific antibody is immobilized on a surface and is allowed to react with the sample. Next, the sample is washed away but bound proteins remain on the surface. Then, a secondary antibody that is linked to an enzyme is allowed to bind to the protein of interest. Finally, a substrate is added that is converted by the enzyme into a coloured substance or fluorescent signal. The signal strength depends on the amount of protein that has bound to the primary antibodies, thus generating quantitative data about the amount of a specific protein present in the sample. [117]

Besides investigating cellular responses by the presence or functionality of a certain protein or gene, other assays can be used to characterize the functionality of the entire cell or tissue. A permeability assay can for example be performed to determine the barrier properties of cellular monolayers. An example of such an assay is fluorescent angiography, in which a fluorescent dye is injected into a blood vessel. Over a predetermined period of time, the dye is allowed to diffuse through the blood vessel wall and into the ECM. Next, the intensity of the fluorescent signal inside and outside of the vessel is measured, which can be used to calculate the permeability coefficient of the barrier. [118] [119] [120]

## **2.3 OXYGEN CONTROL AND SENSING**

Since oxygen is thought to play an important role in vascular function and the development of vascular disease such as PAH, it is desired to study the effects of different oxygen tensions on the cellular behaviour in a 3D sPAoC model. For this purpose, an oxygen control system needs to be integrated into the existing VoC system. Such a control system usually requires two main components: an actuator and a sensor. In this section, various possible oxygen control systems will be discussed and sensing methods will be proposed for use in the 3D VoC system.

### **2.3.1 Oxygen Tension Definitions**

Before going into more detail about the state-of-the-art oxygen control systems, it is important to establish how the actual oxygen concentration or tension can be defined and measured. Most researchers state that their cell culture experiments were performed in 21% oxygen conditions. However, this percentage is only valid for dry air, which is not the case in a regular incubator, where a humidity of 90% or more is common. Besides humidity, the actual oxygen tension also depends on the atmospheric pressure. This can be seen in the fact that the percentage of oxygen is constant at different altitudes, but due to a decrease in atmospheric pressure at higher altitudes, the partial pressure of inspired oxygen is lower at higher altitudes. It is therefore often better to express the oxygen tension in terms of partial pressure. This partial pressure can be given units of Pascal, mmHg or percentages of oxygen (1% = 1013 Pa = 7.6 mmHg). When using this method to express the oxygen tension, most cells cultured in “normoxic” conditions are exposed to 141 mmHg or 18.6% oxygen, accounting for humidity, pressure and added CO<sub>2</sub>. [75] [76] [121]

While controlling the oxygen tension in the gas surrounding the cell culture is fairly easy to achieve, it might not be completely relevant since the cells do not experience the oxygen tension in the gas phase but rather the dissolved oxygen concentration in the medium. To calculate the amount of dissolved oxygen in a certain solution, Henry’s law can be used. This law states that the partial pressure of a gas in the liquid phase is equal to its partial pressure in the gas phase:

$$C_{O_2} = H * p_{O_2} \quad (1)$$

where  $C_{O_2}$  is the concentration of oxygen in the aqueous phase,  $H$  is Henry's adsorption constant ( $H = 1.3 \times 10^{-5} \text{ mol m}^{-3} \text{ Pa}^{-1}$  for oxygen in water at 298.15K) and  $p_{O_2}$  is the partial pressure of oxygen (in Pa). Thus, at 25°C and under normoxic cell culture conditions ( $p_{O_2} = 141 \text{ mmHg}$ ), this gives a dissolved oxygen concentration of around 240  $\mu\text{M}$ . When using the Henry's adsorption constant of oxygen in culture medium or blood plasma at 37°C, this concentration is even lower (177.66  $\mu\text{M}$ ). This solubility of oxygen in culture medium is very low compared to other gasses such as  $\text{CO}_2$  (1140  $\mu\text{M}$  when  $p_{\text{CO}_2} = 38 \text{ mmHg}$  (5%)). Additionally, factors like diffusion limitations and oxygen consumption by the cells ever further reduce the actual oxygen tension that is sensed by the cells. [121] [122]

In the human body, this problem of low oxygen solubility is solved by hemoglobin. This natural oxygen carrier is capable of binding four oxygen atoms at a time in a reversible manner, acting as a buffer system for oxygen. Because it is present in high concentrations (around 15 grams per 100 mL of blood) and generally has a saturation of around 97%, the total amount of oxygen in the blood is approximately 20 ml of oxygen per 100 ml of blood (equal to 6.4 M), which is much higher than the dissolved oxygen concentration of 177.66  $\mu\text{M}$ . Furthermore, the total oxygen concentration in the blood is not linearly dependent on the oxygen partial pressure, as is the case with the dissolved oxygen concentration, but instead follows a sigmoid shape due to changes in the oxygen affinity of hemoglobin at different oxygen partial pressures (see **Figure 14**). For *in vitro* situations, various methods have been developed to increase the total oxygen concentration in the medium using artificial oxygen carriers such as hemoglobin-based artificial oxygen carriers and perfluorocarbons. [7] [123] [124] [125] [126]

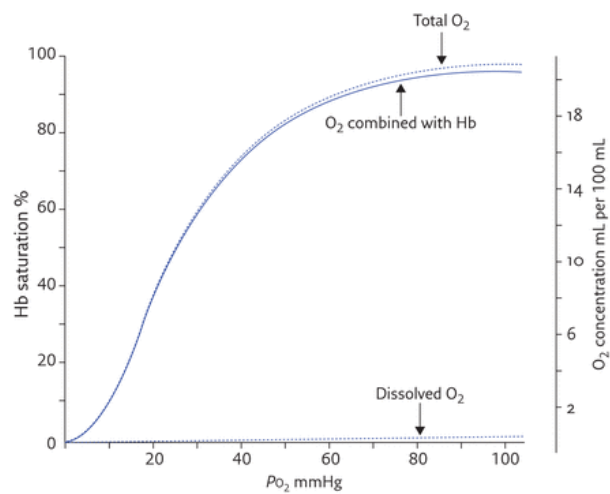


**Figure 14** Oxygen–haemoglobin dissociation curve showing that only a small percentage of the total oxygen concentration in the blood is dissolved, while most oxygen is bound to hemoglobin. From [7].

### 2.3.2 Oxygen Control Systems

A common practice to achieve a specific oxygen concentration in a cell culture is to use a hypoxic incubator. This is a sealed chamber in which the gas composition is regulated using either a pre-defined gas mixture or by introducing a certain amount of nitrogen gas to reduce the partial pressure of oxygen in the chamber. These hypoxic incubators exist in various sizes and complexities (see **Figure 15**). Larger hypoxic workstations such as the Xvivo system [15] allow for manipulation of samples in hypoxic conditions and a large amount of samples can be controlled simultaneously. However, they are bulky, expensive and are unable to create a controlled oxygen gradient which is often present in physiological environments. Smaller hypoxic chambers [22] on the other hand are much cheaper and easier to handle, but can only contain a limited amount of samples and the samples cannot be manipulated within the hypoxic environment. Lastly, advanced microenvironmental control systems are commercially available that allow for control of gas composition and temperature and that are compatible with standard microscopy setups and well plates or microfluidic devices [21]. Although these systems are easy to use, compatible with standard lab equipment and show integrated control of various microenvironmental factors, they are very expensive and often incompatible with custom-made microfluidic devices.

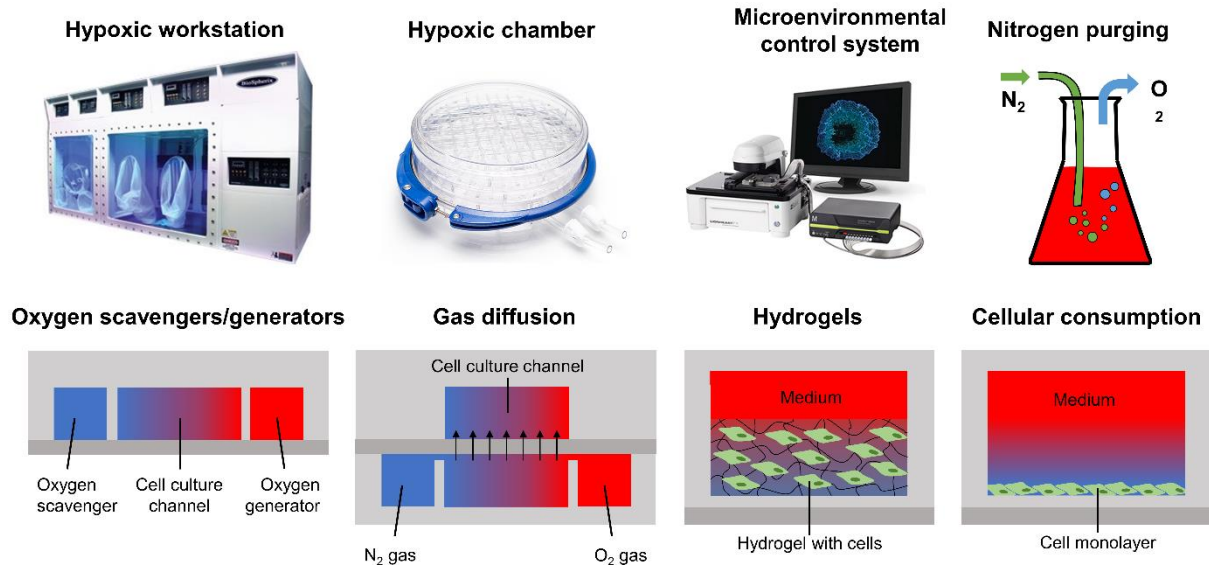


**Figure 15** Overview of various techniques for oxygen control, including hypoxic workstations, hypoxic chamber, microenvironmental control systems, nitrogen purging and the use of oxygen scavengers/ generators, oxygen diffusion, hydrogel diffusion and cellular consumption. Images based on [9] [15] [18] [19] [20] [21] [22]

An alternative possibility to expose the cells to a certain oxygen tension is by directly conditioning the medium. This conditioning can be achieved with several techniques. First of all, a hypoxic incubator can be used to condition the culture medium. However, the equilibration of an entire bottle of medium to low oxygen tension may require days, although this process can be accelerated by agitation of the medium in the incubator. A second method for removal of dissolved oxygen is purging the medium with  $N_2$  gas, but this method might cause significant foaming and protein denaturation in culture media containing fetal bovine serum (FBS) [127] [128]. Instead of purging the gas into the liquid, it is also possible to generate an oxygen tension or gradient on the chip by introducing the gas in a separate channel next to the channel used for cell culture. However, dehydration of the chip might be a problem when using gasses and little to no flow. [129] [130] [131] Similarly, a controlled oxygen tension or gradient can be achieved by using liquids preconditioned with oxygen scavengers or generators which employ chemical reactions to obtain the desired oxygen concentration.

Another process that can be used to generate a certain oxygen tension or gradient is cellular consumption of oxygen. However, this method is hard to control, since the oxygen consumption depends on the cell type, cell density and metabolic rate of the cells. Nevertheless, researchers have been able to generate an oxygen gradient along the length of the channel by controlling the flow rate and oxygen concentration in the medium entering the channels [132]. Lastly, hydrogels can be used to control the diffusion rate of oxygen into the system. By tuning the material, density and thickness of the hydrogel, oxygen gradients can be created in both 2D and 3D cell culture conditions [19] [133] [134] [135]

### 2.3.3 Oxygen Sensing

Many different factors influence the amount of oxygen that is available to the cells, including the oxygen partial pressure, the flow rates through the microchannels, diffusion rates through the gas phase, hydrogels and medium, the oxygen solubility in the medium and the oxygen consumption by the cells. Although computational modelling of such systems might give insights in the optimal flow rates and initial oxygen tensions that can be used to obtain the desired oxygen tension in the microenvironment, it is often difficult to fully predict the oxygen tension that is available to the cells. Especially the oxygen consumption rate is difficult to predict and control, since it depends on cell type, density and metabolic rates of the cells. To get a better picture of the actual oxygen concentration that the cell experience, oxygen sensors are therefore often employed in such systems. When measuring dissolved oxygen in a specific medium, either electrochemical and optical methods can be used. Here, we will focus on

optical oxygen sensing since it knows many advantages for OoC applications (see supplementary material **S1h**). [134] [136]

Optical oxygen sensing is based on fluorescent/phosphorescent quenching of dyes by oxygen [136] [137]. Since the degree of quenching is proportional to the oxygen concentration, measurements of fluorescence or phosphorescence intensity or lifetime can be used to determine the oxygen concentration. For this, the Stern-Volmer equation can be used [138] [136]:

$$\frac{I_0}{I} = \frac{\tau_0}{\tau} = 1 + K_{SV} \cdot P_{O_2} \quad (2)$$

where  $I_0$  and  $I$  are resp. the luminescent intensities in the absence and presence of oxygen,  $\tau_0$  and  $\tau$  are resp. the luminescent lifetimes in the absence and presence of oxygen,  $P_{O_2}$  is the oxygen tension in Torr and  $K_{SV}$  is the quenching constant, which determines the sensitivity of the optical oxygen sensor and is temperature dependent. Rewriting Equation (2) gives us an expression for  $P_{O_2}$  as a function of the measured fluorescence/phosphorescent intensity or lifetime:

$$P_{O_2} = \frac{I_0 - I}{K_{SV} * I} \quad (3)$$

$$P_{O_2} = \frac{\tau_0 - \tau}{K_{SV} * \tau}$$

For an ideal oxygen sensitive dye, this relationship between the oxygen tension  $P_{O_2}$  and the relative fluorescent intensity  $\frac{I_0}{I}$  or lifetime  $\frac{\tau_0}{\tau}$  is linear and can be displayed in a Stern-Volmer plot as shown in **Figure 16**. [139]

Several different molecules can be used as dye for optical oxygen sensing. Currently, most of these dyes are either ruthenium or porphyrin based metal-ligand complexes [6] [136] [137] [140] [141] [142] [143]. To improve the sensitivity, selectivity, response time and biocompatibility of these oxygen-sensitive dyes, they can be modified and/or encapsulated [144] [142] [145] [146]. Soluble dyes are easy to use but often exhibit lower sensitivity and selectivity, potential toxicity and require to be used in high concentrations, which can result in interference and aggregation of the dye [144]. By encapsulating the oxygen sensitive dyes in a film or matrix, these drawbacks can be overcome. The matrix will enable a higher sensitivity, higher signal-to-noise ratio and lower interference of the dye, while still being relatively easy to use and fabricate. By patterning the sensor film, it is possible to create sensor spots to measure at specific locations in the sample. However, the disadvantage of oxygen sensitive films is their increased response time and restriction to 2D imaging. The formulation of oxygen sensitive dyes in particles combines the advantages of both soluble dyes and sensor films. By encapsulating the dyes in small particles, they are shielded from interference and have high selectivity and lower toxicity, similarly to sensor films. However, due to their small size, they have a shorter response time and can be used for 3D

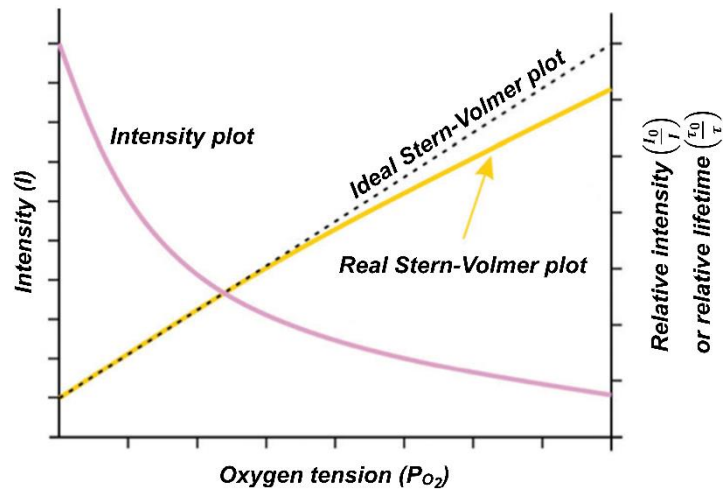


**Figure 16** Intensity plot of the quenching of luminescence intensity by oxygen, and respective Stern–Volmer plot. From [6].

be modified and/or encapsulated [144] [142] [145] [146]. Soluble dyes are easy to use but often exhibit lower sensitivity and selectivity, potential toxicity and require to be used in high concentrations, which can result in interference and aggregation of the dye [144]. By encapsulating the oxygen sensitive dyes in a film or matrix, these drawbacks can be overcome. The matrix will enable a higher sensitivity, higher signal-to-noise ratio and lower interference of the dye, while still being relatively easy to use and fabricate. By patterning the sensor film, it is possible to create sensor spots to measure at specific locations in the sample. However, the disadvantage of oxygen sensitive films is their increased response time and restriction to 2D imaging. The formulation of oxygen sensitive dyes in particles combines the advantages of both soluble dyes and sensor films. By encapsulating the dyes in small particles, they are shielded from interference and have high selectivity and lower toxicity, similarly to sensor films. However, due to their small size, they have a shorter response time and can be used for 3D

imaging, which is not possible with sensor films. Especially for oxygen sensing *in vitro* or *in vivo*, the size, charge and hydrophilicity of the particles is very important, since these parameters determine whether the particles will be taken up by the cells or not. [6] [138] [144] [147] [148]

To be able to measure the oxygen concentration using the aforementioned oxygen sensitive dyes and formulations, various different measurement techniques have been exploited. Depending on the application, it is possible to measure either the intensity or the lifetime of the dye to obtain the oxygen concentration. Although intensity measurements might be easier to implement, life-time measurements known many advantages since they are independent on the dye concentration and most optical parameters. Additionally, factors such as drift in the light source intensity and the sensitivity of the detector can be eliminated and the effect of photobleaching can often be excluded. Two main types of life-time measurements can be distinguished, namely fluorescence life-time imaging microscopy (FLIM) and phosphorescence life-time imaging microscopy (PLIM). While FLIM has very short detection times and therefore a high temporal resolution, it requires sensitive detectors and femtosecond lasers to excite the dyes in very short pulses. PLIM on the other hand is much more sensitive due to longer decay times and higher quenching constants of oxygen. This results in higher accuracy at lower oxygen concentrations, but it also takes longer to acquire the data due to the longer detection times. [6] [149] [150]

While many different solutions have been proposed in literature to measure oxygen for OoC applications, only a limited number of these sensors are commercially available. They can be divided into oxygen sensor probes, oxygen sensor films/spots and oxygen sensitive particles (see **Figure 17**). To measure the oxygen tension in the bulk medium, oxygen sensor probes are most suitable, where the oxygen sensitive dyes are integrated on the end of an optical fiber which both excites light and collects emitted light. Instead of combining the optical fiber and oxygen sensitive dye in a single probe, they can also be separated into a separate optical fiber and a sensor film or spot. Even though these oxygen sensor spots generally have a diameter in the order of millimetres, they can provide more information regarding the oxygen tension at different locations within the microfluidic channel. Lastly, oxygen sensitive particles can be used in combination with a microscope objective to obtain high spatial resolution images of the oxygen tension in the OoC system. Some examples of commercially available oxygen sensor particles are the CPOx-beads from Colibri Photonics [151], Nano<sub>2</sub> nanoparticles from Luxcel [152] and OXnano Nanoprobes from PyroScience [153]. [154] [155] [156] [157] [158] [159] [160]

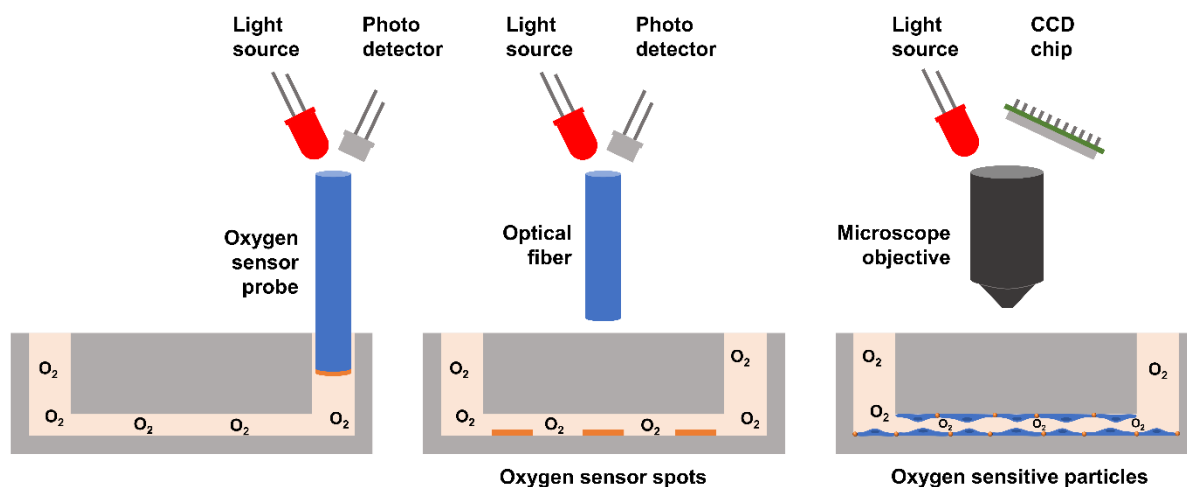


**Figure 17** Types of commercially available oxygen sensors, including oxygen sensor probes, oxygen sensor spots and oxygen sensitive particles.

## 2.4 FLOW CONTROL AND SENSING

Besides oxygen tension, it is also desired to study the effect of flow and shear stress on the behaviour of vascular cells. As earlier discussed, vascular ECs *in vivo* are continuously exposed to blood flow and shear stress, which influences their morphology and behaviour. To mimic this behaviour *in vitro*, a microfluidic chip with integrated flow control can be used. In this section, definitions of fluid, flow and shear stress will be given before possible flow control and sensing systems are discussed.

### 2.4.1 Fluid and Flow Definitions

A fluid can be regarded as either incompressible, having a constant density, or compressible, having a varying density. When the relationship between the shear stress  $\tau$  and shear rate  $\frac{\partial v}{\partial y}$  is linear, such that the fluid has a constant viscosity  $\mu$  that is only dependent on temperature, it is called a Newtonian fluid [161]:

$$\tau = \mu \frac{\partial v}{\partial y} = \frac{F}{A} \quad (4)$$

Flow is the quantity of fluid that is moved by unbalanced forces and is expressed by the volumetric flow rate  $Q$  with units of  $\text{m}^3/\text{s}$ . To induce such a flow, a pressure difference  $dP$  between the inlet and outlet of a channel can be applied, causing the fluid to flow from the area of high pressure to the area of low pressure. Laminar flow is the smooth, constant motion of fluid, where viscous forces dominate over inertial forces and the Reynolds number is less than 2000. Turbulent flow on the other hand is characterized by irregular movement and Eddies, where the inertial forces dominate over viscous forces and the Reynolds number is higher than 3000 [161]. Shear stress can be defined as the stress created when a tangential force acts on a surface and is expressed in units of Pascal or  $\text{dyne}/\text{cm}^2$  ( $10 \text{ dyn}/\text{cm}^2$  is equal to 1 Pa). When regarding biology and microfluidics, the WSS is defined as the frictional force of a (biological) fluid flow acting on cells or tissues. This WSS depends on the viscosity of the fluid and the geometry of the channel which dictates the flow profile. [48] [161]

### 2.4.2 Flow Control and Sensing

To obtain flow in a microfluidic system, various flow control systems can be considered (see **Figure 18**). The easiest method to integrate flow in microfluidic systems is by using hydrostatic pressure. Hydrostatic flow occurs due to unequal volume heights in the inlet and outlet, which generates a pressure difference between the inlet and the outlet. For example, when inserting an empty pipette tip in the outlet and a full pipette tip with 200  $\mu\text{l}$  of water in the inlet of a microfluidic chip, the water will flow from the inlet towards the outlet until both pipette tips contain 100  $\mu\text{l}$  of water. Although such a system is easy to implement, the obtained flow rate is not constant and decreases over time. To maintain flow for longer periods of time, a rocker platform can therefore be used. This platform periodically changes the height of the inlet and outlet, thereby inducing a hydrostatic pressure difference and thus a flow through the microchannel. However, this flow is still not constant and its direction alternates. Additionally, the flow rate is difficult to control and it is difficult to achieve very low or very high flow rates with this technique. [162]

Syringe pumps are most commonly used for active flow control in microfluidic systems. With such a system, two possible setups can be imagined. In a push system, the syringe is filled with liquid, connected via tubing to the chip and the liquid is pushed through the chip into a waste reservoir. On the contrary, a pull system uses a reservoir of liquid which is pulled through the chip into the syringe. The flow rate in such systems is controlled by the speed at which a motor pushes the piston of the syringe. Advantages of syringe pumps are that they are easy to use and allow for a wide range of flow rates and pressures. They also enable relative precise control of the flow rate and small volumes can be injected into the chip. However, at low flow rates stability might become an issue and syringe pumps suffer from a low responsiveness.

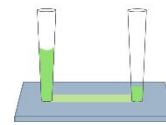
Because the system uses volumetric flow control instead of pressure control, increases in fluidic resistance due to channel clogging for example can increase the pressure and damage the device. Lastly, syringe pumps can only dispense a limited volume, which might pose problems for long term experiments. [5] [163] [164] [165] [166]

Another commonly used flow control system for microfluidic applications is a pressure controller. These operate by pressurizing a liquid containing tank, thereby forcing the liquid out of the tank and into the microfluidic device. Although pressure controllers are quite expensive and cannot operate at high pressures, they know many advantages over other flow control systems. For one, they are able to generate stable flows with high precision and high responsiveness for a large range of flow rates. Furthermore, the pressure source enables smooth, pulseless flow and large volumes can be pumped with this system. By integrating flow sensors and a feedback loop, both the pressure and the flow rate in the system can accurately be controlled. Lastly, valves can be used for fluid recirculation and multiple reservoirs can be pressurized simultaneously with only a single pressure channel for sequential solution injections. [5] [165] [166]

Finally, peristaltic pumps (also called recirculation pumps) can be used to continuously pump a liquid through a closed system. This way, an infinite amount of liquid can be dispensed in a continuous and unidirectional manner and it is possible to recirculate the same sample multiple times through the microfluidic device. However, these kind of pumping systems do not allow for precise flow control and might cause strong pulsation in the flow rate. [5]

To get more insight in the flow and shear stresses that are generated in a microfluidic system, thermal or Coriolis flow sensors can be applied. Alternatively, microparticle velocimetry or Laser Doppler Velocimetry can be employed to obtain more detailed information about the flow profile. Once the flow rate of the fluid moving through the chip is determined, the shear stress that is experienced by the cells can be estimated with computational modelling. It can also be estimated using liquid crystals or by transfecting the cells with a reporter plasmid which is transcribed in response to shear stresses. Expression of this plasmid then generates a fluorescent signal such that the measured fluorescent intensity can be corresponded to the locally experienced shear stress.

### Hydrostatic pressure



### Syringe pump



### Pressure controller



### Peristaltic pump

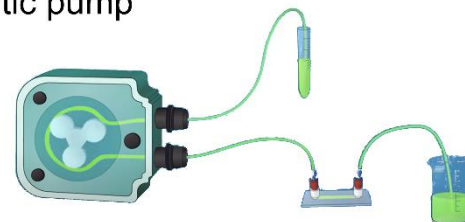


**Figure 18** Overview of various flow control systems, including peristaltic pumps, syringe pumps and pressure controllers. Adapted from [5].

## 3 PROPOSED SOLUTION

---

### 3.1 SYSTEM REQUIREMENTS

Now that more is understood about the physiology of the sPAs, characteristics of vascular cells, possible materials and methods for chip fabrication and integration of oxygen and flow control, it is possible to apply this knowledge in the design of an ideal microfluidic system that can be used to answer the main research question. However, before coming up with such an ideal design, it is necessary to determine the system requirements regarding the microfluidic device itself and the cell culture inside, but also concerning the fluidic interface and the oxygen sensing setup.

#### 3.1.1 Microfluidic Device

Regarding the microfluidic device used to model an sPA, it is important to consider the following requirements:

1. The chip dimensions should be **sufficiently small** to fit under a microscope. It is therefore desired to create a chip that is not larger than 10 x 10 cm, with a maximum height of 2 cm. These dimensions are roughly based on the size of a regular microscope slide (7.5 x 2.5 cm) and the thickness of a standard well plate (roughly 2 cm).
2. The **channel dimensions need to resemble the size of the sPAs *in vivo***, which are the vessels that are mainly affected in patients with PAH. The diameter of these vessels is in the range of 70-500  $\mu\text{m}$ .
3. It is desired to obtain a 3D model of the sPA which allows for mimicking of the physiological **3D architecture** as found *in vivo*.
4. In the initial stages of the device fabrication, the chip should be **easy to fabricate** and replicate in small batches to allow for rapid prototyping. In a later phase, it might be necessary to switch to different methods for mass-production of the devices, but this phase is not regarded yet in this thesis.
5. Regarding material properties, the chip material should be **biocompatible and optically transparent** to allow for cell culture inside the device and visualization with standard microscopes.
6. Additionally, the materials used for chip fabrication should **promote cell adhesion** and stimulate the cells to proliferate. This can for example be achieved by using a material or coating that mimics the properties of the ECM as found in the sPAs.
7. The chip material and design should allow for **control of oxygen tension on the chip** itself. The need for a hypoxic workstation or chamber is undesired because it reduces the ease-of-use of the system. The desired oxygen tensions that need to be maintained in the chip range between 1% and 20% with an accuracy of  $\pm 1\%$ .
8. Lastly, the chip design should allow for **control of the flow rate** and shear stress to obtain shear stresses that are in a physiological and pathophysiological range. In this case, a shear stress range of 0-120 dynes/cm<sup>2</sup> is preferred with an accuracy of  $\pm 5$  dynes/cm<sup>2</sup>.

#### 3.1.2 Cell Culture

For the culture of cells inside this microfluidic device, several additional requirements should be taken into account

1. To mimic the sPA as found *in vivo*, it is needed to include all important native cell types in the microfluidic model. Therefore, a **co-culture of ECs, SMCs and fibroblasts** is aspired.
2. A **sustainable cell source** is desired to ensure continuous availability of cells and reproducibility of the system. For this purpose, hiPSCs are the preferred cell type to use, also because they can be used to study the genetic impact of a disorder such as PAH in this system.

3. The phenotype of the cells in the chip should correspond as much as possible to the **cellular behaviour as observed *in vivo***. To achieve this, a high maturity of the cells should be induced, either before culture in the device or because of exposure to stimuli in the device.
4. The cells should be able to **adhere strongly** to the material inside the microfluidic device and form a structure corresponding to the **3D architecture as found in the human body**. For example, the ECs should organize into a strong monolayer on top of a multi-layered structure of SMCs to create both a barrier and contractile layer that function similar to the layers found in sPAs.

### 3.1.3 Oxygen sensing

To monitor the oxygen concentration in the sPAoC system, oxygen sensors might need to be integrated in the microfluidic device. These sensors should adhere to the following requirements:

1. **Extracellular measurements** are desired to prevent alterations in cell behaviour. This means the sensor should be biocompatible, not cytotoxic and should not be taken up by the cells. Furthermore, the sensor material should not get lost over time, for example by disintegration or erosion, and should not be flushed out by the flow of medium through the channel.
2. There should be a possibility for **3D sensing**, since the VoC is a 3D cylindrical structure. *In vivo*, the sPA is approximately 70-500  $\mu\text{m}$  in diameter and has a wall thickness of tens to hundreds of micrometers. With the oxygen sensing setup, it should be possible to measure the oxygen concentration everywhere within this vessel wall.
3. A **high resolution** sensing technique is required, allowing for measurements of oxygen across the thickness of the vessel wall. Since it is hypothesized that the oxygen concentration will change when you move further away from the medium flow, it is necessary to be able to measure oxygen close to the medium flow, as well as in areas located further away from the medium flow.
4. Since it is desired to measure the oxygen concentration throughout the duration of the experiments, the chosen measurement setup should allow for **life-cell imaging**. It is therefore undesirable if the measurement technique requires fixated or cleared samples, since this will only allow for end-point oxygen measurements.
5. In case of optical oxygen sensing, a **high penetration depth and/or adaptable focal point** is required to allow for the fluorescent/phosphorescent signal to be measured across the thickness of the vessel. Here, a sample thickness of approximately 10  $\mu\text{m}$  needs to be considered.

### 3.1.4 Fluidic Interface

To be able to connect the microfluidic device to the outside world, a fluidic interface is needed. Such an interface should meet the following requirements:

1. First of all, the fluidic interface should be easy to use and connect to the chip and it should allow for a **strong connection** to prevent leakage without damaging the device. Furthermore, dead volume should be minimized and the fluidic interface should not introduce air bubbles into the fluid channel of the chip.
2. It should be possible to actuate flow rates and corresponding **shear stresses that are in the physiological and pathophysiological range** as mentioned earlier. For this purpose, the fluidic interface should allow for the maintenance of a constant flow rate, not pressure. Since no quick changes in flow rate are needed, a fast response rate of the system is not necessary, but could be helpful when setting up the system.
3. Finally, materials used for the fluidic interface should, like the chip itself, display **limited diffusion of oxygen**. This is thought necessary, since oxygen might diffuse into the controlled chip environment through the fluidic interface if oxygen permeable materials are used.

### 3.2 EXISTING SOLUTIONS

To my knowledge, no solutions exist yet that meet up to all the previously described requirements. As of yet, there are only a very limited number of solutions that try to mimic the 3D architecture and physiological environment of the sPAs *in vitro*. Although several 3D VoC systems have been created in the size range of 70-500  $\mu\text{m}$  [13] [17] [51] [52] [167], these models do not yet mimic the physiological oxygen tensions and shear stresses as found in the sPAs *in vivo*. Only low shear stresses of up to 0.9 dyne/cm<sup>2</sup> have been generated in these 3D VoCs [13]. However, a few attempts have been made to integrate both flow control and oxygen control in other VoC systems [168] [169] [170]. These system are able to recapitulate the physiological flow and oxygen tension in the sPA and include either primary or embryonic stem cell derived ECs and SMCs. Nonetheless, they often employ 2D<sup>+</sup> cell cultures of cellular monolayers in rectangular channels instead of using a 3D hydrogel lumen to mimic the 3D ECM architecture as found in the native environment of the sPAs.

### 3.3 PROPOSED IDEAL SETUP

Since no VoC system currently exists that both recapitulates the 3D architecture of the sPA and allows for control of flow and oxygen in a physiological range, a novel, ideal setup is proposed that meets all the stated requirements and could answer the main question of this research. This setup is roughly based on the earlier described 3D hydrogel VoC system as developed by the AST group at the University of Twente [13] [17] (see **Figure 3**), where a 3D collagen lumen is fabricated in a PDMS device and lined with a monolayer of hiPSC-ECs. However, a different chip design and material is desired to allow for control of flow and oxygen tension at physiological ranges. This ideal setup and chip design can be found in **Figure 19**.

The proposed ideal chip setup consists of a PMMA chip with two compartments separated by a permeable membrane. These two compartments or channels are required to mimic the different oxygen tensions found in the blood of the sPA (5%) and the air in the alveoli adjacent

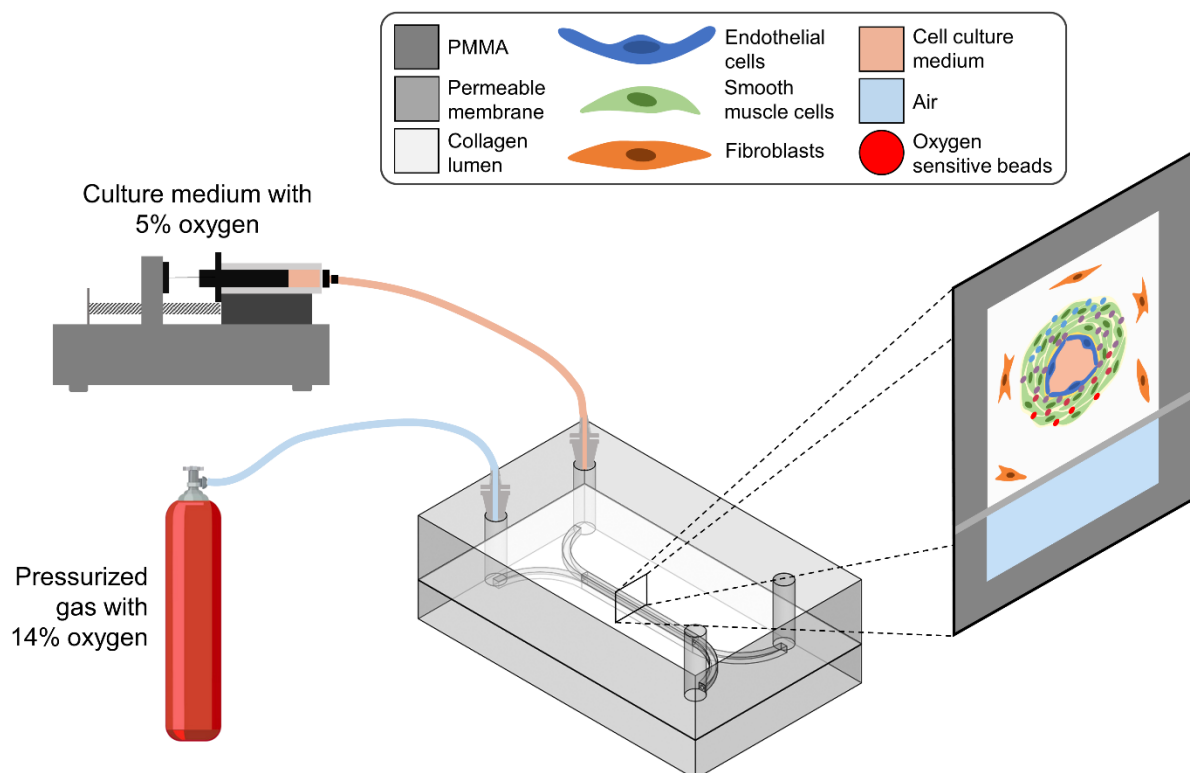


**Figure 19** Proposed ideal chip setup consisting of a PMMA chip with two compartments separated by a permeable membrane. The bottom compartment contains gas with 14% oxygen, mimicking the alveoli, while the top compartment mimics the sPA via a 3D collagen lumen lined with hiPSC derived ECs, SMCs and fibroblasts. This lumen is perfused with culture medium containing 5% oxygen at a physiological flow rate.

to the sPA (14%), which are expected to generate a gradient across the wall of the sPA. This second, alveolar compartment is thought to be critical, since it has been shown that perfusion of the pulmonary vasculature with a hypoxic solution is far less effective to generate vasoconstriction than ventilation of the airways with a hypoxic air mixture [74]. A permeable membrane is used to separate the two compartments and allow for diffusion of oxygen between both compartments. This membrane can for example be made from PDMS. PMMA was chosen for the chip material because of its low oxygen permeability (see **Table 1**), optical transparency and ease-of-use for rapid prototyping.

The channels and inlets can easily be fabricated from a slab of PMMA using CNC milling and drilling techniques. The desired channel dimensions are 500 x 500  $\mu\text{m}$  with a minimum length of 1 cm for the top channel. These dimensions correspond with the size of the sPAs *in vivo*, which are 70-500  $\mu\text{m}$  in diameter. For the bottom channel, the dimensions do not need to be exact, but 500 x 200  $\mu\text{m}$  was used for the initial design with a length equal to the length of the top channel. Inlet dimensions are designed in such a way to allow for insertion of pipette tips for lumen fabrication and cell seeding, but also for insertion of commercially available fluidic connectors needed for flow control.

After chip assembly, a 3D collagen lumen is created in the top compartment via VFP. This method has been optimized within the AST group and can be used to create a circular lumen of approximately 300  $\mu\text{m}$  in diameter inside a rectangular channel. Collagen is used since it mimics the structure of the native ECM and promotes adhesion and proliferation of cells. A collagen density of 5 mg/ml is chosen to limit invasion of the cells into the hydrogel [171]. The formed lumen is then lined with hiPSC derived ECs, SMCs and fibroblasts. hiPSC derived cells are preferred because of their sustainable availability and the possibility to create diseased sPA models to study the effect of genetic modifications on disease development of for example PAH.

After cell seeding, the lumen is perfused with culture medium containing 5% oxygen at a physiological flow rate. A syringe pump is chosen because of its ability to maintain a constant flow rate and thus a constant shear stress within the lumen. To prevent oxygen diffusion via the fluidic interface, a glass syringe is used which is filled with culture medium containing 5% oxygen at the beginning of the experiment. For tubing material, ETFE is preferred because of its optical transparency and low oxygen permeability (see **Table 1**). This tubing can then easily be connected to the chip using male Luer slip connectors, allowing for a leak-free connection without damaging the chip. The bottom compartment is at the same time perfused with a gas containing 14% oxygen, 81.5% nitrogen and 4.5%  $\text{CO}_2$  to mimic the gas mixture as found in the alveoli. Here, the same connector and tubing materials can be used, but they are then connected to a pressurized gas container instead of a syringe.

To measure the oxygen tension in this ideal chip design, CPOx-beads [151] are used. These PS beads are approximately 50  $\mu\text{m}$  in diameter and contain the oxygen-sensitive dye platinum(II) tetra pentafluoro phenyl porphyrin, which can be visualized using PLIM. Optical sensing is preferred over electrochemical sensing, since optical sensing allows for 3D extracellular measurements and there is no need for a direct connection between the chip and the readout probe. By using beads instead of spots or an immersible probe, the oxygen tension in between the cellular layers can be measured to visualize the oxygen gradient within the sPA vessel wall. Life-time imaging is preferred over intensity imaging, since it is independent on the dye concentration and shows minimal drift. PLIM is chosen as a readout method because of its high sensitivity and accuracy.

### 3.4 TIMELINE AND PLANNING

Because the presented ideal design contains many different components, cell types, mechanical factors and readout methods, a project roadmap is designed as a step-by-step guide towards this ideal design (see supplementary material **S2**). Since completion of this roadmap was not deemed feasible within the timeframe of the project (12 months), it was decided to focus only on characterization and integration of ECs in 2D and 3D culture and leave co-culture with SMCs and fibroblasts for a later time. ECs were chosen as initial cell type

since they are readily available at the AST group and have previously been integrated in the 3D oxygen permeable VoC system made from PDMS. Besides characterization of the ECs, a second focus was directed at the development of a 3D oxygen impermeable sPAoC system made from PMMA with integrated flow and oxygen control. In the following sections, the computational and experimental progress on these initial steps in stage 1 and 3 is reported and discussed.

## 4 COMPUTATIONAL MODELLING

Before fabricating the proposed sPAoC which can be used to study the effect of various oxygen tensions and flow rates on the cellular behaviour, it was decided to validate whether the proposed design theoretically allowed for control of oxygen tension and flow rates in the desired ranges. As mentioned previously, the desired oxygen range lies between 1% and 20% while the shear stresses in the channel should be controlled between 0 and 120 dynes/cm<sup>2</sup>. Additionally, it is desired to generate an oxygen gradient across the vessel wall. To study whether these conditions could be created and maintained in the proposed chip design, computational modelling in COMSOL was performed.

### 4.1 MODELLING OF FLOW CONTROL

To determine which flow rates are required to generate the desired range of shear stresses to which the ECs will be exposed, the collagen lumen inside the chips was modelled as a circular tube with a diameter of 300  $\mu\text{m}$  and a length of 1 cm. The fluid flowing through this channel (blood or culture medium) is regarded to be similar to water, with a density of 998.2 kg/m<sup>3</sup> and a dynamic viscosity of  $1 \times 10^{-3}$  Pa s at a temperature of 293.15 K. It is considered a Newtonian fluid which moves with a fully developed, incompressible laminar flow through the channel. Gravity is neglected and backflow is suppressed. The walls are thought to be impermeable and have no slip. The flow rate is varied between 0 and 2 ml/min. The result of this stationary Navier-Stokes simulation for a flow rate of 1 ml/min can be seen in **Figure 20a**.

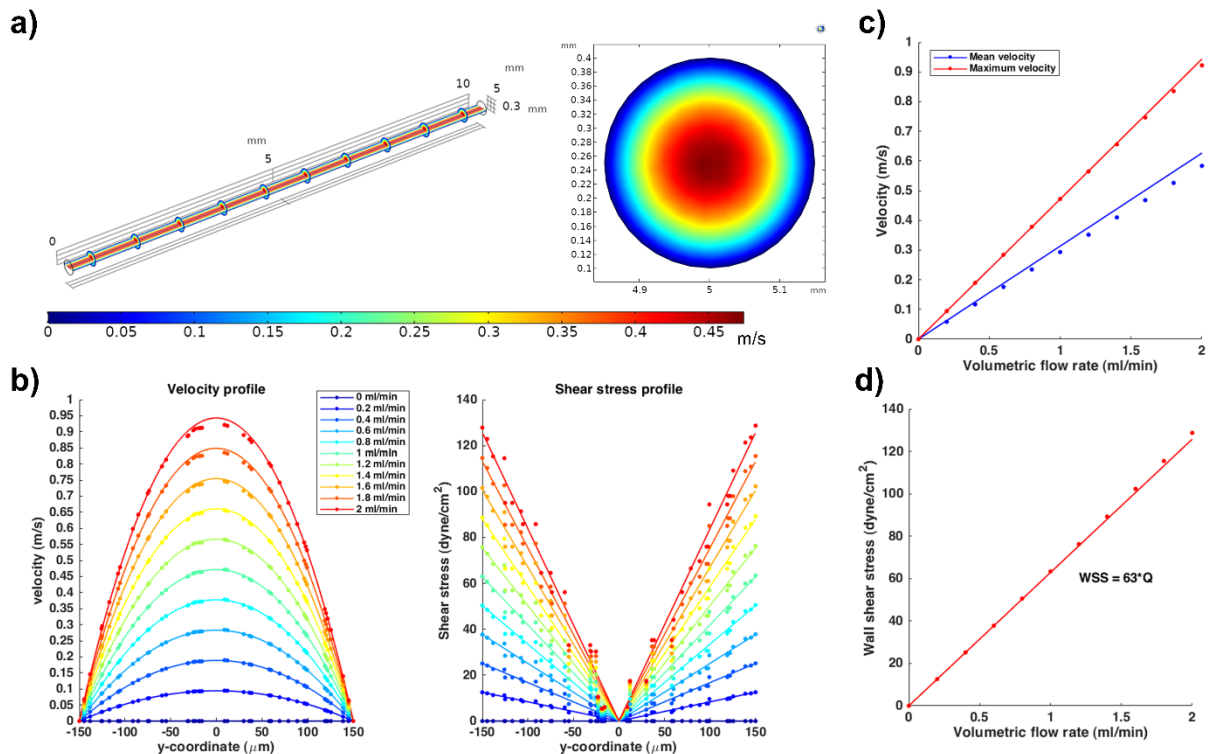


**Figure 20** a) 3D and 2D velocity profile in a cylindrical channel with a flow rate of 1 ml/min as modelled with COMSOL. b) 1D velocity profile and shear stress profile halfway a cylindrical channel for various volumetric flow rates. c) Correlation between the volumetric flow rate and the maximum and mean velocity. d) Correlation between the volumetric flow rate and wall shear stress. In b-d, dots depict results from numerical modelling with COMSOL while lines are analytically calculated with MATLAB.

In **Figure 20b**, the velocity profile for different flow rates is plotted as determined with COMSOL as well as using Equation (5), which describes the velocity profile in a circular channel:

$$v(r) = \frac{dP}{4\mu L}(R^2 - r^2) \quad (5)$$

where  $v$  gives the fluid velocity at a position  $r$  from the center of the channel,  $\mu$  is the dynamic viscosity of the fluid ( $1 \cdot 10^{-3}$  Pa s),  $L$  is the length of the channel (1 cm) and  $R$  is the radius of the channel (150  $\mu$ m).  $dP$  is the pressure difference between the inlet and the outlet of the channel, which depends on the volumetric flow rate  $Q$  according to Equation (6):

$$dP = \frac{8\mu L Q}{\pi R^4} \quad (6)$$

As can be seen, there is a good correspondence between the velocity profiles found with COMSOL and Equations (5) and (6), where a flow rate of 2 ml/min generates a maximum velocity of  $0.93 \pm 0.01$  m/s in the center of the channel. Using this flow profile, it is then possible to calculate and model the shear stress inside the channel. In COMSOL, the shear stress is calculated by multiplying the shear rate as found with the laminal flow model by the dynamic viscosity. With MATLAB, the shear stress is determined by multiplying the derivative of the flow profile with the dynamic viscosity, resulting in Equation (7):

$$\tau(r) = \frac{dP}{2L} r \quad (7)$$

The result of these shear stress calculations in COMSOL and MATLAB for a range of flow rates can also be found in **Figure 20b**. As can be seen, there is also a good correspondence between the shear stress profiles found with COMSOL and MATLAB, where a flow rate of 2 ml/min generates a wall shear stress of  $127 \pm 2$  dyne/cm<sup>2</sup>.

In **Figure 20c**, the maximum and mean velocity are plotted as a function of the volumetric flow rate. In both cases, a linear correlation is found with a minor discrepancy between the solutions found with COMSOL and MATLAB. It is thought that the COMSOL results might be slightly lower than the results found with MATLAB due to approximations in the numerical COMSOL model compared to the analytical solution as calculated with MATLAB, which are influenced by factors such as the meshing of the channel in COMSOL.

Similarly, a linear correlation is found between the volumetric flow rate and the wall shear stress (**Figure 20d**). Here, the predicted values with COMSOL are slightly higher than the values calculated with MATLAB, most likely due to the same reasons. Based on the analytical MATLAB calculations, it was found that the wall shear stress in a circular channel of 300  $\mu$ m in diameter is equal to 63 times the volumetric flow rate. With this data, it is possible to establish the desired flow rates that can be used in experiments to obtain physiological and pathophysiological shear stresses. An overview of these flow rates, velocities and shear stresses can be found in **Table 2**.

**Table 2** Required volumetric flow rates and corresponding mean and maximum velocities for different desired wall shear stresses in a 3D collagen lumen.

Desired shear stress (dyne/cm <sup>2</sup> )	Required volumetric flow rate (ml/min)	Mean velocity (m/s)	Maximum velocity (m/s)
0	0	0	0
5	0.080	0.025	0.038
20	0.318	0.100	0.150
60	0.954	0.299	0.450
90	1.431	0.449	0.675
120	1.908	0.598	0.900

## 4.2 MODELLING OF OXYGEN CONTROL

Now that it has been established that the proposed design is theoretically capable of recapitulating shear stresses in the range of 0-120 dynes/cm<sup>2</sup>, it is also of interest to see whether the same design can be used to create an oxygen gradient between the lumen and the alveoli channel. For this purpose, a COMSOL model was created simulating both laminar flow in the lumen and transport of diluted species along the length of the chip (see **Figure 21**).

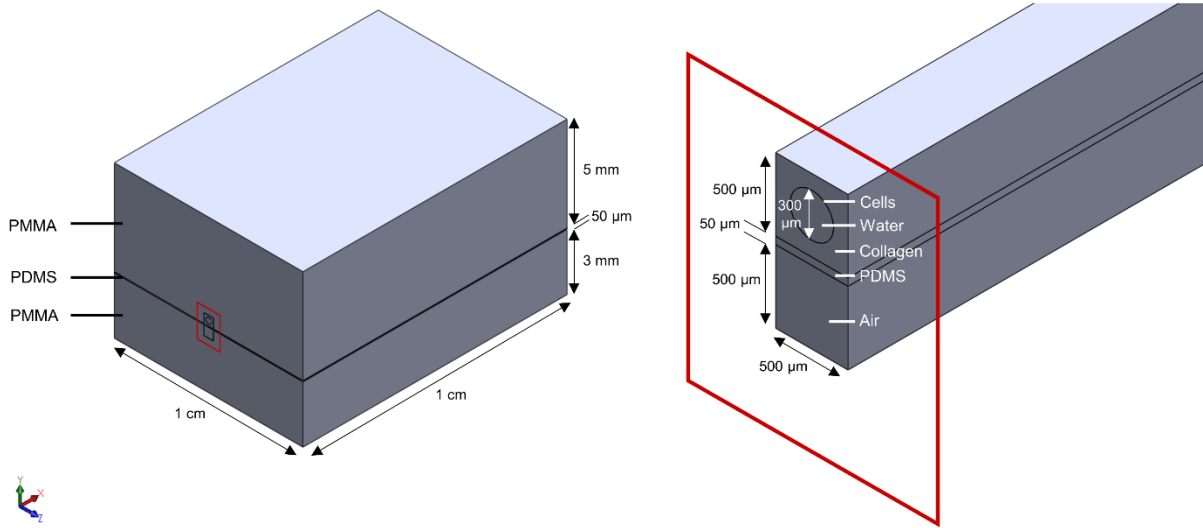


**Figure 21** 3D representation of the ideal chip design used to model the oxygen concentration within the chip with COMSOL.

To reduce computing time, oxygen transport in the chip was modelled in 2D to visualize the oxygen tension in various cross-sections. Initially, a cross-section in the x-y plane was used to determine the oxygen gradient along the length of the channel. Flow through the lumen was modelled using the same assumptions and parameters as mentioned earlier, with the only difference that a mean velocity was used as input instead of a volumetric flow rate. This mean velocity was ranged between 0 and 0.6 m/s, corresponding to a range of 0 to 2 ml/min (see **Figure 20c** and **Table 2**).

To model the oxygen transport in the chip, Fick's first and second law of diffusion were used for stationary and time dependent models respectively. Both of these laws were adjusted to account for permeability instead of solely diffusion. Equation (8) was used to relate the permeability to the diffusion coefficient, where  $P$  is the oxygen permeability coefficient (in mol m<sup>-1</sup> s<sup>-1</sup> Pa<sup>-1</sup>),  $D$  is the oxygen diffusion coefficient (in m<sup>2</sup> s<sup>-1</sup>) and  $H$  is Henry's adsorption constant (in mol m<sup>-3</sup> Pa<sup>-1</sup>) of the material [172].

$$P = DH \quad (8)$$

To relate the oxygen concentration to the oxygen tension, Henry's law was used (Equation (1)). By substituting these equations into Fick's first and second law of diffusion, the following Equations could be obtained [172]:

$$J = -P \frac{\partial p}{\partial x} \quad (9)$$

$$\frac{\partial p}{\partial t} = -D \frac{\partial^2 p}{\partial x^2} \quad (10)$$

The initial oxygen concentration in the entire chip was assumed to be equal to the oxygen concentration in the outside air (21% or 2.13\*10<sup>4</sup> Pa). The oxygen concentration in the culture

medium (approximated as water) at the inlet of the lumen is taken to be 5% ( $5.07 \cdot 10^4$  Pa). The air in the alveolar channel is assumed to flow with an average velocity of 1 m/s and have a concentration at the inlet of 14% ( $1.42 \cdot 10^4$  Pa).

In **Table 3**, the diffusion and permeability coefficients used for each material can be found. The permeability coefficients for air and collagen could not be found in literature, but were assumed to be high ( $1 \cdot 10^{-13}$  mol  $m^{-1}$   $s^{-1}$   $Pa^{-1}$ ) and equal to the permeability of water ( $2.68 \cdot 10^{-14}$  mol  $m^{-1}$   $s^{-1}$   $Pa^{-1}$ ) respectively. For the cells in the lumen, the average oxygen consumption by the cells was incorporated as a reaction with a reaction rate of  $-4 \cdot 10^{-3}$  mol  $m^{-3}$   $s^{-1}$  based on an average cell density of 1090  $kg/m^3$  [173].

**Table 3** Overview of oxygen diffusion, permeability and adsorption coefficients for various materials as used to simulate the oxygen transport in the chip with COMSOL. Values from [92] [93] [94] [95] [96] [97] [98] [99] [174] [175] [176] [177] [178] [179] [180] [181].

Material	Oxygen diffusion constant ( $m^2 s^{-1}$ )	Oxygen permeability constant (mol $m^{-1}$ $s^{-1}$ $Pa^{-1}$ )	Oxygen adsorption constant (mol $m^{-3}$ $Pa^{-1}$ )
PMMA	$3 \cdot 10^{-12}$	$3.16 \cdot 10^{-17}$	$1.05 \cdot 10^{-5}$
PDMS	$3.5 \cdot 10^{-9}$	$2.04 \cdot 10^{-14}$	$5.83 \cdot 10^{-6}$
Water	$1.9 \cdot 10^{-9}$	$2.68 \cdot 10^{-14}$	$1.41 \cdot 10^{-5}$
Air	$2 \cdot 10^{-5}$	$1 \cdot 10^{-13}$	$5 \cdot 10^{-9}$
Collagen	$3 \cdot 10^{-10}$	$2.68 \cdot 10^{-14}$	$8.93 \cdot 10^{-5}$

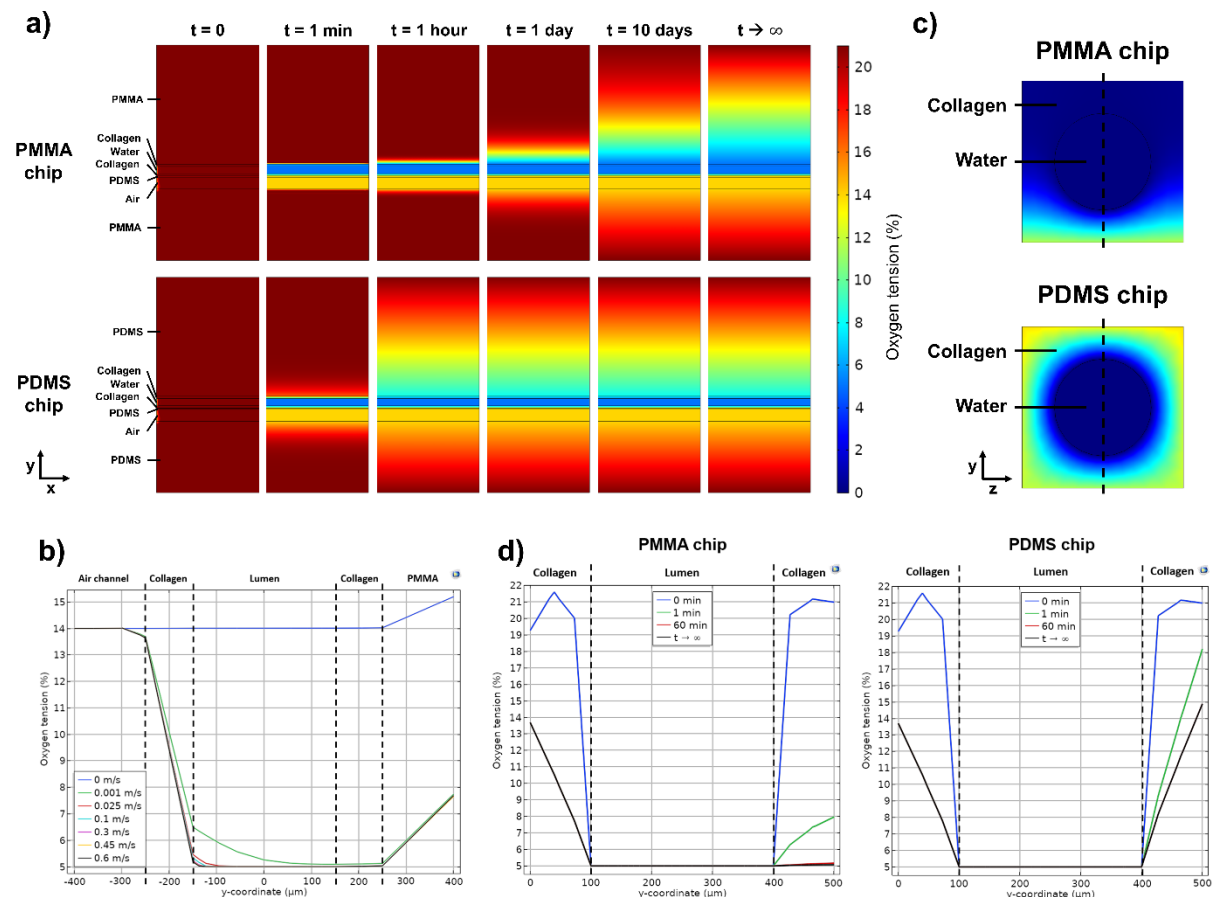


**Figure 22** a) Oxygen concentration over time in a PMMA chip (top) and PDMS chip (bottom) as viewed in the  $x$ - $y$  plane cross-section. b) Oxygen gradient across the collagen lumen inside a PMMA chip when flushing the lumen with water containing 5% oxygen for various average velocities and the air channel with 14% of oxygen gas. c) Oxygen concentration in a PMMA and PDMS chip as viewed in the  $y$ - $z$  plane cross-section. d) Oxygen gradient across the collagen lumen inside a PMMA and PDMS chip at different time points. All data was simulated with COMSOL.

In **Figure 22a**, the result of the time dependent simulation can be seen for various times after turning on the flow with a mean flow velocity of 0.3 m/s. At this flow rate, no significant differences are observed in the oxygen gradient between the beginning and end of the channel. When comparing the results of the PMMA and PDMS chips, it can be observed that equilibrium is reached much faster in a PDMS chip compared to a PMMA chip. This can be explained by the fact that the permeability and diffusion constants are much higher for PDMS compared to PMMA. Additionally, it can be seen that after 1 hour, the oxygen tension at the top edge of the lumen is still 15% in the PDMS chip, while in the PMMA chip it has already been reduced to 5% oxygen (data not shown). When looking at the oxygen gradient that is formed after 1 day in the middle of the collagen lumen using different flow rates, the graph as shown in **Figure 22b** is found. From these results, it can be concluded that a similar oxygen gradient can be generated within the chip for each of the physiological flow conditions.

In **Figure 22c**, the oxygen gradient can be observed in the lumen, but then using a cross-section in the y-z plane. Additionally, the oxygen concentration at different points in time is plotted along the height of the channel (y-direction), as can be seen in **Figure 22d**. For these simulations, a constant concentration of oxygen in the culture medium (approximated as water) and air channel is assumed, which is approximately the case for all flow velocities of interest except stationary culture. From these results it can be observed that the generated oxygen gradient differs between the PDMS and PMMA chips. In the PDMS chip, a fairly homogenous gradient is obtained that is similar in all directions, while in the PMMA chip the oxygen gradient decreases from the air channel (14%) towards the lumen (5%) and remains low on the other side of the lumen. Together, these results confirm the hypothesis that it is preferable to use a PMMA chip for oxygen control instead of PDMS to minimize effects of the oxygen tension outside of the chip on the cellular behaviour in the lumen.

### 4.3 DISCUSSION

Using the outcomes of the simulations as described above, it has been possible to estimate the flow rates that need to be used to achieve certain wall shear stresses within the collagen lumen. Furthermore, it has been shown that the chip design theoretically allows for the creation of an oxygen gradient in both PDMS and PMMA chips. However, in the PDMS chips this gradient seems to be affected more strongly by the oxygen tension in the ambient air. Nevertheless, it is important to recognise certain limitations and shortcomings of these simulations that could have an influence on the behaviour of these processes when examined experimentally.

First of all, in these simulations it is assumed that the lumen formed within the collagen is always 300  $\mu\text{m}$  in diameter, while this is often not as easy to control experimentally using the VFP method. Depending on the exact protocol, lumen diameters can vary between 200 and 400  $\mu\text{m}$  in different channels but even within the same lumen [13]. By combining Equations (6) and (7), it can be seen that the WSS ( $r = R$ ) depends strongly on the radius of the channel (see Equation (11)), where a channel that is twice as small will generate a WSS that is 8 times as large. It is therefore recommended to determine the diameter of each lumen before calculating the volumetric flow rate that is required to generate the desired physiological or pathophysiological WSS.

$$WSS = \frac{4\mu Q}{\pi R^3} \quad (11)$$

Another point of discussion is the permeability and diffusion coefficients that were used to model the oxygen gradient in the chips. These coefficients depend on the exact material and fabrication method that will be used, as well as on the temperature and pressure of the room. Especially for PDMS and collagen, the oxygen diffusion depends strongly on the degree of crosslinking of the material and the addition of cells in and on the collagen will most likely also alter the oxygen diffusion through the material. These simulations can therefore only be used

as a general indication of the gradient that will be created, but oxygen sensing is required for exact detection of the oxygen tension inside the chip.

Lastly, the oxygen consumption by the cells that was incorporated in these models is an average value, while in reality this reaction rate depends on many factors such as cell type, cell density, cellular activity and the oxygen tension surrounding the cells. For example, it was theoretically possible to generate negative oxygen concentrations during the simulations because a constant oxygen consumption rate was used, while actually this is not possible. By measuring the oxygen tension in the chips during experiments, a better approximation of the real oxygen consumption rate of the cells used in this project might be established.

## 5 EXPERIMENTAL PROGRESS

---

After validation of the proposed design *in silico*, it is possible to start with the fabrication and characterization of the sPAoC system *in vitro*. In this section, the experimental progress that was made during the time frame of this project will be discussed. In the first subsection, characterization of the hiPSC-ECs is discussed regarding their micro/macrovacular behaviour, arterial/venous behaviour, response to hypoxia and systemic/pulmonary behaviour. Secondly, the results of the chip fabrication are presented including the design process, micro milling of PMMA and VFP. Additionally, the results of initial oxygen sensing and flow experiments are demonstrated and integration of cells in the microfluidic device is shown. All protocols and scripts can be found in supplementary material **S3** and **S4**.

### 5.1 CHARACTERIZATION OF CELLULAR BEHAVIOUR

Since immature hiPSCs will be used as a preferred cell type for integration into the sPAoC, it is essential to characterize them regarding their micro/macrovacular behaviour, arterial/venous behaviour and systemic/pulmonary behaviour. Only then, when their current state is known, is it possible to determine changes in their behaviour due to the 3D environment, oxygen tension or shear stress. Since currently only hiPSC-ECs were available and these cells are in their native environment the first to experience changes in oxygen tension and shear stress, it was decided to start with characterization of the hiPSC-ECs and leave characterization and integration of hiPSC-SMCs and hiPSC derived fibroblasts for a later moment.

#### 5.1.1 Materials and Methods

##### 5.1.1.1 Cell Culture

hiPSC-ECs were differentiated using the protocol from Orlova *et al.* [115]. hPAECs (CC-2530), hMVECs (CC-2527) and human umbilical vein endothelial cells (HUVECs, C2519A) were purchased from Lonza. Cells were thawed and resuspended in culture medium. hiPSC-ECs were cultured in serum-free medium (SFM, Gibco, 11111-044) supplemented with 1% platelet-poor-derived serum (PPP, Biomedical Technologies, BT-214), 0.2 µl/ml fibroblast growth factor (bFGF, Miltenyi Biotec, 130-093-842) and 0.6 µl/ml VEGF (Miltenyi Biotec, 130-109-384). For hMVECs, endothelial cell growth medium MV 2 (EGM-MV2, PromoCell, C-22111) was used and for all other cell types, endothelial cell growth medium 2 (EGM-2, PromoCell, C-22121) was used. All culture media were supplemented with Penicillin-Streptomycin (Pen/Strep, 5,000 U/mL, Gibco, 15070063).

hiPSC-ECs were plated on culture flasks and plates coated with 0.1% gelatine (Sigma Aldrich, G1890), while other cell types were plated on 0.1 mg/ml collagen Rat tail I (Thermo Fisher, A1048301) coated culture flasks and plates. After 3-4 days, when cells were nearly confluent by visual inspection, cells were harvested using 0.05% Trypsin-EDTA (Thermo Fisher, 15400054), counted and reseeded in the appropriate culture medium on coated culture plates. Seeding densities between 5.000 and 30.000 cells/cm<sup>2</sup> were used depending on available number of cells. Cells were cultured for 2-4 days until confluent in a normoxic incubator (20% oxygen, 5% CO<sub>2</sub> and 75% N<sub>2</sub>, 90% humidity). For hypoxia experiments, cells were moved into a hypoxic incubator (Xvivo System Model X3, BioSpherix) set at 1% or 5% oxygen, 5% CO<sub>2</sub>, 94% or 90% N<sub>2</sub> and 90% humidity for the duration of the hypoxic exposure before sample collection.

##### 5.1.1.2 Immunostaining

After a monolayer was formed, culture medium was aspirated and cells were fixated with a 4 w/v% formaldehyde (37%, Sigma Aldrich, 252549) in phosphate buffered saline (PBS), washed three times with PBS and stored in PBS at 4°C until further use. Before each immunostaining, samples were incubated at room temperature for 60 minutes in a permeabilization and blocking buffer solution (PBB) containing of 0.1 v/v% Triton X-100

(Sigma Aldrich, T8787) and 1 w/v% bovine serum albumin (BSA, Sigma Aldrich, A9418) in PBS.

For VE-cadherin/F-actin staining, samples were incubated with 2 µg/ml VE-cadherin goat anti-human primary antibody (R&D Systems, AF938) in PBB over night at 4°C. Samples were washed 3 times shortly with PBS, followed by 3 washing steps of 20 minutes each and subsequently incubated with 5 µg/ml Alexa Fluor 546 donkey anti-goat secondary antibody (Thermo Fisher, A11056), 2 drops/ml ActinGreen™ 488 ReadyProbes™ reagent (Invitrogen™, R37110) and 12.5 µg/ml 4',6-Diamidino-2-Phenylindole (DAPI, Invitrogen™, D1306) in PBB for 2 hours at room temperature in the dark. Samples were washed again 3 times shortly with PBS, followed by 3 washing steps of 20 minutes each. Samples were then stored in PBS wrapped in aluminium foil at 4°C until imaging with an EVOS™ FL Auto 2 Imaging System (Thermo Scientific™, AMAFD2000).

Lectin staining was based on the protocol of Comhair *et al.* [16]. Samples were incubated with 5 µg/ml fluorescein isothiocyanate (FITC) labelled GSL (bioWORLD, 21511062-1) and/or 5 µg/ml HPA Alexa Fluor™ 647 conjugate (Invitrogen™, L32454) and 12.5 µg/ml DAPI for 1 hour at room temperature in the dark. Samples were washed 3 times shortly with PBS, followed by 3 washing steps of 20 minutes each. Samples were then stored in PBS wrapped in aluminium foil at 4°C until imaging with an EVOS™ FL Auto 2 Imaging System (Thermo Scientific™, AMAFD2000).

### 5.1.1.3 Western Blotting

Cells were exposed to either 1% or 5% normoxia for different lengths of time (t=0, 6, 12, 24 or 48 hours). 100 µM cobalt(II) chloride hexahydrate (CoCl<sub>2</sub>, Sigma Aldrich, 60818) was added as a positive control. After exposure, cells were washed with 1X PBS and lysed with lysis buffer containing 0.12M tris(hydroxymethyl)aminomethane (TRIS, pH 6.8, Millipore, 1.08382), 4 w/v% sodium dodecyl sulphate (SDS, Sigma, L3771) and 20 v/v% glycerol (Calbiochem, 356350) in milliQ supplemented with 1X Halt™ Protease Inhibitor Cocktail (Thermo Fisher Scientific, 78430). Samples were then scraped, collected and stored at -80°C until further use.

Protein quantification was performed using the DC Protein Assay (Bio-Rad, 5000112) and a BSA calibration curve according to the manufacturers instructions. Absorption was measured with a microplate spectrophotometer (Multiskan™ Go, Thermo Scientific). Next, sodium dodecyl sulphate polyacrylamide gel electrophoresis (SDS-PAGE) gel electrophoresis was executed using the Mini-PROTEAN® 3 Cell setup (Bio-Rad, 165-3301) following the manufacturers manual. An 8% running gel was used containing 25 v/v% 1.5M TRIS solution (pH 8.8), 26 v/v% 30% bis/acrylamide (Bio-Rad, #1610156), 0.1 w/v% SDS, 0.1 w/v% ammonium persulfate (APS, Sigma Aldrich, 215589) and 0.2 v/v% Tetramethyl ethylenediamine (TEMED, Sigma Aldrich, T22500) in milliQ. A 5% stacking gel was added on top containing 12.5 v/v% 1M TRIS solution (pH 6.8), 17 v/v% 30% bis/acrylamide, 0.1 w/v% SDS, 0.1 w/v% APS and 0.2 v/v% TEMED in milliQ. Samples were diluted 1:4 in Laemmli sample buffer containing 0.25M TRIS solution (pH 6.8), 10 w/v% SDS, 0.008% bromophenol blue (Bio-Rad, 1610404), 40 v/v% glycerol and 2.86M of B-mercapto ethanol (Sigma, 63689). Samples were loaded with a protein mass of 8-20 mg per lane depending on available protein concentration and run at 100V in running buffer containing 25 mM TRIS, 19.2 mM glycine (G8898, Sigma) and 3.5 mM SDS in milliQ.

Proteins were then transferred onto a PVDF membrane (Immobilon-P, Millipore, IPVH00010) in transfer buffer containing 25 mM TRIS and 19.2 mM glycine in 20% methanol in milliQ, which was run at 100V for 90 minutes at 4°C. Membranes were blocked for 1 hour at room temperature in a 5% milk (Carl Roth, T145.1) in a tris-buffered saline solution with Tween 20 (TBST, pH 6.8) containing 0.02M TRIS, 0.15M NaCl (1.06404, Supelco) and 0.005% Tween® 20 (Sigma, P7949) in milliQ. After blocking, membranes were incubated with primary antibodies for HIF-1α (0.5 µl/ml, Abcam, ab16066), HIF-2α (0.5-1 µl/ml, Abcam, ab199), β-Actin (ACTB, 0.05-0.5 µl/ml, Abcam, ab8224) or glyceraldehyde 3-phosphate dehydrogenase (GAPDH, 0.05 µl/ml, Merck Millipore, MAB374) in 5% milk in TBST over night at 4°C.

After washing 3x 5 minutes in TBST solution, membranes were incubated with horseradish peroxidase (HRP) conjugated secondary antibodies for anti-mouse (0.33 µl/ml for HIF-1α,

0.02-0.05  $\mu\text{l/ml}$  for  $\beta$ -Actin and 0.02  $\mu\text{l/ml}$  for GAPDH, Promega, W4021) or anti-rabbit (0.2-0.33  $\mu\text{l/ml}$  for HIF-2 $\alpha$ , Promega, #1706515) in 5% milk in TBST for 1 hour at room temperature. Membranes were washed 3x 10 minutes in TBST solution and 2x 2 minutes in PBS before incubation with SuperSignal™ West Pico/Femto PLUS HRP substrate (Thermo Scientific™, 34577) for 1 to 5 minutes at room temperature. Finally, membranes were imaged with FluorChem M imaging system from Protein Simple.

#### 5.1.1.4 ELISA Assay

Cells were exposed to either 1% or 5% normoxia for different lengths of time ( $t=0, 6, 12, 24$  or 48 hours). 100  $\mu\text{M}$   $\text{CoCl}_2$  was added as a positive control. After exposure, culture medium was collected and stored at  $-80^\circ\text{C}$  until further use. ET-1 content in undiluted samples was determined with an Endothelin 1 ELISA Kit (Abcam, ab133030) according to manufacturers instructions. Absorption was measured with Multiskan™ Go.

#### 5.1.1.5 Colorimetric Assay

Cells were exposed to either 1% or 5% normoxia for different lengths of time ( $t=0, 6, 12, 24$  or 48 hours). 100  $\mu\text{M}$   $\text{CoCl}_2$  was added as a positive control. After exposure, culture medium was collected and stored at  $-80^\circ\text{C}$  until further use. Before analysis, samples were deproteinized using an Amicon Ultra-0.5 Centrifugal Filter Unit (Merck Millipore, UFC5003). NO content in deproteinized, undiluted samples was determined with a Nitric Oxide Assay Kit (Colorimetric, Abcam, ab65328) according to manufacturers instructions. Absorption was measured with Multiskan™ Go.

### 5.1.2 Results and Discussion

#### 5.1.2.1 Characterization of Cell Morphology

To characterize general cell morphology, hMVECs, hiPSC-ECs and hPAECs were stained for VE-cadherin, f-actin and nuclei (see **Figure 23a**). As can be seen, hiPSC-ECs seem slightly smaller and more elongated than both hMVECs and hPAECs. Quantification using a CellProfiler™ pipeline confirms a higher cell count and lower mean cell area for hiPSC-ECs compared to hMVECS and hPAECs (see **Figure 23b**). Additionally, the mean cell eccentricity,

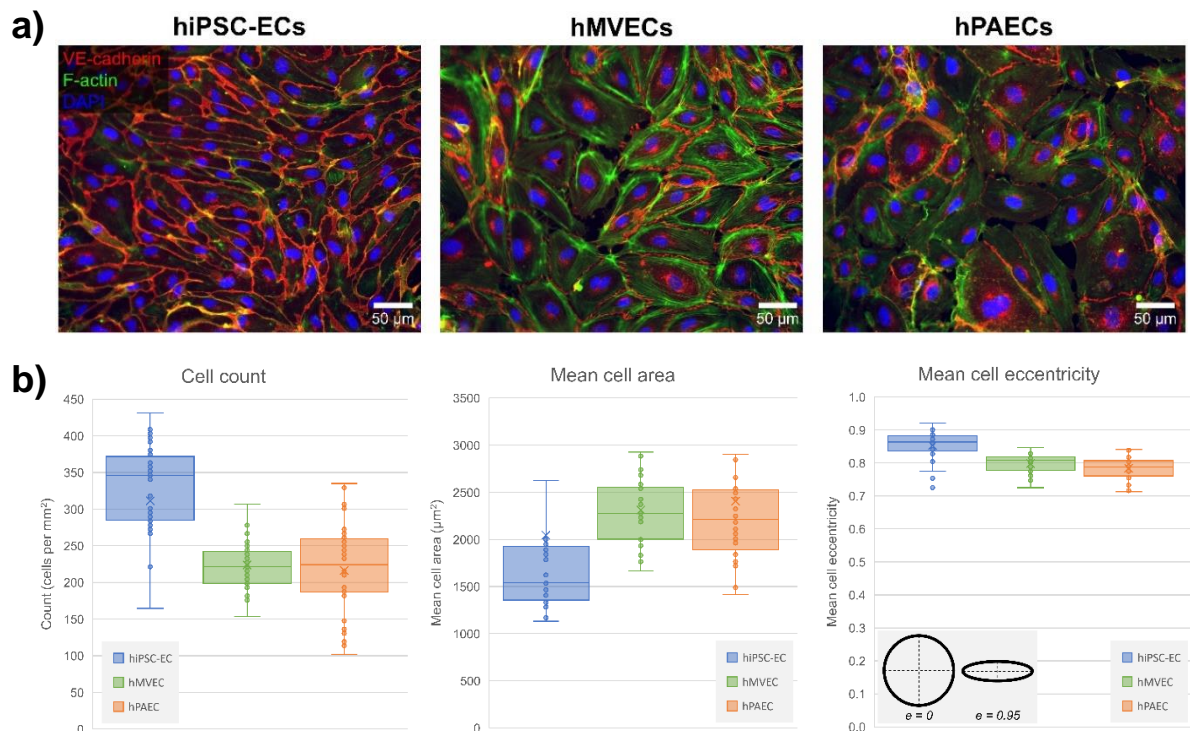


**Figure 23** a) Fluorescent images of hMVECs, hiPSC-ECs and hPAECs stained for VE-cadherin in red, F-actin in green and nuclei in blue. b) Cell count, mean cell area and mean cell eccentricity of hiPSC-ECs, hMVECs and hPAECs as determined with CellProfiler after staining for VE-cadherin, F-actin and DAPI.

which represents elongation of the cell, is slightly higher for hiPSC-ECs. F-actin filaments were most clearly visible in hMVECs, while VE-cadherin staining was found to be strongest for hiPSC-ECs. Based on these results, it was not yet possible to determine whether the hiPSC-ECs behave more like microvascular or macrovascular ECs. However, clear differences could be observed between the mature primary cells (hMVECs and hPAECs) and the immature stem cells (hiPSC-ECs).

### 5.1.2.2 Characterization of Micro/Macrovascular Behaviour

To determine whether hiPSC-ECs behave more like micro- or macrovascular ECs, binding of GSL and HPA lectins was investigated. Based on literature, GSL lectins bind to microvascular ECs from vessels smaller than 40  $\mu\text{m}$  in diameter, while HPA lectins are thought to bind to macrovascular ECs (see **Figure 7**). However, this difference could not be observed between the hMVECs and hPAECs used as a positive control in this experiment (see **Figure 24**).

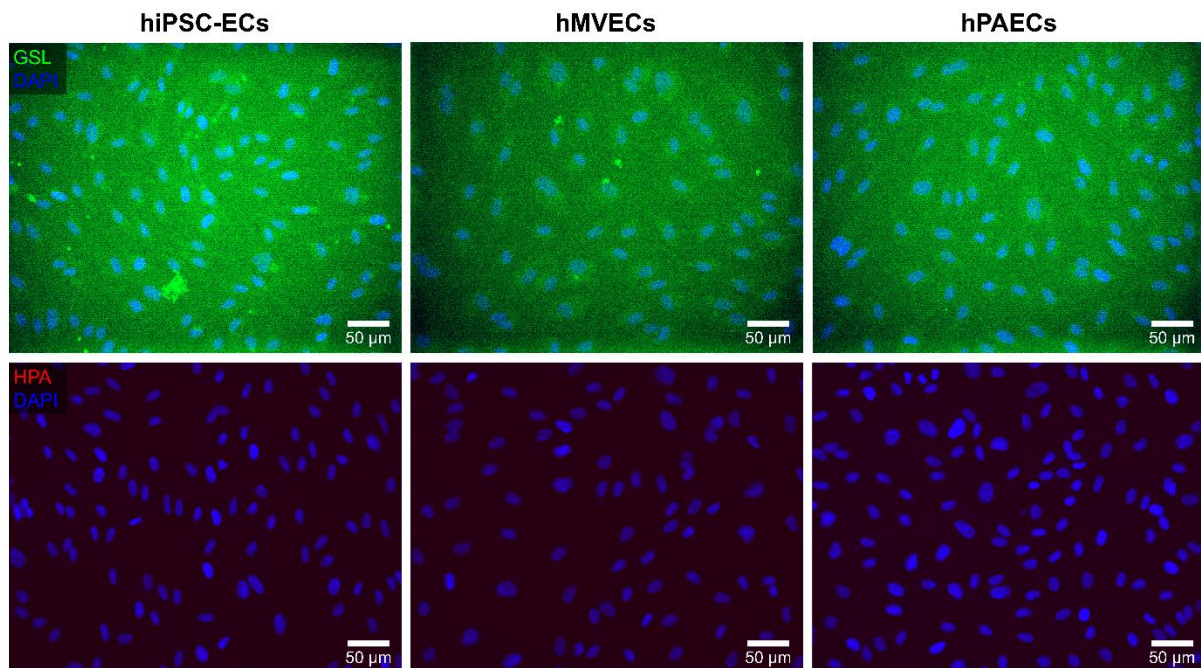


**Figure 24** Fluorescent images of hiPSC-ECs, hMVECs and hPAECs stained with GSL in green (top) or HPA in red (bottom) and nuclei in blue.

It is unclear why the intensity of the staining for both GSL and HPA was very weak. Repeating the staining protocol with a much higher concentration of lectins (1 mg/ml instead of 5  $\mu\text{g}/\text{ml}$ ) did not significantly improve the staining intensity. Alternative explanations of an unsuccessful staining could be differences in the blocking and permeabilization buffer that was used compared to literature, the amount of washing that was performed after the staining, the fluorescent lectins used or the cells that were used as control conditions.

Due to these results, it is not possible to determine whether hiPSC-ECs behave more like micro- or macrovascular ECs in 2D normoxic static culture. For next experiments, it is therefore suggested to use 2% FBS for blocking and block only for 15 minutes instead of 1 hour. Additionally, washing steps should be reduced and fluorescently labelled lectins from a different manufacturer might be tested to see what is the cause of this weak signal.

### 5.1.2.3 Characterization of Arterial/Venous Behaviour

Characterization of the arterial and venous behaviour of hiPSC-ECs can be achieved with qPCR, by looking at the expression of the arterial marker Ephrin B2 and the venous marker COUP-TFII. It was found that this experiment was already performed by Halaidych *et al.* [11] using the same differentiation protocol for the hiPSC-ECs as used in this research. In **Figure 25**, the results from this research can be seen. From these results, it can be observed that hiPSC-ECs express both venous and arterial markers, but in lower concentrations than their arterial or venous controls. It can therefore be concluded that the hiPSC-ECs are not fully arterial nor fully venous yet, but exhibit an immature phenotype after culture in a 2D normoxic, static culture.

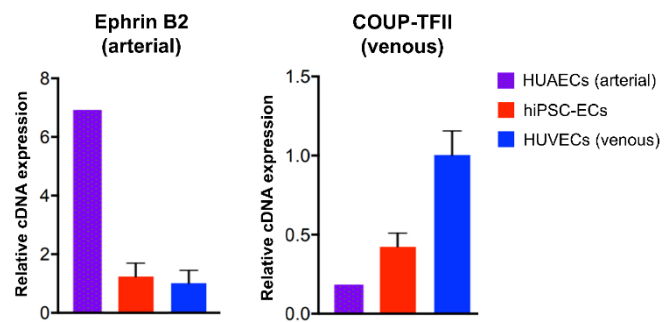


**Figure 25** Relative cDNA expression of arterial marker Ephrin B2 and venous marker COUP-TFII in hiPSC-ECs, arterial primary cells (HUAECs) and venous primary cells (HUVECs). Adapted from [11].

### 5.1.2.4 Response to Hypoxia

To determine pulmonary and systemic behaviour of the hiPSC-ECs, it is desired to quantify changes in expression of ET-1 and NO in response to hypoxia. However, it has not previously been investigated how these hiPSC-ECs respond to hypoxia in general. Therefore, expression of HIF-1 $\alpha$  and HIF-2 $\alpha$  was analysed in response to hypoxia with WB. In **Figure 26**, images of the stained membrane can be seen for three cell types exposed to different oxygen concentrations for various lengths of time. The intensity of the observed bands, which corresponds to the expression of HIF-1 $\alpha$  and HIF-2 $\alpha$ , was quantified using ImageJ.

From these results it can be observed that the expression of both HIF-1 $\alpha$  and HIF-2 $\alpha$  is higher after exposure to 1% oxygen than to 5% oxygen compared to the positive control. For all cell types, HIF-1 $\alpha$  expression seems to increase after 6 hours of exposure to hypoxia and decrease after 48 hours, which corresponds with literature [182]. Interestingly, it is observed that for all cell types HIF-2 $\alpha$  expression is high even in normoxic culture conditions, which is not expected based on literature [182]. It is unknown why this is the case for these cell types, although high HIF-2 $\alpha$  expression in normoxic conditions has been observed for certain tumor cells [183]. In hypoxic conditions, HIF-2 $\alpha$  expression seems to be fairly constant for HUVECs exposed to 5% oxygen as expected based on literature, while HIF-2 $\alpha$  expression decreases over time in hiPSC-ECs independent of the oxygen tension. For hPAECs, a peak can be observed after 6 hours of exposure to 1% oxygen after which expression decreases, while at 5% oxygen expression remains high even after 48 hours but shows significant fluctuations over time.

Based on these results, it can be concluded that hiPSC-ECs do respond to hypoxia by expression of both HIF-1 $\alpha$  and HIF-2 $\alpha$  after exposure to either 1% or 5% oxygen. The expression seems to decrease over time, which is expected for HIF-1 $\alpha$  but not for HIF-2 $\alpha$ , as this should remain elevated even after 48 hours. It is unknown why this trend is observed in these results. Similarly, it is unknown why a high expression of HIF-2 $\alpha$  is observed in normoxic conditions. However, it should be noted that these experiments were only conducted once and even after extensive optimization only a very weak expression of HIF-1 $\alpha$  could be detected. Additionally, the expression of ACTB as a housekeeping protein was not always constant for different exposure times to hypoxia, influencing the quantified results. It is therefore recommended to repeat these experiments at least two more times, preferably with an even higher primary antibody concentration for HIF-1 $\alpha$ , to validate whether the observed trends can consistently be detected. Additionally, different cell types, donors and normoxic incubators might be tested to determine whether HIF-2 $\alpha$  expression remains consistently high in normoxic conditions.

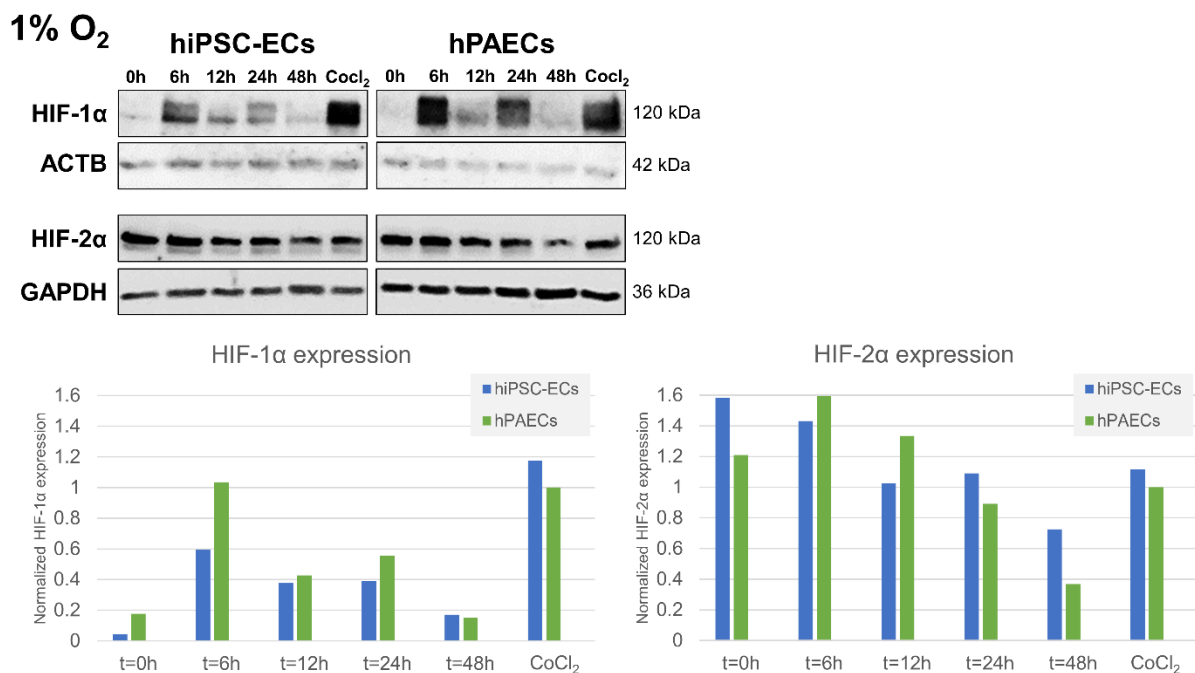
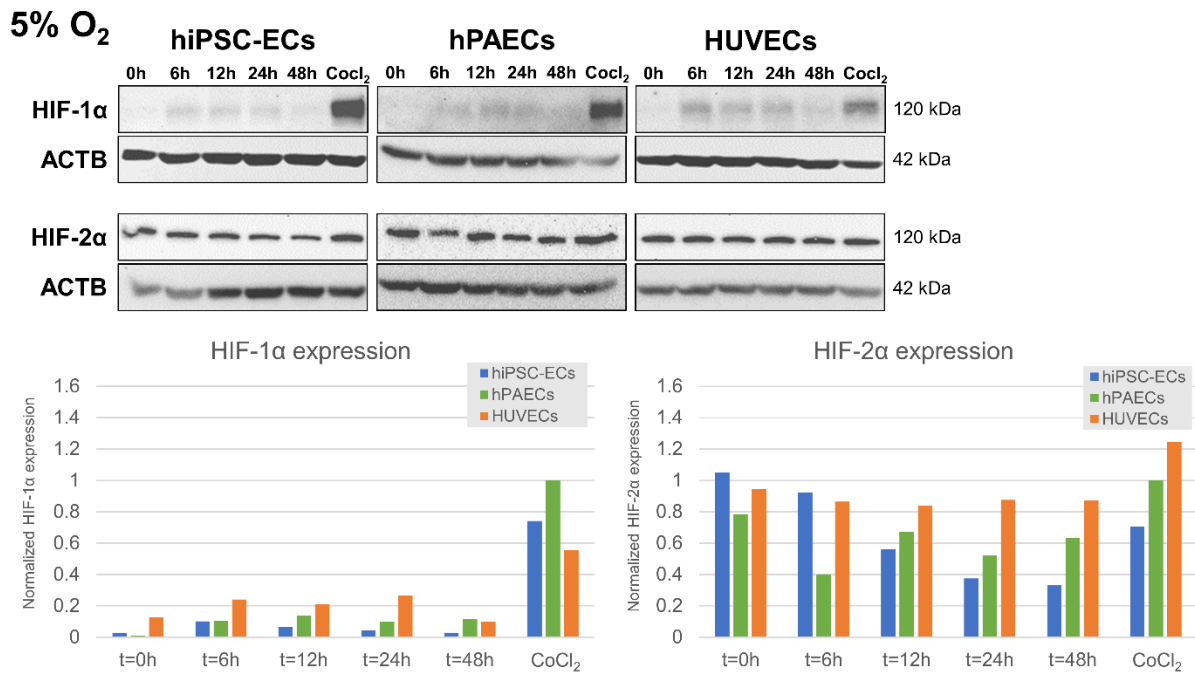


**Figure 26** WB images and quantified results of HIF-1α and HIF-2α expression in hiPSC-ECs, hPAECs and HUVECs after exposure to 1% or 5% oxygen for 0, 6, 12, 24 or 48 hours. Exposure to 100 μM CoCl<sub>2</sub> is used as positive control. Data is normalized to ACTB or GAPDH expression and CoCl<sub>2</sub> exposure in hPAECs is set to 1.

### 5.1.2.5 Characterization of Pulmonary/Systemic Behaviour

As mentioned earlier, pulmonary and systemic behaviour of the hiPSC-ECs can be investigated by quantifying changes in expression of ET-1 and NO in response to hypoxia. ET-1 concentration in culture medium of cells exposed to 5% hypoxia for different lengths of time was analysed with an ELISA assay (see **Figure 27a**). NO content in the same culture medium was determined via a colorimetric assay (see **Figure 27b**). For NO measurements, data was normalized to blank controls. For both assays, ET-1 and NO concentration in culture medium without cells was subtracted and concentration was normalized to residual culture medium volume and protein concentration to accommodate for evaporation and cell number.

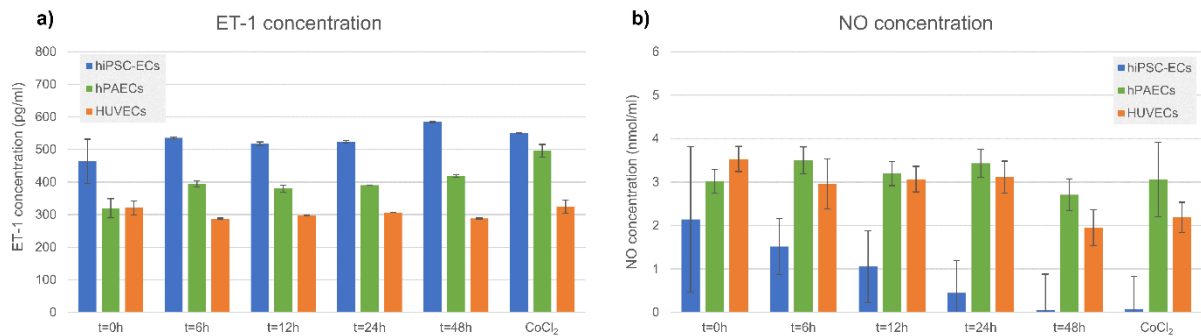


**Figure 27** a) ET-1 concentration in culture medium of cells exposed to 5% hypoxia for different lengths of time as analysed with an ELISA assay. b) NO concentration in the same culture medium as determined via a colorimetric assay. ET-1 and NO concentration in culture medium without cells was subtracted and concentration was normalized to residual culture medium volume and protein concentration to accommodate for evaporation and cell number.

From this data a slight increase of ET-1 expression can be observed for hPAECs after exposure to hypoxia as expected based on literature (see **Figure 10**), while for HUVECs a slight decrease can be seen. For hiPSC-ECs, expression of ET-1 also seems to increase due to exposure to hypoxia, indicating a pulmonary phenotype. When looking at the NO expression, a clear decrease can be observed for hiPSC-ECs, while both hPAECs and HUVECs do not show a clear trend. For hiPSC-ECs this would also suggest a pulmonary phenotype, although control cell types do not show the expected behaviour.

Nevertheless, it is very difficult to draw any conclusions from these results, since for the ET-1 assay the measured concentrations are almost 6 times as high as the highest concentration used for the calibration curve. It is therefore recommended to dilute the samples at least 10 times before repeating the assay. The measured NO concentrations on the other hand are all below the detection limit of 10 nmol/ml, which could explain the large standard deviations, especially as observed for the hiPSC-ECs. It is therefore suggested to culture cells in a lower volume of medium in next experiments and perform the colorimetric assay quickly after sample collection to prevent sample degradation. Additionally, a fluorescent assay (ab65327, Abcam) can be used instead which has a lower detection limit than the currently used colorimetric assay.

Furthermore, it is important to note that although the concentration in culture medium without cells was subtracted, observed differences might be influenced by the fact that a different culture medium was used for hiPSC-ECs compared to the other cell types. Furthermore, both culture media contained FBS in different concentrations which is known to affect ET-1 production [184]. Although it was unsuccessfully attempted to culture cells without FBS, this could be a way to reduce this effect. Lastly, HUVECs might not be the preferred cell type representing systemic ECs, since the umbilical circulation shows significant differences with the systemic circulation regarding physiological oxygen tension [185]. It is therefore recommended to use another cell type such as aortic ECs as a systemic control instead of HUVECs.

### 5.1.3 Conclusions and Recommendations

Based on general cell morphology, differences in cell number, mean cell area and mean eccentricity could be observed between immature hiPSC-ECs and mature hPAECs and hMVECs. It has not been possible to determine whether hiPSC-ECs behave more like micro- or macrovascular cells due to unsuccessful lectin staining. Issues with low intensity of fluorescently labelled lectins might be resolved by reducing blocking time, using a different buffer for blocking and permeabilization, reducing washing steps and using similar labelled lectins from a different manufacturer. From the research by Halaidych *et al.* [11] it can be concluded that the hiPSC-ECs are not fully arterial nor fully venous yet, but exhibit an immature phenotype after culture in a 2D normoxic static culture.

Response of hiPSC-ECs to hypoxia was confirmed with expression of HIF-1 $\alpha$  and HIF-2 $\alpha$ . HIF-1 $\alpha$  expression showed an increase after exposure to hypoxia, where a stronger increase

was observed after exposure to 1% oxygen compared to 5% oxygen. HIF-2 $\alpha$  expression was high in both normoxic and hypoxic conditions, but seemed to decrease with longer exposure times. To confirm these results, it is recommended to repeat these experiments at least two more times, preferably with an even higher primary antibody concentration for HIF-1 $\alpha$ , to validate whether the observed trends can consistently be detected. Additionally, different cell types, donors and normoxic incubators might be tested to determine whether HIF-2 $\alpha$  expression remains consistently high in normoxic conditions.

Expression patterns of ET-1 and NO showed a respective increase and decrease with increasing exposure times to 5% hypoxia, indicative of a pulmonary phenotype. However, because measured concentrations were outside the range that could be reliably measured with either assay, these conclusions need to be questioned. It is therefore recommended to repeat the measurements by diluting the samples for ET-1 at least 10x and use a fluorescent assay for the detection of NO in culture media.

Taken together, these results give a preliminary indication of the phenotype of the hiPSC-ECs, Nonetheless, all experiments need to be repeated multiple times before strong conclusions can be drawn. After this is achieved, the same experimental methods can be used to characterize the hiPSC-ECs in a 3D VoC model to determine the effects of 3D cell architecture, shear stress and oxygen tension on the cellular behaviour. In this way it could also be investigated whether flow and hypoxia can be used as stimuli for maturation and development of a more physiologically and/or pathophysiologically relevant sPA model.

## **5.2 CHIP FABRICATION WITH OXYGEN AND FLOW CONTROL**

Besides cellular characterization, the second aim of this project was to develop a sPAoC chip system which would allow for control of both oxygen and flow. In this section, the fabrication procedures and results of both oxygen permeable PDMS chips and oxygen impermeable PMMA chips are discussed, including collagen lumen creation. Furthermore, initial results of integration of cells, flow and oxygen sensing are presented.

### **5.2.1 Materials and Methods**

#### **5.2.1.1 PDMS Chip Fabrication**

Master-moulds for PDMS casing were designed in SolidWorks (Dassault Systèmes SolidWorks Corp.) and fabricated from PMMA using a CNC milling machine (DATRON neo). Polydimethylsiloxane (PDMS, Sylgard 184, Dow Corning) base agent was mixed 10:1 with a curing-agent and poured onto the master-mould to yield a PDMS slab with a thickness of approximately 2.5 mm. The PDMS was then degassed for at least 30 min at room temperature in a desiccator. In the mean time, glass cover slides (24 x 50 x 0.15 mm, Menzel Gläser, Fisher Scientific) were spin-coated for 30 seconds at 1500 rpm using the same PDMS mixture. Both chips and coated cover slides were then cured at 65 °C over night. After curing, the PDMS was cooled to room temperature and carefully peeled off the mould. The microfluidic chips were cut to fit the cover glasses and inlet holes were punched with a Uni-Core punch (1.0 mm, GE Healthcare). Finally, coated cover slides and chips were air plasma treated (2 min, 50 mA at 20 Pa) and contact bonded.

#### **5.2.1.2 PMMA Chip Fabrication**

PMMA chips were designed in SolidWorks (Dassault Systèmes SolidWorks Corp.) and fabricated using a CNC milling machine (DATRON neo). Chips were cut using a band saw and cleaned with pressurized air followed by ultrasonication in DI water and detergent for 10 minutes to remove all loose PMMA debris. Next, PMMA chips were rinsed subsequently in clean DI water, ethanol and IPA and dried with nitrogen gas. Cleaned chips were then secured onto a glass Petri dish cover lid using Scotch tape. Chloroform (Sigma Aldrich) was poured into a glass Petri dish until the bottom surface was covered and the cover lid with attached PMMA chips was placed on top. The lid was removed after 5 minutes and the chips were left in a fume hood over night to allow for the residual chloroform to evaporate. Finally, chips were

sealed with qPCR sealing film (Z734438, Merck) which was cut into the size of the PMMA chip and manually applied.

#### **5.2.1.3 Surface Activation**

Two different methods were used for surface activation of the chips to promote adhesion of the collagen to the chip material, namely an APTES treatment and a PDA treatment. For APTES treatment, microfluidic channels were filled with 3% (3-aminopropyl)triethoxysilane (APTES, Sigma Aldrich) in milliQ immediately after contact bonding of PDMS. For PMMA, chips were air plasma treated (2 min, 50 mA at 20 Pa) before sealing with qPCR sealing film when using this treatment. After 5 minutes, channels were rinsed with ethanol and left in fresh ethanol for at least 2 minutes to leech the remaining APTES. Chips were then one by one rinsed with ethanol, dried with nitrogen gas and channels were filled with 10% glutaraldehyde (50% GA in dH<sub>2</sub>O, Sigma Aldrich) in 1x PBS. After 5 minutes, channels were rinsed with milliQ and left in fresh milliQ for at least 30 minutes to leech all remaining GA. This step is essential, since any residual GA will affect cell viability. Finally, chips are rinsed with milliQ and ethanol, dried with nitrogen gas and stored overnight at 65 °C to evaporate any residual GA and ethanol.

For PDA treatment, a 2 mg/ml dopamine hydrochloride (Sigma Aldrich, H8502) in 10mM TRIS HCl (pH 8.5) solution was sterile filtered using a 0.2 µm filter. Channels were filled with the dopamine solution and incubated at room temperature for 1-2 hours until the solution turned black. Channels were washed 3 times thoroughly with milliQ, dried with nitrogen gas and stored at room temperature until use.

#### **5.2.1.4 Viscous Finger Patterning**

After surface activation, chips were placed in a regular incubator (18.6% O<sub>2</sub>, 5% CO<sub>2</sub>, 37 °C, humidity >90%) to equilibrate them to cell culture conditions. A master mix solution was then prepared by mixing 10x PBS + phenol red (Gibco), 1M sodium hydroxide (NaOH, Sigma Aldrich) and 0.2 µm sterilized milliQ in appropriate volumes to obtain a final collagen concentration of 5 mg/ml. Next, the master mix was carefully added to the required volume of high concentration rat tail collagen I (Corning). pH was measured and adjusted with 1M NaOH if needed to obtain a pH of approximately 7.0. The mixture was then spun down to remove air bubbles and kept on ice during the procedure. Mixed collagen was used within 1 hour.

Depending on the chip design, 10-30 µl of mixed collagen was then injected in a microfluidic channel. Immediately after, a 200 µl pipette tip (without filter), filled with 20-30 µl of DPBS (Gibco), was inserted in the inlet of the channel. When a meniscus started to form at the outlet of the channel, an empty 200 µl pipette tip (without filter) was inserted in the outlet. VFP was repeated for each channel. Chips were then incubated in a regular incubator for approximately 2 hours to allow for the collagen to start crosslinking, after which culture medium (37 °C) was added to the DPBS in the pipette tips using a gel loader pipette tip (Greiner Bio-one). The next day, when the collagen was is crosslinked, pipette tips were carefully removed from the inlets by twisting and pipette tips with fresh culture medium were inserted to keep the hydrogels hydrated until cell seeding.

#### **5.2.1.5 Cell culture**

hiPSC-ECs, hPAECs and hMVECs were cultured as described before. After 3-4 days, when cells were nearly confluent by visual inspection, cells were harvested using 0.05% Trypsin-EDTA, counted and resuspended in EGM-2 medium. Cells were then seeded in fabricated 3D VoC systems containing collagen hydrogel lumens by adding 5 µL of cell suspension (containing 5.8-7.5 \*10<sup>6</sup> cells/ml depending on available number of cells) to either inlet of each channel using a gel loader pipette tip. Chips were flipped upside down and placed in a normoxic incubator for 1 hour to allow for cell attachment to the top of the collagen lumens. Next, cell seeding was repeated and chips were placed right side up to ensure cell attachment on the bottom of the collagen lumens. Cells were cultured on a rocker platform for 2-4 days in a normoxic incubator until a monolayer was formed.

### 5.2.1.6 Permeability Assay

Fresh dextran solution was prepared by diluting 10 mg/ml 40 kDa FITC-Dextran (Invitrogen, D1845) in EGM-2 medium to obtain a 60 µg/ml FITC-dextran solution. Syringe, tubing and blunt needle were connected and flushed with ethanol. Syringe and tubing were then filled with PBS to prevent air entering the channels. Syringe was fixed in syringe pump (PHD ULTRA, Harvard Apparatus) set to withdraw liquid with a constant volumetric flow rate of 15 µl/min. The blunt needle was inserted in the outlet of the channel without introducing air and a pipette tip without filter was inserted in the inlet to function as a reservoir. The chip was then placed under a microscope and time-lapse recording was started to record every 9 seconds. After 5 images were taken, 150 µl of FITC-dextran solution was injected into the pipette tip reservoir. Images were taken for at least 5 minutes or until no significant change in intensity across the image could be observed. Protocol was repeated for each lumen. To determine apparent permeability  $P_{app}$  of the cell layer, equation (12) was used [17] [186].

$$P_{app} = \frac{1}{I_0} \frac{dI}{dt} \frac{r}{2} \quad (12)$$

Total fluorescence intensity in the chip was determined for each image using ImageJ and plotted as a function of time. It was assumed that fluorescent intensity inside the lumen remained constant during perfusion. Background intensity was established from the first 5 images and subtracted from all data. Initial intensity  $I_0$  was obtained from the time when the increase in intensity was less than  $0.01 \text{ s}^{-1}$  and the average slope  $\frac{dI}{dt}$  was calculated from this timepoint until the end of the measurement. Radius of the lumen  $r$  was measured from brightfield images.

### 5.2.1.7 Immunostaining

After a monolayer was formed, culture medium was aspirated and cells were fixated with a 4 w/v% formaldehyde in PBS<sup>++</sup>, washed three times with PBS<sup>++</sup> and stored in PBS<sup>++</sup> at 4°C until further use. Before each immunostaining, samples were incubated at room temperature for 60 minutes in PBB. Samples were incubated with 5 µg/ml VE-cadherin goat anti-human primary antibody in PBB over night at 37°C. Samples were washed 3 times shortly with PBS<sup>++</sup>, followed by 3 washing steps of 20 minutes each and subsequently incubated with 10 µg/ml Alexa Fluor 546 donkey anti-goat secondary antibody, 4 drops/ml ActinGreen<sup>TM</sup> 488 ReadyProbes<sup>TM</sup> reagent and 12.5 µg/ml DAPI in PBB for 4 hours at room temperature in the dark. Samples were washed again 3 times shortly with PBS<sup>++</sup>, followed by 3 washing steps of 20 minutes each. Samples were then stored in PBS<sup>++</sup> wrapped in aluminium foil at 4°C until imaging with a Nikon Instruments A1 Confocal Laser Microscope.

### 5.2.1.8 Integration of Flow

Syringe, tubing, blunt needle and male mini Luer fluid connectors were connected and flushed with ethanol. Syringe and tubing were then filled with PBS to prevent air entering the channels. Syringe was fixed in syringe pump set to withdraw liquid with a constant volumetric flow rate of 15 µl/min. The blunt needle or Luer connector was inserted in the outlet of the channel without introducing air and a pipette tip with 100 µl of PS microspheres (1:50 dilution) was inserted in the inlet to function as a reservoir. The chip was then placed under a microscope and a video recording was started. Protocol was repeated for each lumen.

### 5.2.1.9 Oxygen Sensing in VoC systems

Oxygen sensor spots of 400-500 µm in diameter were fabricated by the group of Torsten Mayr of Graz University [141] [147] and embedded on qPCR tape. In short, oxygen sensitive dye (platinum(II) tetraphenyl tetra benzo porphyrin) [187] was mixed with silicone rubber and PS and dissolved in chloroform to obtain a sensor “cocktail”. This “cocktail” was then deposited onto qPCR tape using a photomask as a stencil and an in-house developed computerized numerical control (CNC) air-brush spraying device. Finally, the sensor spots were cured at 60 °C for 24 hours. Sensor spots were integrated into the center of a microfluidic channel by

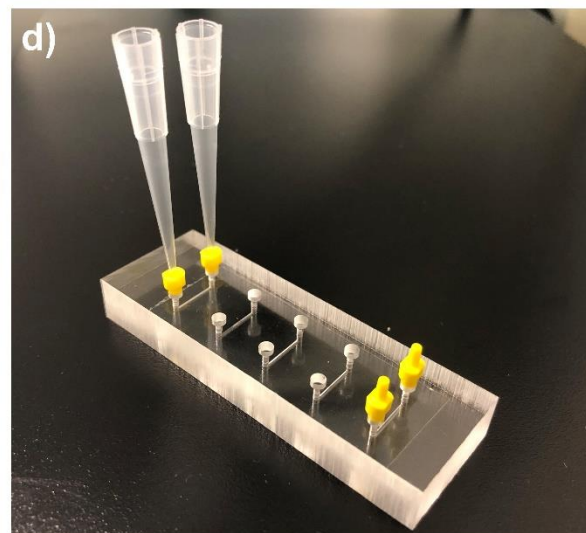
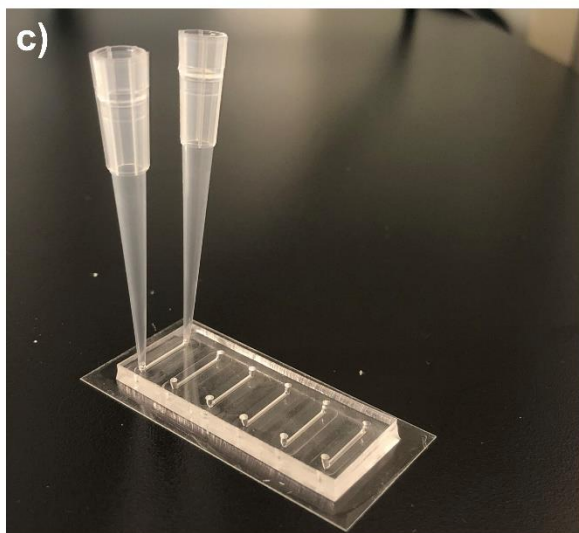
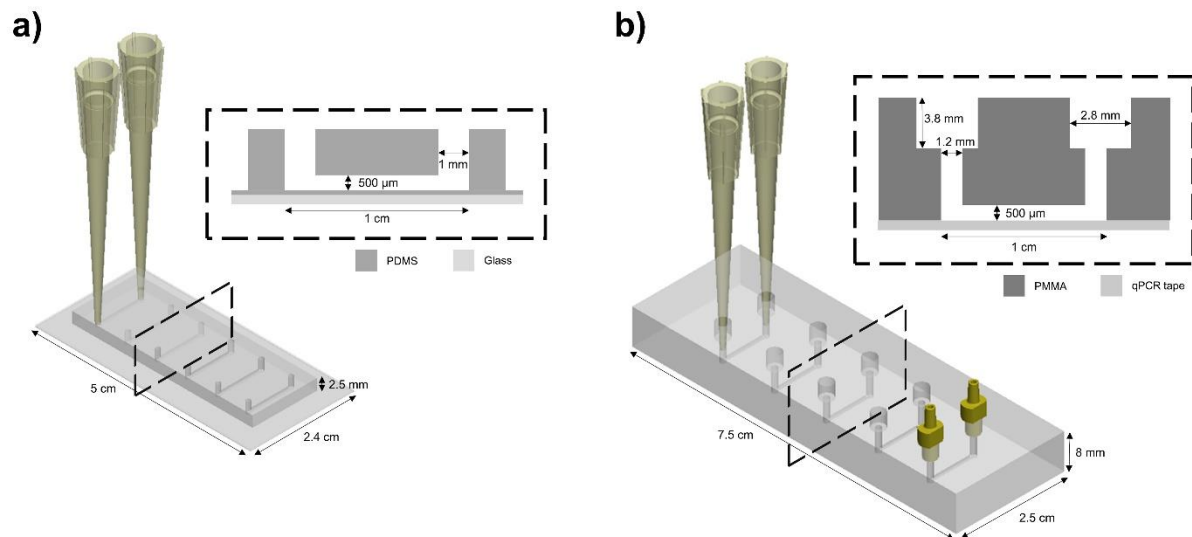
manually sealing the chips with the qPCR tape containing the sensor spots. To reduce oxygen permeability through the tape, a glass microscope slide (Fisherbrand™, 22-310397) was sealed onto the bottom of each chip using scotch tape.

Oxygen measurements were performed using the FireSting-PRO Multi-Analyte Meter (Pyroscience GmbH, FSPRO-4) in combination with 1 mm diameter optical fibers (Pyroscience GmbH, SPFIB-BARE), a 3 mm diameter oxygen probe (Pyroscience GmbH, OXROB10) and a Pt100 temperature probe (Pyroscience GmbH, TDIP15). Pressure was measured with an internal pressure sensor. Calibration of the sensor spots was performed in gas using ambient air as 100% oxygen and N<sub>2</sub> gas as 0% oxygen. Calibration of the oxygen probe was performed in ambient air for 100% oxygen and in 0.5 M sodium sulphite (Na<sub>2</sub>SO<sub>3</sub>, Sigma, 71988) in milliQ for 0% oxygen. After calibration, oxygen measurements were conducted by injecting oxygen deprived EGM-2 culture medium, as placed in an hypoxic incubator (set at 0.1% oxygen) for at least 2 days, into the channels and measuring the change of oxygen tension over time.

## 5.2.2 Results and Discussion

### 5.2.2.1 Chip Design and Fabrication

PDMS chip were fabricated based on the design as used in previous research [13]. For the fabrication of an oxygen impermeable PMMA chip, several different designs were explored. In **Figure 28a-b**, the dimensions for the final version of both chips can be found. For both chip designs, pipette tips can be inserted directly into the inlets. Blunt needles can be used for perfusion of the PDMS chips due to the flexibility of the material, but for the PMMA chips a different method was needed to connect the chip to the tubing for flow experiment. Therefore,



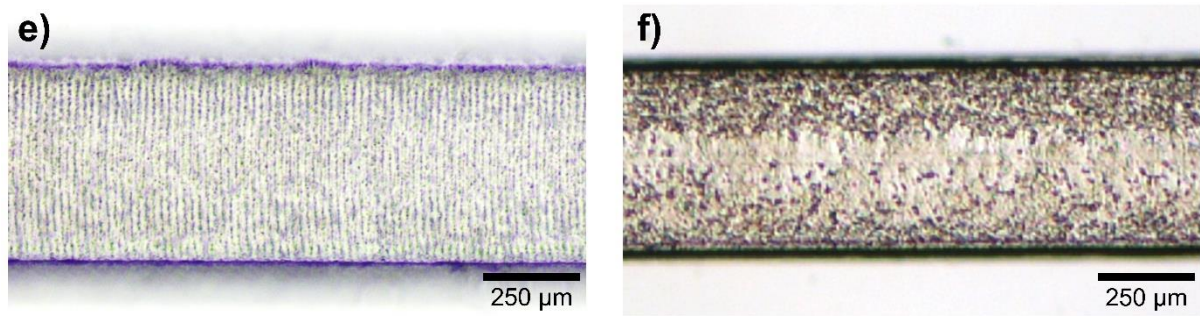


**Figure 28** Final chip designs and dimensions of a PDMS chip (a) and PMMA chip (b), as well as pictures of a fabricated PDMS chip (c) and PMMA chip (d) and microscopic images of the microfluidic channels inside the PDMS chip (e) and PMMA chip (f).

small reservoirs were added in the chip design in which male mini Luer fluid connectors (Fluidic 331, ChipShop) could be inserted to allow for application of continuous flow via tubing.

For initial experiments, it was decided to focus first on the top compartment of the PMMA chip containing the collagen lumen lined with hiPSC-ECs and disregard the second compartment mimicking the alveoli. Thus, instead of sealing the chip with a semi-permeable membrane and a second piece of PMMA containing an air channel, the chips were sealed with polyolefin qPCR sealing film which is regarded inert until pressed onto a surface. This qPCR tape was chosen since it allowed for easy integration of optical oxygen sensor spots in the channels in a later stage, which could be used for initial oxygen measurements in the microfluidic channels without the need to integrate oxygen sensor beads in between the cultured cells.

In **Figure 28c-f** images of the fabricated chips are shown as well as microscope images of the channel surface. As can be seen, the channel surface in the PDMS chips is fairly smooth and homogenous, while in the PMMA chips a lot of debris and a high surface roughness was observed. Most likely, this is caused during the micro milling process, when pieces of PMMA melt because of friction and are deposited on the channel surface. This debris caused issues later on during the VFP, especially regarding visualization of the lumens. Although small alterations in the micro milling procedure slightly reduced debris deposition, it was decided to polish the PMMA channels with chloroform vapour based on the protocol by Ogilvie *et al.* [188] to improve visibility and transparency of the channels.

Chloroform vapour polishing was optimized by varying the time during which the PMMA channels were exposed to chloroform vapour from 1 to 10 minutes (see **Figure 29a**). Surface roughness was quantified with a MATLAB script where for each image the percentage of pixels above a threshold was determined (**Figure 29b**). From these results it can be observed that 5 minutes of exposure to chloroform vapour yields the lowest surface roughness and was therefore used in following experiments. No significant modifications in channel geometry were observed after exposure to chloroform vapour for 5 minutes.

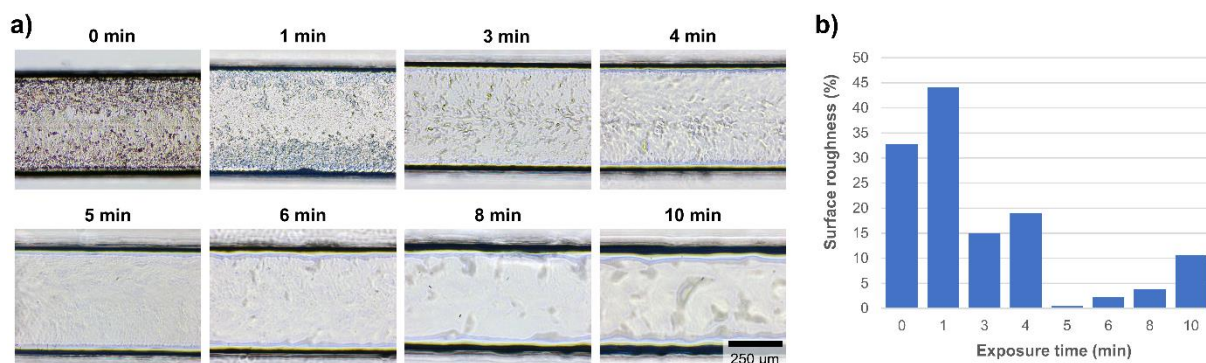


**Figure 29** a) Microscope images and b) surface roughness quantification with MATLAB of microfluidic channels in PMMA chips polished with chloroform vapour for different lengths of time.

### 5.2.2.2 Collagen Lumen Fabrication

After chip fabrication and polishing, collagen lumens were fabricated in the chips using VFP. In **Figure 30a**, the process of VFP in a PDMS chip is visualized using red food dye in PBS as a liquid displacing the collagen inside the channel. In the last image, a lumen fabricated with PBS is perfused with red food dye for visualization. In these images, a clear lumen can be observed inside the channel filled with collagen.

When attempting to perform the same protocol in the PMMA chips, bubble formation was encountered which affected the lumen formation (see **Figure 30b**). Various methods were explored to reduce bubble formation, including more careful sealing of the channels with qPCR tape, different methods of VFP, switching to a fresh batch of collagen, spinning down the collagen mixture for a longer time and changing the temperature and liquid used for lumen formation. Although some of these methods did seem to reduce bubble formation, none of them seemed to consistently prevent bubble formation in the channels. It was therefore hypothesized that the bubbles may be formed due to air pockets at the interface between the PMMA chip and the qPCR tape, as the chloroform vapour polishing might have slightly rounded the edges of the channel.

To overcome this problem, it was suggested to prefill the channels with another liquid before injecting the collagen mixture to fill up the air pockets and prevent bubble formation. For this to work, a liquid with a high wetting ability and thus a low contact angle is preferred. Various liquids were investigated including water, PBS, ethanol and 10% SDS in water. Images were taken immediately after lumen formation and after crosslinking for 2 or 24 hours to monitor bubble growth. In **Figure 30b**, an example can be seen of a lumen formed after prefilling the channel with ethanol, which clearly reduced bubble formation compared to the situation without prefilling.

Bubble formation was quantified from the obtained images using edge detection with MATLAB (see **Figure 30c**). From this data, it can be seen that prefilling with either ethanol or 10% SDS seems to significantly reduce bubble formation in the lumens, while prefilling with water or PBS still results in bubble formation as seen without prefilling. This can possibly be explained by the fact that both ethanol and a 10% SDS solution are liquids with a high wettability, thereby being able to fill all air pockets in the channel, while water and PBS have a lower wettability on PMMA and are unable to fill all air pockets. However, both ethanol and

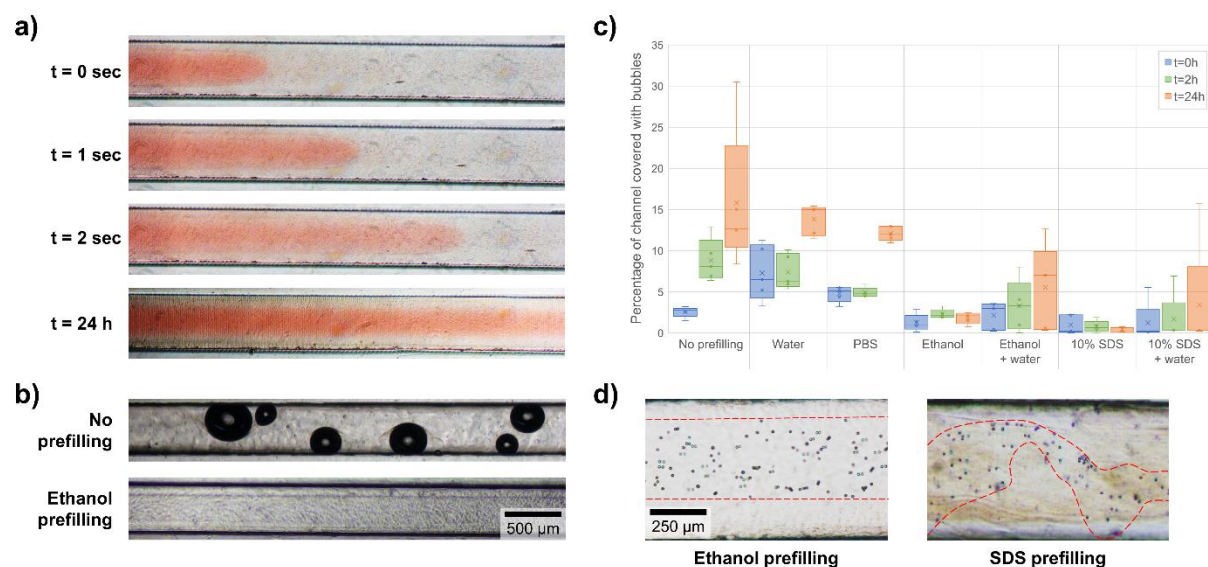


**Figure 30** a) Process of VFP in PDMS chips as visualized with red food dye. For the top three images, red food dye in PBS was used to create the lumen. For the bottom image, a lumen was formed with PBS and after collagen crosslinking for 24 hours the lumen was perfused with red food dye. b) Collagen lumens formed in PMMA chips without prefilling and after prefilling the channels with ethanol. c) Quantification of bubble formation in PMMA channels pre-filled with different liquids immediately after lumen formation and after crosslinking for 2 and 24 hours. d) Collagen lumens in PMMA chips as visualized with PS beads after prefilling with ethanol or 10% SDS in water. Red dotted lines are drawn manually to indicate the edges of the formed lumens.

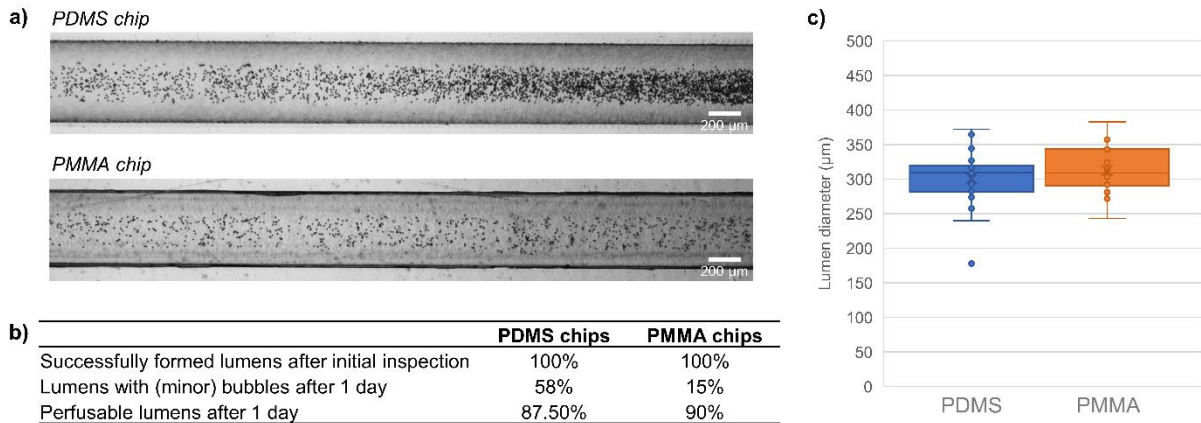


**Figure 31** a) Images of collagen lumens formed in PDMS and PMMA chips and perfused with PS beads. b) Success rates of lumen formation immediately after formation and after crosslinking for 1 day, as well as the percentage of lumens with bubbles before perfusion in PDMS chips ( $n=24$ ) and PMMA chips ( $n=20$ ). c). Average lumen diameter of lumens formed in PDMS ( $n=21$ ) and PMMA chips ( $n=18$ ).

10% SDS solutions might have a negative effect on the lumen formation and cell viability [189] [190]. Therefore, it was attempted to wash the lumens with water after prefilling with ethanol or 10% SDS. However, this seemed to increase the amount of bubbles formed in some channels.

When investigating the lumens formed in channels prefilled with either ethanol or 10% SDS by flushing them with 10  $\mu\text{m}$  PS microspheres (PolyScience), it was observed that with ethanol prefilling straight lumens could be obtained while with the 10% SDS prefilling the lumens seemed much more irregular (see **Figure 30d**). This might be because the surfactants in the 10% SDS solution influence the balance in surface tension that is needed to form a nice and straight lumen with the VFP technique. Thus, it was decided to use prefilling with ethanol in further experiments. To remove residual ethanol, lumens were perfused with water and culture medium before cell seeding.

Once a successful protocol was established for lumen formation in the PMMA chips, the formed lumens were quantified regarding the success rate of fabrication and their diameter and compared to lumens formed in PDMS chips (see **Figure 31**). From this data, it can be seen that in both chip materials, a success rate of 100% could be achieved immediately after lumen formation ( $n=24/20$ ). However, after 1 day of crosslinking in a normoxic incubator, bubbles were formed in 58% of the lumens in the PDMS chips and 15% of the lumens in the PMMA chips. Nevertheless, most of these bubbles could be removed and eventually 87.5% of the lumens formed in the PDMS chips could be perfused with PS microspheres compared to 90% in the PMMA chips. These success rates indicate that a protocol has successfully been established for the formation of lumens in the PMMA chips with a success rate comparable to that achieved in PDMS chips. When manually analysing the diameter of the formed lumens after crosslinking and perfusion with PS microspheres using a MATLAB script, an average diameter of  $301 \pm 40 \mu\text{m}$  was found for the PDMS chips and for the PMMA chips this was  $313 \pm 34 \mu\text{m}$  (**Figure 31c**). Based on these numbers it can be concluded that similar lumens can be formed in PDMS and PMMA chips.

To characterize lumen formation in 3D, optical coherence tomography (OCT) was used. In **Figure 32**, a cross-section of a collagen lumen formed in a PMMA chip after prefilling with ethanol is shown. From this image it can be seen that a cylindrical lumen is successfully formed in the PMMA chip. However, the lumen is not perfectly circular but has a height of approximately 325  $\mu\text{m}$  and

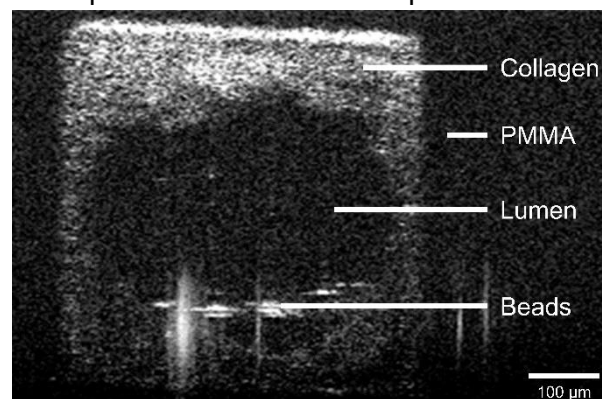


**Figure 32** OCT image of collagen lumen in PMMA chip.

a width of 440  $\mu\text{m}$ . It is unknown why the lumen does not have a circular cross-section, but since only a small part of a single channel was imaged, no conclusions can be drawn from this data about the general shape and size of the lumens formed in the channels.

### 5.2.2.3 Integration of hiPSC-ECs in Oxygen Permeable PDMS Chips

Once 3D collagen lumens could successfully be created in both oxygen permeable and impermeable chips, the next step would be integration of vascular cell into these systems. First, hiPSC-ECs, hMVECs and hPAECs were integrated in the oxygen permeable PDMS chips. In **Figure 33**, brightfield images of hMVECs cultured in such an oxygen permeable PDMS VoC system with collagen lumen can be seen directly after cell seeding and after 24 hours of culture in a normoxic incubator. From these images a lumen can clearly be observed and an increase in cell coverage is observed after 24 hours of culture, resulting in the formation of a monolayer inside the lumen. Similar results were observed for hPAECs and hiPSC-ECs (data not shown).

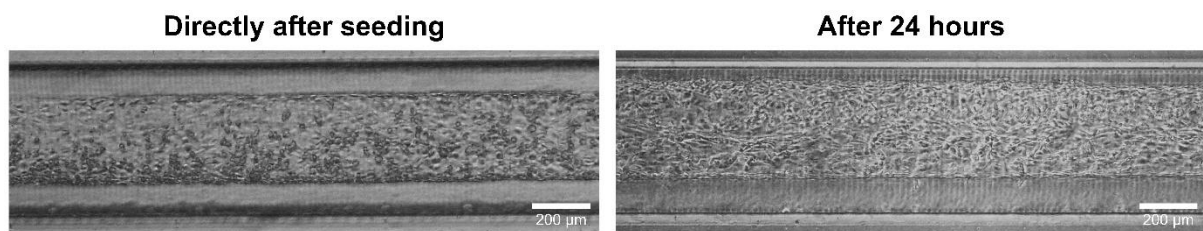


**Figure 33** Images of hMVECs cultured in oxygen permeable PDMS VoC system with collagen lumen directly after cell seeding (left) and after 24 hours of culture in normoxic incubator (right).

After cell culture for 2 days, a permeability assay was performed to determine the integrity of the vessel wall. In **Figure 34**, the results of this assay can be found. **Figure 34a** shows an example of a fluorescent overlay image of FITC-Dextran in a hPAEC lumen, which was used to determine the total fluorescence intensity in the channel as a function of time (see **Figure 34b**). Although in this example a clear jump is visible after injection of FITC-dextran as is

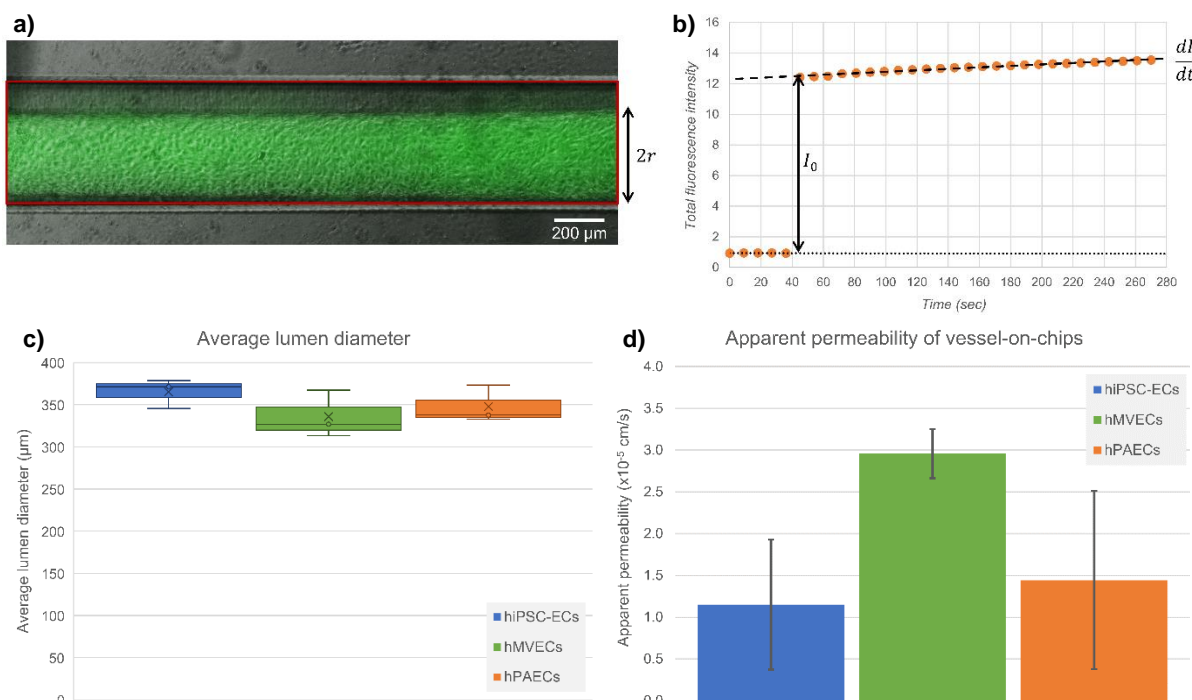


**Figure 34** Results of permeability assay for hiPSC-ECs, hMVECs and hPAECs cultured in oxygen permeable PDMS VoC systems. a) Overlay image of FITC-Dextran perfused through hPAEC lumen. b) Example of measured fluorescence intensity over time. c) Average vessel diameter for each cell type. d) Calculated apparent permeability for each cell type.

desired, in other channels this increase was found to be more gradual. This is most likely caused due to differences in perfusability between lumens and manual addition of FITC-Dextran resulting in delayed infusion. In **Figure 34c**, average lumen diameters for each cell type are plotted. From this data, it can be seen that all lumens had a diameter between 300 and 400  $\mu\text{m}$ , with hiPSC-ECs having slightly larger and hMVECs slightly smaller diameter lumens. However, these minor differences might not be related to cell type but rather due to lumen fabrication.

Lastly, the calculated apparent permeability of the VoCs created with each cell type can be seen in **Figure 34d**. Here, a clear difference in permeability is observed between hMVECs and the other cell types. Where both hiPSC-ECs and hPAECs display a relatively low permeability, the permeability of vessels cultured with hMVECs is significantly higher. This is relatable to the physiological situation, since microvessels need to be more permeable to allow for exchange of fluids and small solutes while larger vessels need a low permeability to reduce losses during transport [3].

To evaluate general cell morphology and further characterize the created lumens, they were stained for VE-cadherin, f-actin and nuclei and imaged with confocal microscopy (see **Figure 35**). First of all, it can be observed that the hMVEC lumen displays sprouting of cells into the collagen lumen, which could be a signal of angiogenesis as is characteristic for microvessels but not macrovessels [3]. Secondly, gaps are observed in the cellular layer of the hPAEC lumen but not in the other lumens. This might have influenced the measured permeability of the hPAEC lumens, although it is not known whether the measured lumens also contained such gaps.

Another interesting observation is the fact that hMVECs seem to express more VE-cadherin and less f-actin than hiPSC-ECs and hPAECs, even though VE-cadherin is known to play a role in the maintenance of a restrictive endothelial barrier [191]. This observation therefore clashes with the previous conclusion where an increased permeability was observed for hMVECs compared to hiPSC-ECs and hPAECs. However, a significant amount of nonspecific VE-cadherin staining can be seen in all lumens, making it difficult to tell whether VE-cadherin expression is really higher for hMVECs. Additionally, only a single lumen was imaged per cell type, making it impossible to draw any significant conclusions on these images.

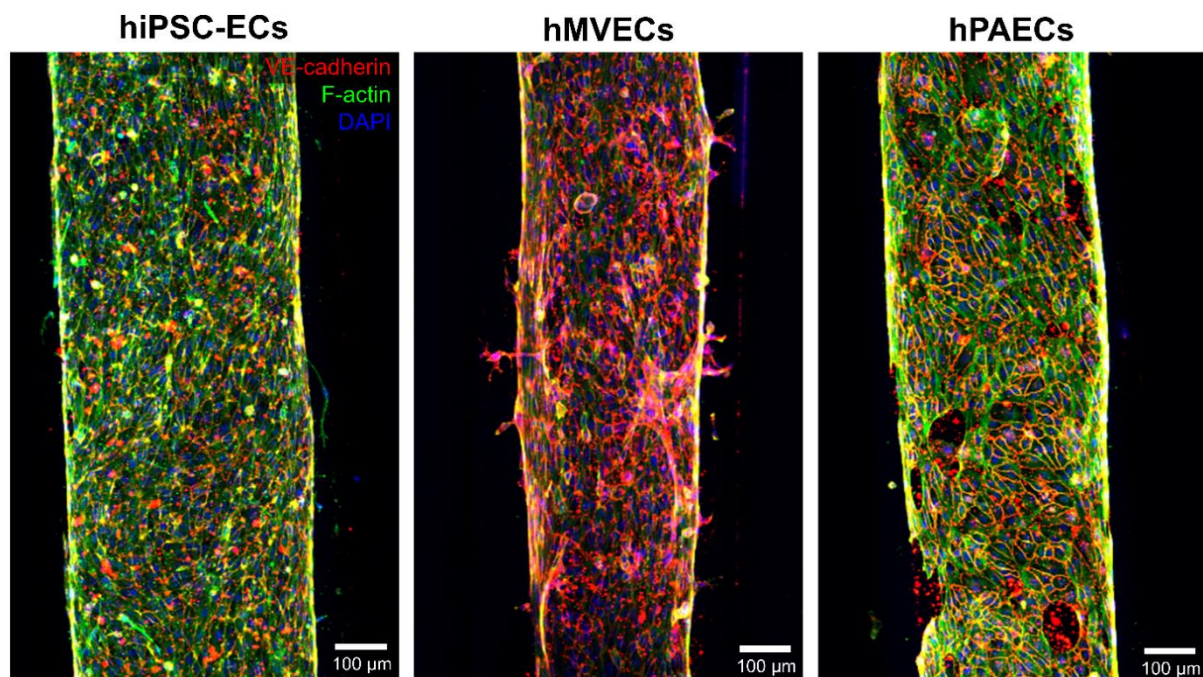


**Figure 35** Images of hiPSC-ECs, hMVECs and hPAECs cultured in oxygen permeable PDMS VoC systems with collagen lumens stained for VE-cadherin in red, F-actin in green and nuclei in blue.

#### 5.2.2.4 Integration of hiPSC-ECs in Oxygen Impermeable PMMA Chips

Besides integration of cells in the oxygen permeable PDMS chips, it was also attempted to integrate cells in the oxygen impermeable PMMA chips. In **Figure 36**, brightfield images of hiPSC-ECs cultured in an oxygen impermeable PMMA VoC system with collagen lumen can be seen directly after cell seeding and after 24 hours of culture in a normoxic incubator. From these images it can be seen that although initial cell seeding seemed successful, cells died after 24 hours of culture on a rocker platform in a normoxic incubator. It is thought that this might be due to lack of oxygen in the chip as supplied by the rocking culture medium. It is therefore suggested to repeat the experiment after successful integration of controlled flow into the chip to ensure sufficient supply of oxygen and nutrients to the cells during culture.

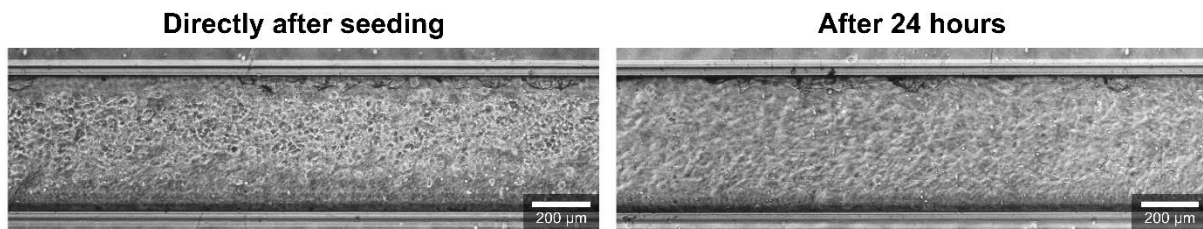


**Figure 36** Images of hiPSC-ECs cultured in oxygen impermeable PMMA VoC system with collagen lumen directly after cell seeding (left) and after 24 hours of culture in normoxic incubator (right).

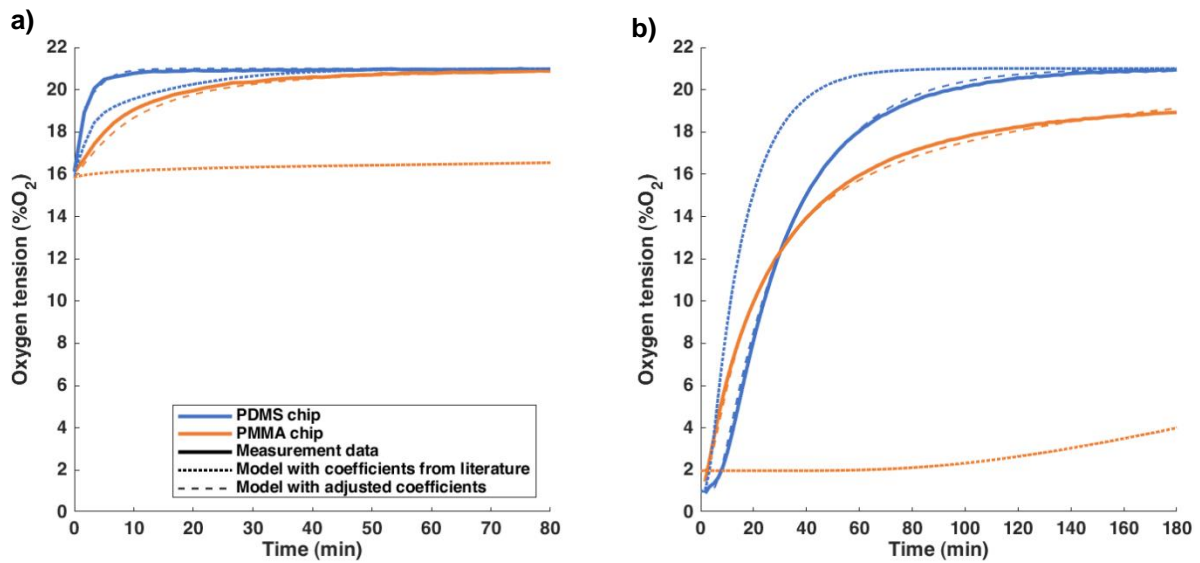
#### 5.2.2.5 Integration of Controlled Flow

Lumens in both PDMS and PMMA chips could successfully be perfused with PS microspheres (see videos in supplementary material **S5**) at a flow rate of 15  $\mu\text{l}/\text{min}$ . Due to lack of time it has not been possible to analyse the flow profile in these lumens, e.g. by bead tracking algorithms, or to experiment with different flow rates to determine which flow rates can be reached before the lumens are damaged or the bond between the collagen and the chip material is broken. If this were to happen below the desired maximum flow rate of 2 ml/ml (corresponding to a shear stress of 120 dynes/cm<sup>2</sup>), it could be beneficial to switch to an APTES/GA coating to promote adhesion of collagen to the chip material.

#### 5.2.2.6 Oxygen Sensing in VoC systems

To determine whether it is possible to measure the oxygen tension in the current chip designs, oxygen sensor spots were integrated in a PDMS and PMMA chip and the oxygen tension was measured after injection of oxygen deprived EGM-2 culture medium (see **Figure 37**). Oxygen tension of the culture medium at the time of injection as measured with the oxygen probe was estimated to be approximately 3% (data not shown). This is higher than the expected oxygen tension of 0.1% to which the hypoxic incubator was set, most likely because it took around 5 minutes to take the culture medium out of the incubator and inject it into the chips. Additionally, two days in an hypoxic incubator without mixing might not be sufficient to remove enough oxygen from the medium to obtain medium with 0.1% oxygen.

As can be seen from the graphs in **Figure 37a**, the oxygen tension increased significantly during injection into the chips, since in both chips the minimum oxygen tension that could be measured was 16%. This initial oxygen tension also varied strongly between measurements and chips. At first it was thought that this variation might be caused by the fact that injection of the medium was not simultaneously, since medium was first injected into the PDMS chip and then in the PMMA chip. However, in some measurements the oxygen tension was found to be lower in the PMMA chips, so it is unlikely that the oxygen tension in the culture medium strongly changed in the seconds between injection of the two chips. It is therefore thought that these differences might be caused during the manual injection of the culture medium, when oxygen can diffuse into the medium through the pipette tips and air in the channel. Possibly slight differences in the speed of injection or available oxygen in the porous chip materials have also had an effect on the initial oxygen tension that was measured, which could vary as much as 8.5-19% for different measurements in the same chip.



c)	Chip material	Preconditioned in hypoxia?	Initial oxygen tension (kPa)		Diffusion coefficient ( $\text{m}^2 \text{s}^{-1}$ )			
			Chip	Medium/ water	qPCR tape	Medium/ water	PMMA	PDMS
Coefficients from literature	PMMA	✗	21	14.5	$10^{-11}$	$1.9 \times 10^{-9}$	$3 \times 10^{-12}$	-
		✓	2	2	$10^{-11}$	$1.9 \times 10^{-9}$	$3 \times 10^{-12}$	-
	PDMS	✗	21	13.5	$10^{-11}$	$1.9 \times 10^{-9}$	-	$3.5 \times 10^{-9}$
		✓	1	1	$10^{-11}$	$1.9 \times 10^{-9}$	-	$3.5 \times 10^{-9}$
Adjusted coefficients	PMMA	✗	21	12.5	$10^{-11}$	$6 \times 10^{-8}$	$5 \times 10^{-10}$	-
		✓	2	2	$10^{-11}$	$6 \times 10^{-8}$	$5 \times 10^{-10}$	-
	PDMS	✗	21	13.5	$10^{-11}$	$6 \times 10^{-8}$	-	$10^{-8}$
		✓	1	1	$10^{-11}$	$10^{-10}$	-	$10^{-8}$

**Figure 37** Oxygen tension measurements over time in PDMS and PMMA chips after injection of oxygen deprived culture medium in a) chips that were stored in ambient air and b) chip that were preconditioned in an hypoxic incubator (0.1%  $\text{O}_2$ ) for 2 days. Oxygen tension in chip as modelled using diffusion coefficients found in literature is shown with dotted lines and oxygen tension as modelled with adjusted diffusion coefficients is shown with dashed lines. c) Overview of initial oxygen tensions and diffusion coefficients used for each model.

The idea that residual oxygen in the chip caused an increase in the measured oxygen tension in the culture medium was confirmed by a measurement of hypoxic culture medium injected into chips that were placed in a hypoxic incubator (0.1%  $\text{O}_2$ ) for two days (see **Figure 37b**). Here it can be seen that initial oxygen tension in these chips is much lower and varied between 1-2%, after which a gradual increase is observed towards 21% oxygen. The time in which the oxygen tension reaches 21% was found to be significantly shorter for the PDMS chip compared to the PMMA chip independent of the oxygen tension in the chip material. However, for the preconditioned chips the initial increase seemed to be faster for the PMMA chips, while this was not observed in the chips that were stored in ambient air. It is unknown why this behaviour is observed, since it is expected that the oxygen tension in the PDMS chip would increase faster compared to the PMMA chip.

In an attempt to explain these measured oxygen patterns and relate them to the material properties of the different chip systems, the previously described computation model was compared to the measured data. The initial oxygen tension was set to match the measured initial oxygen tension and diffusion through the glass and qPCR tape covering the bottom of the channel was neglected. When using the diffusion constants for water, PDMS and PMMA as found in literature (see **Table 3**) a poor fit was found with the measured data (as shown by dotted lines in **Figure 37a**). Unfortunately it was not possible to perform a parameter estimation in COMSOL to determine an optimal fit due to lack of computational power. Nevertheless, a better fit was obtained by manually adjusting the diffusion constants to  $6 \times 10^{-8} \text{ m}^2/\text{s}$  for water,  $10^{-8} \text{ m}^2/\text{s}$  for PDMS and  $5 \times 10^{-10} \text{ m}^2/\text{s}$  for PMMA (shown by dashed lines in **Figure 37a**). For all

conditions these values gave good results except the preconditioned PDMS chip where a diffusion constant of  $10^{-10}$  m<sup>2</sup>/s was used. Similarly to literature, the found diffusion constant for PMMA is significantly lower than the one found for PDMS, although for both materials the found diffusion constants were higher than the values found in literature. The found diffusion constant for water is also higher than the values found in literature, which can be explained by the fact that proteins, salts and sugars are present in the culture medium that could alter the oxygen diffusion compared to water.

### **5.2.3 Conclusions and Recommendations**

3D collagen lumens were successfully fabricated in both oxygen permeable PDMS chips and oxygen impermeable PMMA chips. Chloroform polishing was used to reduce surface roughness and improve visibility of the formed lumens in the channel. To prevent bubble formation due to air pockets in the chip, channels were prefilled with various solutions, from which ethanol showed the largest reduction in bubble formation while still allowing for the creation of straight lumens. An average diameter of  $301 \pm 40$   $\mu$ m was found for lumens in the PDMS chips and  $313 \pm 34$   $\mu$ m for the lumens in the PMMA chips, with a respective success rate of 87.5% and 90%. 3D OCT imaging also confirmed successful formation of a cylindrical lumen in the PMMA chips.

Although these results look promising, various issues are still encountered during the fabrication of these lumens. First of all, visualization of the formed lumens remains difficult, even when perfusing the lumens with a coloured dye or PS microspheres, which makes it difficult to accurately determine the lumen diameter. This visualization problem could become an issue when selecting functional lumens before cell seeding as not to waste cells and might also be important for the integration of controlled shear stresses.

Secondly, some variability between lumens could be observed regarding lumen dimensions and success rate, depending on the day, chip design and collagen batch. This is most likely due to the high sensitivity of the VFP procedure, which is affected by many factors such as the exact composition of the collagen mixture, temperature of the solutions, timing and the precision with which the PBS is introduced into the channel. Other methods of lumen fabrication such as needle patterning might be more robust and could solve the issue of variability between lumens. Additionally, it might be easier to control the exact shape and diameter of the lumens with needle patterning. This could also be important when controlling the shear stress in a later stage, which strongly depends on the geometry and size of the lumen. However, needle patterning knows other disadvantages, such as a low throughput and limiting geometries that can be fabricated, and still requires a lot of optimization.

Lastly, it is important to note that the oxygen sensor spots are incompatible with ethanol and cannot be used with this method of lumen formation. Thus, it might be necessary in the future to find a different technique to prevent bubble formation during lumen formation that does not require ethanol or another nonaqueous solvent. Nonetheless, when oxygen sensitive beads will be used, the use of ethanol should not pose a problem since the beads will be integrated after lumen formation.

After successful lumen formation, hiPSC-ECs, hPAECs and hMVECs could be integrated in oxygen permeable VoC systems. Characterization revealed a higher permeability of lumens formed with hMVECs compared to hPAECs and hiPSC-ECs. This is relatable to the physiological situation, since microvessels need to be more permeable to allow for exchange of fluids and small solutes while larger vessels need a low permeability to reduce losses during transport. However, VE-cadherin staining intensity was also found to be increased for hMVECs, refuting this conclusion. Nonetheless, despite a high amount of nonspecific staining and limited data it can be considered that hiPSC-ECs behave more like macrovascular cells in 3D culture than microvascular cells based on permeability and immunostaining data. Yet more experimental data is required to support this conclusion.

Unfortunately it has not yet been possible to create a cellular lumen in the oxygen impermeable PMMA VoC system, most likely due to lack of oxygen in the cellular environment when using a rocker platform. Although it has been possible to integrate continuous flow in the PMMA chip systems, lack of time prevented analysis of the flow profile in these lumens and

experimentation with different flow rates to determine which flow rates can be reached before the lumens are damaged or the bond between the collagen and the chip material is broken. Once this characterization is completed, it is recommended to again attempt culture of hiPSC-ECs in the PMMA VoC system using continuous flow with various flow rates. It is expected that continuous flow should provide sufficient oxygen and nutrients to the cells to promote the formation of a monolayer in the lumens.

Regarding control and sensing of oxygen in the chip systems, it has been possible to integrate oxygen sensor spots in the PDMS and PMMA chips and measure the oxygen tension after exposure to oxygen deprived culture medium. Here, a difference could be observed between the PDMS and PMMA chips, where the oxygen tension in the PDMS chips seemed to increase faster compared to the PMMA chips. This behaviour could be confirmed with the computational model, although data fitting revealed that the apparent diffusion constants of the chips and the culture medium were higher than those found in literature.

The next step in the integration of oxygen sensors in the sPAoC would be to measure the oxygen tension in a chip with collagen lumen. For the PDMS chips this should easily be achieved by performing VFP in a chip that is sealed with a piece of qPCR tape containing a sensor spot. However, for the PMMA chips this cannot be done, since the ethanol used to prevent bubble formation is incompatible with the hydrogel in which the sensor spots are embedded. Thus, it is necessary to either find a different method to prevent bubble formation without the need of a nonaqueous solvent such as ethanol, or to measure the oxygen tension with oxygen sensitive beads which could be integrated after lumen formation. Since no SMCs are integrated as of yet, these oxygen sensitive beads might need to be (covalently) bonded to the collagen to prevent leaching. Yet, this could affect the VFP procedure.

When 3D hiPSC-EC lumens can successfully be created in the PMMA chips and flow and oxygen tension can be controlled and measured, the cells can be characterized in 3D dynamic normoxic and hypoxic conditions similarly to characterization in 2D and 3D lumens in PDMS chips. General characterization can be performed by staining with VE-cadherin, f-actin and DAPI and permeability can be assessed using the permeability assay previously described. Lectin staining can be used to investigate differences in micro/macrovacular phenotype between 2D and 3D culture, while expression of COUP-TFII and Ephrin B2 should be analysed to determine arterial/venous behaviour. For this purpose, a hiPSC-EC COUP-TFII reporter line as created by the University of Leiden could be used. To determine pulmonary/systemic behaviour of the hiPSC-ECs, medium from the lumens should be collected and ET-1 and NO content must be measured. However, it is expected that this expression will strongly be diluted when using high flow rates. Therefore, it might be necessary to use a recirculation pump or fluidic circuit board which allows recirculation of the medium to ensure that the ET-1 and NO content are within the range of the detection assays. Using these readout methods, the effect of different shear stresses and oxygen tensions can finally be studied in the sPAoC systems.

## 6 DISCUSSION

---

In this research, a sPAoC model is proposed that recapitulates the 3D architecture of the sPA and allows for control of flow and oxygen in a physiological range. hiPSC derived vascular cells are preferred for this purpose because of the genetic nature of some pulmonary vascular diseases such as PAH, but it is unknown whether these cells exhibit the characteristic behaviour of cells found in the sPAs. Although some researchers claim that a pulmonary phenotype is not necessary and that immature, heterogenous hiPSC-ECs are good surrogates for PAH modelling and drug testing in 2D [192], it is unknown whether this is also the case for culture in a 3D OoC model with ECM, multiple cell types and physiological oxygen and flow conditions.

As of yet, limited protocols exist for the creation of hiPSC-ECs and most of these focus on the creation of a heterogenous population of ECs, while cell behaviour is known to depend on the location within the vascular tree [193]. Regarding vessel types, some methods have been proposed for further differentiation into arterial or venous ECs, but no protocols yet exist to generate microvascular ECs [10] [193]. Only a few tissue specific ECs have been created so far, mostly focussing on the blood-brain barrier, retina or heart, but none concentrating on the pulmonary circulation [193]. One of the reasons which makes it so hard to come up with protocols for differentiation of type and tissue specific hiPSC-ECs is the fact that little is known about the differences between ECs *in vivo* on a molecular and function level. If no molecular signature of functional distinction has been established for the required specific ECs *in vivo*, it is very difficult to recreate and characterize them in an *in vitro* model. Most researchers therefore use general EC biomarkers such as VE-cadherin, CD31 and von Willebrand Factor vWF and a lack of actin- $\alpha 2$  to confirm EC cell behaviour [115]. To characterize arterial or venous branching, Ephrin B2 and COUP-TFII have previously been used [11]. However, for the creation of a sPAoC this characterization is not deemed sufficient and it is therefore necessary to further characterize the cells using markers that specify a sPA phenotype.

In this study, extensive characterization of hiPSC-ECs has been presented for the first time to identify sPA specific hiPSC-ECs. Although micro/macrovascular characterization has not yet proven successful, initial results do show that hiPSC-ECs exhibit a pulmonary phenotype based on their expression pattern of ET-1 and NO in response to hypoxia. Additionally, the general response to hypoxia as indicated by the expression of HIF-1 $\alpha$  and HIF-2 $\alpha$  is similar to the response found in primary hPAECs. These results are of great importance when integrating the cells into a sPAoC system, since they provide previously unknown information about the current phenotype of the hiPSC-ECs. Additionally, biomarkers and assays have been identified and optimized to assess this phenotype in both 2D and 3D cell culture conditions. With this characterization and after integration into a sPAoC system it will finally be possible to study the changes in cellular phenotype due to (patho)physiological oxygen tensions and shear stresses.

A second aspect that has been covered in this research is the design and creation of an oxygen impermeable sPAoC system in which hiPSC derived vascular cells can be cultured and where the flow rate and oxygen tension can be controlled. Although the 3D VoC system from as developed within the AST group [17] does contain the 3D ECM architecture as found in the sPAs and hiPSC-ECs have previously been integrated in this system, only low shear stresses could be generated and oxygen control is prevented due to the high oxygen permeability of the chip material. Other systems [168] [169] [170] are able to stimulate the cells with controlled oxygen tensions and shear stresses, but do not mimic the 3D ECM architecture as found in the native environment of the sPAs and have not previously been used with hiPSC derived cells.

Here, a novel sPAoC design is proposed which combines the 3D ECM architecture and use of hiPSC derived cells with control of oxygen tension and flow rate. With this chip design, it is possible to study the effects of shear stress and two oxygen tensions (as found in the alveoli and the blood) in a (patho)physiological range, which has not been realized before. Although primary or embryonic stem cell derived ECs and SMCs have been integrated in oxygen

controlled 2D<sup>+</sup> OoC systems, no oxygen controlled 3D VoC system exists yet that contains patient-specific hiPSCs derived ECs, SMCs and fibroblasts. To study more complex vascular processes such as vasoconstriction and vascular remodelling, tissue engineered blood vessels [194] or bioprinted ring assays [195] are currently the best solutions. However, these do not allow for control of flow and/or oxygen tension and are not specified towards patient-specific, pulmonary studies. Thus, since no 3D human *in vitro* models yet exist to study these processes, the proposed system could be the first realistic, patient-derived sPA model in which the effects of shear stress and oxygen tension on complex vascular processes can be studied.

Initial experimental progress towards this proposed solution demonstrate the integration of a 3D collagen lumen fabricated with VFP to mimic the native ECM architecture in an oxygen impermeable PMMA chip, which has not been shown before. Furthermore, it has been established that this system can be perfused with a syringe pump and that oxygen measurements can be performed within the microfluidic channel, revealing a clear difference between the PDMS and PMMA systems. When comparing the novel PMMA chip to the existing PDMS chip, its main advantage is the fact that it allows for control of oxygen tension without being influenced by the oxygen tension of the ambient air, which is expected to be the case for the PDMS chip based on initial oxygen measurements and computational modelling of the system. This greatly improves the physiological relevance of the model, since cells in the sPAs are expected to receive most oxygen from the blood (5%) and air in the alveoli (14%), which is significantly lower in concentration than the ambient air (21%). Although it might be possible to simulate these physiological conditions in the PDMS chip, this will require a hypoxic workstation which limits ease-of-use, has limited capacity and might pose problems when combining it with a fluidic setup.

All in all, it is believed that with the proposed sPAoC system it will be possible to recreate the (patho)physiological environment as found in the sPAs *in vivo* using patient-specific cells. The system can then be used to determine which stimuli, including oxygen tensions and shear stresses, could initiate or progress the vasoconstriction and vascular remodelling as observed in various vascular diseases such as PAH. Obtaining this knowledge is deemed crucial for a better understanding of diseases development. Additionally, these stimuli can be used to mimic the disease in an *in vitro* situation, which could be a turning point in the development of an effective treatment or cure.

## 7 CONCLUSIONS

---

In this research it was aspired to determine how the influence of oxygen tension and shear stress on the behaviour of vascular cells can be studied in a 3D VoC system. Towards this end, a 3D sPAoC chip design is proposed based on extensive literature studies which allows for integration of ECs, SMCs and fibroblasts in a 3D hydrogel-based PMMA chip with control of physiological oxygen tensions and flow rates. A concept version of this chip system without the alveolar compartment was successfully fabricated via micro milling, chloroform polishing, ethanol prefilling and VFP. Microscopy and OCT imaging confirmed successful formation of a cylindrical collagen lumen in the PMMA chips with an average diameter of  $313 \pm 34 \mu\text{m}$  and a success rate of 90%. Furthermore, the system could be perfused with a syringe pump and oxygen measurements within the microfluidic channels demonstrated a clear difference between the PDMS and PMMA systems, which was confirmed with computational modelling. Finally, extensive characterization of hiPSC-ECs was performed previous to integration into the chip system, revealing a pulmonary arterial phenotype based on the cellular response to hypoxia and expression patterns of ET-1 and NO.

Thus, significant theoretical and experimental progress has been booked in this research regarding the development of a sPAoC for *in vitro* small pulmonary artery studies. Even though most presented results still require optimization and replication, it is believed that by continuation of the project according to the presented roadmap, a physiologically relevant sPAoC can be obtained which has the potential to be used for studying various complex vascular processes in both healthy and diseased situations.

## 8 REFERENCES

- [1] Chen A., Liu J., Zhu J., et al., *Fgf21 attenuates hypoxia-induced dysfunction and apoptosis in hpaecs through alleviating endoplasmic reticulum stress*, Int J Mol Med, 2018, Volume 42, Issue 3, pp. 1684-1694, DOI: 10.3892/ijmm.2018.3705
- [2] Pugliese S.C., Poth J.M., Fini M.A., et al., *The role of inflammation in hypoxic pulmonary hypertension: From cellular mechanisms to clinical phenotypes*, American journal of physiology. Lung cellular and molecular physiology, 2015, Volume 308, Issue 3, pp. L229-L252, DOI: 10.1152/ajplung.00238.2014
- [3] Marieb E.N., Hoehn K.N., Chapter: 19, *The cardiovascular system: Blood vessels*, pp. 692-750, In: *Human anatomy & physiology*, 9th Edition, 2014, Pearson, ISBN: 978-1-292-02649-7
- [4] Marieb E.N., Hoehn K.N., Chapter: 18, *The cardiovascular system: The heart*, pp. 658-691, In: *Human anatomy & physiology*, 9th Edition, 2014, Pearson, ISBN: 978-1-292-02649-7
- [5] Elveflow, *How to choose the right microfluidic flow control system?*, Access date: 04/05/2021, From: <https://www.elveflow.com/microfluidic-reviews/microfluidic-flow-control/how-to-choose-right-microfluidic-flow-control-system/>
- [6] Wang X.-D., Wolfbeis O.S., *Optical methods for sensing and imaging oxygen: Materials, spectroscopies and applications*, Chemical Society Reviews, 2014, Volume 43, Issue 10, pp. 3666-3761, DOI: 10.1039/C4CS00039K
- [7] Collins J.-A., Rudenski A., Gibson J., et al., *Relating oxygen partial pressure, saturation and content: The haemoglobin-oxygen dissociation curve*, Breathe, 2015, Volume 11, Issue 3, p. 194, DOI: 10.1183/20734735.001415
- [8] Li M., Stenmark K.R., Shandas R., et al., *Effects of pathological flow on pulmonary artery endothelial production of vasoactive mediators and growth factors*, Journal of Vascular Research, 2009, Volume 46, Issue 6, pp. 561-571, DOI: 10.1159/000226224
- [9] Adler M., Polinkovsky M., Gutierrez E., et al., *Generation of oxygen gradients with arbitrary shapes in a microfluidic device*, Lab on a Chip, 2010, Volume 10, Issue 3, pp. 388-391, DOI: 10.1039/B920401F
- [10] Rosa S., Praça C., Pitrez P.R., et al., *Functional characterization of ipsc-derived arterial- and venous-like endothelial cells*, Scientific Reports, 2019, Volume 9, Issue 1, p. 3826, DOI: 10.1038/s41598-019-40417-9
- [11] Halaidych O.V., Freund C., Van Den Hil F., et al., *Inflammatory responses and barrier function of endothelial cells derived from human induced pluripotent stem cells*, Stem Cell Reports, 2018, Volume 10, Issue 5, pp. 1642-1656, DOI: 10.1016/j.stemcr.2018.03.012
- [12] Cao J., Ehling M., März S., et al., *Polarized actin and ve-cadherin dynamics regulate junctional remodelling and cell migration during sprouting angiogenesis*, Nature Communications, 2017, Volume 8, Issue 1, p. 2210, DOI: 10.1038/s41467-017-02373-8
- [13] De Graaf M.N.S., Cochrane A., Van Den Hil F.E., et al., *Scalable microphysiological system to model three-dimensional blood vessels*, APL Bioengineering, 2019, Volume 3, Issue 2, p. 026105, DOI: 10.1063/1.5090986
- [14] Gold K., Gaharwar A.K., Jain A., *Emerging trends in multiscale modeling of vascular pathophysiology: Organ-on-a-chip and 3D printing*, Biomaterials, 2019, Volume 196, pp. 2-17, DOI: 10.1016/j.biomaterials.2018.07.029
- [15] Biospherix, *Xvivo system model x3*, Access date: 30/04/2021, From: <https://www.biospherix.com/products/xvivo-system-model-x3>
- [16] Comhair S.a.A., Xu W., Mavrakis L., et al., *Human primary lung endothelial cells in culture*, American journal of respiratory cell and molecular biology, 2012, Volume 46, Issue 6, pp. 723-730, DOI: 10.1165/rcmb.2011-0416TE
- [17] Herland A., Van Der Meer A.D., Fitzgerald E.A., et al., *Distinct contributions of astrocytes and pericytes to neuroinflammation identified in a 3D human blood-brain barrier on a chip*, PLOS ONE, 2016, Volume 11, Issue 3, p. e0150360, DOI: 10.1371/journal.pone.0150360
- [18] Chen Y.-A., King A.D., Shih H.-C., et al., *Generation of oxygen gradients in microfluidic devices for cell culture using spatially confined chemical reactions*, Lab on a Chip, 2011, Volume 11, Issue 21, pp. 3626-3633, DOI: 10.1039/C1LC20325H
- [19] Lewis D.M., Tang V., Jain N., et al., *Collagen fiber architecture regulates hypoxic sarcoma cell migration*, ACS Biomaterials Science & Engineering, 2018, Volume 4, Issue 2, pp. 400-409, DOI: 10.1021/acsbmaterials.7b00056
- [20] Lo J.F., Sinkala E., Eddington D.T., *Oxygen gradients for open well cellular cultures via microfluidic substrates*, Lab on a Chip, 2010, Volume 10, Issue 18, pp. 2394-2401, DOI: 10.1039/c004660d
- [21] Merck Millipore, *CellASIC® onix2 microfluidic system*, Access date: 30/04/2021, From: [https://www.merckmillipore.com/NL/en/product/CellASIC-ONIX-Microfluidic-Platform,MM\\_NF-C117908](https://www.merckmillipore.com/NL/en/product/CellASIC-ONIX-Microfluidic-Platform,MM_NF-C117908)
- [22] Stemcell Technologies, *Hypoxia incubator chamber*, Access date: 30/04/2021, From: <https://www.stemcell.com/how-to-create-a-hypoxic-environment-for-cell-culture.html>
- [23] World Health Organization, *Cardiovascular diseases (cvds)*, Access date: 15/02/2021, Last updated: 17/05/2017, From: [https://www.who.int/en/news-room/fact-sheets/detail/cardiovascular-diseases-\(cvds\)](https://www.who.int/en/news-room/fact-sheets/detail/cardiovascular-diseases-(cvds))
- [24] Medlineplus, *Vascular diseases*, Access date: 16/02/2021, Last updated: 11/12/2020, From: <https://medlineplus.gov/vascular-diseases.html>
- [25] VascularCures, *Types of vascular diseases*, Access date: 16/02/2021, From: <https://vascularcures.org/types-of-vascular-diseases/>

- [26] Humbert M., Guignabert C., Bonnet S., et al., *Pathology and pathobiology of pulmonary hypertension: State of the art and research perspectives*, European Respiratory Journal, 2019, Volume 53, Issue 1, p. 1801887, DOI: 10.1183/13993003.01887-2018
- [27] Feldman J., *Pulmonary hypertension*, Access date: 02/09/2020, From: <https://pulmonaryhypertensionrn.com/>
- [28] Lai Y.-C., Potoka K.C., Champion H.C., et al., *Pulmonary arterial hypertension: The clinical syndrome*, Circulation Research, 2014, Volume 115, Issue 1, pp. 115-130, DOI: 10.1161/CIRCRESAHA.115.301146
- [29] National Organization for Rare Diseases, *Pulmonary arterial hypertension*, Access date: 02/09/2020, Last updated: 2018, From: <https://rarediseases.org/rare-diseases/pulmonary-arterial-hypertension/>
- [30] U.S. National Library of Medicine, *Bmpr2 gene*, Access date: 02/09/2020, Last updated: 17/08/2020, From: <https://ghr.nlm.nih.gov/gene/BMPR2>
- [31] Chan S.Y., Loscalzo J., *Pathogenic mechanisms of pulmonary arterial hypertension*, Journal of molecular and cellular cardiology, 2008, Volume 44, Issue 1, pp. 14-30, DOI: 10.1016/j.yjmcc.2007.09.006
- [32] Morrell N.W., Aldred M.A., Chung W.K., et al., *Genetics and genomics of pulmonary arterial hypertension*, European Respiratory Journal, 2019, Volume 53, Issue 1, p. 1801899, DOI: 10.1183/13993003.01899-2018
- [33] Pugh M.E., Hemnes A.R., *Metabolic and hormonal derangements in pulmonary hypertension: From mouse to man*, International journal of clinical practice. Supplement, 2010, Volume 64, Issue 168, pp. 5-13, DOI: 10.1111/j.1742-1241.2010.02523.x
- [34] Pober J.S., Sessa W.C., *Evolving functions of endothelial cells in inflammation*, Nature Reviews Immunology, 2007, Volume 7, Issue 10, pp. 803-815, DOI: 10.1038/nri2171
- [35] Itoh T., Nagaya N., Ishibashi-Ueda H., et al., *Increased plasma monocyte chemoattractant protein-1 level in idiopathic pulmonary arterial hypertension*, Respirology, 2006, Volume 11, Issue 2, pp. 158-163, DOI: <https://doi.org/10.1111/j.1440-1843.2006.00821.x>
- [36] Hurst L.A., Dunmore B.J., Long L., et al., *Tnfa drives pulmonary arterial hypertension by suppressing the bmp type-ii receptor and altering notch signalling*, Nature Communications, 2017, Volume 8, pp. 14079-14079, DOI: 10.1038/ncomms14079
- [37] Kumar R., Graham B., *How does inflammation contribute to pulmonary hypertension?*, European Respiratory Journal, 2018, Volume 51, Issue 1, p. 1702403, DOI: 10.1183/13993003.02403-2017
- [38] Giaid A., Yanagisawa M., Langleben D., et al., *Expression of endothelin-1 in the lungs of patients with pulmonary hypertension*, New England Journal of Medicine, 1993, Volume 328, Issue 24, pp. 1732-1739, DOI: 10.1056/NEJM199306173282402
- [39] Lei W., He Y., Shui X., et al., *Expression and analyses of the hif-1 pathway in the lungs of humans with pulmonary arterial hypertension*, Mol Med Rep, 2016, Volume 14, Issue 5, pp. 4383-4390, DOI: 10.3892/mmr.2016.5752
- [40] Tang H., Babicheva A., Mcdermott K.M., et al., *Endothelial hif-2 $\alpha$  contributes to severe pulmonary hypertension due to endothelial-to-mesenchymal transition*, American journal of physiology. Lung cellular and molecular physiology, 2018, Volume 314, Issue 2, pp. L256-L275, DOI: 10.1152/ajplung.00096.2017
- [41] Mirrakhimov A.E., Strohl K.P., *High-altitude pulmonary hypertension: An update on disease pathogenesis and management*, The open cardiovascular medicine journal, 2016, Volume 10, pp. 19-27, DOI: 10.2174/1874192401610010019
- [42] Vessières E., Freidja M., L., Loufrani L., et al., *Flow (shear stress)-mediated remodeling of resistance arteries in diabetes*, Vascular Pharmacology, 2012, Volume 57, Issue 5-6, pp. 173-178, DOI: 10.1016/j.vph.2012.03.006
- [43] Tang B.T., Pickard S.S., Chan F.P., et al., *Wall shear stress is decreased in the pulmonary arteries of patients with pulmonary arterial hypertension: An image-based, computational fluid dynamics study*, Pulmonary circulation, 2012, Volume 2, Issue 4, pp. 470-476, DOI: 10.4103/2045-8932.105035
- [44] Moses S.R., Adorno J.J., Palmer A.F., et al., *Vessel-on-a-chip models for studying microvascular physiology, transport, and function in vitro*, American Journal of Physiology-Cell Physiology, 2020, Volume 320, Issue 1, pp. C92-C105, DOI: 10.1152/ajpcell.00355.2020
- [45] Van Den Eijnden-Van Raaij J., Meer B.V., Mummery C., et al., *Mini organs-on-chips*, 2020, Dutch Foundation for Biosciences and Society (BWM), ISBN: 978-94-93232-01-3
- [46] Huh D., Matthews B.D., Mammoto A., et al., *Reconstituting organ-level lung functions on a chip*, Science, 2010, Volume 328, Issue 5986, p. 1662, DOI: 10.1126/science.1188302
- [47] Booth R., Kim H., *Characterization of a microfluidic in vitro model of the blood-brain barrier ( $\mu$ bbb)*, Lab on a Chip, 2012, Volume 12, Issue 10, pp. 1784-1792, DOI: 10.1039/C2LC40094D
- [48] Kim H.J., Huh D., Hamilton G., et al., *Human gut-on-a-chip inhabited by microbial flora that experiences intestinal peristalsis-like motions and flow*, Lab on a Chip, 2012, Volume 12, Issue 12, pp. 2165-2174, DOI: 10.1039/C2LC40074J
- [49] Pollet A.M.a.O., Den Toonder J.M.J., *Recapitulating the vasculature using organ-on-chip technology*, Bioengineering, 2020, Volume 7, Issue 1, DOI: 10.3390/bioengineering7010017
- [50] Zheng Y., Chen J., Craven M., et al., *In vitro microvessels for the study of angiogenesis and thrombosis*, Proceedings of the National Academy of Sciences, 2012, Volume 109, Issue 24, p. 9342, DOI: 10.1073/pnas.1201240109
- [51] Bischel L.L., Lee S.-H., Beebe D.J., *A practical method for patterning lumens through ecm hydrogels via viscous finger patterning*, Journal of Laboratory Automation, 2012, Volume 17, Issue 2, pp. 96-103, DOI: 10.1177/2211068211426694

- [52] Bischel L.L., Young E.W.K., Mader B.R., et al., *Tubeless microfluidic angiogenesis assay with three-dimensional endothelial-lined microvessels*, *Biomaterials*, 2013, Volume 34, Issue 5, pp. 1471-1477, DOI: <https://doi.org/10.1016/j.biomaterials.2012.11.005>
- [53] Krüger-Genge A., Blocki A., Franke R.-P., et al., *Vascular endothelial cell biology: An update*, *International journal of molecular sciences*, 2019, Volume 20, Issue 18, p. 4411, DOI: 10.3390/ijms20184411
- [54] Ranchoux B., Antigny F., Rucker-Martin C., et al., *Endothelial-to-mesenchymal transition in pulmonary hypertension*, *Circulation*, 2015, Volume 131, Issue 11, pp. 1006-1018, DOI: 10.1161/CIRCULATIONAHA.114.008750
- [55] Alberts B, Johnson A, Lewis J, et al., Chapter: 22, *Blood vessels and endothelial cells*, In: *Molecular biology of the cell*, 4th Edition, 2002, Garland Science, New York, From: <https://www.ncbi.nlm.nih.gov/books/NBK26848/>
- [56] Hemnes A.R., Humbert M., *Pathobiology of pulmonary arterial hypertension: Understanding the roads less travelled*, *European Respiratory Review*, 2017, Volume 26, Issue 146, p. 170093, DOI: 10.1183/16000617.0093-2017
- [57] Goncharov N.V., Nadeev A.D., Jenkins R.O., et al., *Markers and biomarkers of endothelium: When something is rotten in the state*, *Oxidative medicine and cellular longevity*, 2017, Volume 2017, pp. 9759735-9759735, DOI: 10.1155/2017/9759735
- [58] Stevens T., Phan S., Frid M.G., et al., *Lung vascular cell heterogeneity: Endothelium, smooth muscle, and fibroblasts*, *Proceedings of the American Thoracic Society*, 2008, Volume 5, Issue 7, pp. 783-791, DOI: 10.1513/pats.200803-027HR
- [59] Sandoo A., Van Zanten J.J.C.S.V., Metsios G.S., et al., *The endothelium and its role in regulating vascular tone*, *The open cardiovascular medicine journal*, 2010, Volume 4, pp. 302-312, DOI: 10.2174/1874192401004010302
- [60] Bacakova L., Trávníčková M., Filová E., et al., *The role of vascular smooth muscle cells in the physiology and pathophysiology of blood vessels*, 2018, ISBN: 978-1-78984-005-6
- [61] Wang H.D., Rätsep M.T., Chapman A., et al., *Adventitial fibroblasts in vascular structure and function: The role of oxidative stress and beyond* this review is one of a selection of papers published in a special issue on oxidative stress in health and disease, *Canadian Journal of Physiology and Pharmacology*, 2010, Volume 88, Issue 3, pp. 177-186, DOI: 10.1139/Y10-015
- [62] An S.J., Liu P., Shao T.M., et al., *Characterization and functions of vascular adventitial fibroblast subpopulations*, *Cellular Physiology and Biochemistry*, 2015, Volume 35, Issue 3, pp. 1137-1150, DOI: 10.1159/000373939
- [63] Weber S.C., Gratopp A., Akanbi S., et al., *Isolation and culture of fibroblasts, vascular smooth muscle, and endothelial cells from the fetal rat ductus arteriosus*, *Pediatric Research*, 2011, Volume 70, Issue 3, pp. 236-241, DOI: 10.1203/PDR.0b013e318225f748
- [64] Lee S.-H., *Concept of large artery and small vessel*, pp. 31-36, In: *Stroke revisited: Pathophysiology of stroke: From bench to bedside*, 2020, Springer Singapore, Singapore, ISBN: 978-981-10-1430-7, From: [https://doi.org/10.1007/978-981-10-1430-7\\_3](https://doi.org/10.1007/978-981-10-1430-7_3)
- [65] Chi J.-T., Chang H.Y., Haraldsen G., et al., *Endothelial cell diversity revealed by global expression profiling*, *Proceedings of the National Academy of Sciences*, 2003, Volume 100, Issue 19, p. 10623, DOI: 10.1073/pnas.1434429100
- [66] Wu S., Zhou C., King J.a.C., et al., *A unique pulmonary microvascular endothelial cell niche revealed by weibel-palade bodies and griffonia simplicifolia*, *Pulmonary circulation*, 2014, Volume 4, Issue 1, pp. 110-115, DOI: 10.1086/674879
- [67] Geiger M., Stone A., Mason S.N., et al., *Differential nitric oxide production by microvascular and macrovascular endothelial cells*, *The American journal of physiology*, 1997, Volume 273, Issue 1 Pt 1, pp. L275-281, DOI: 10.1152/ajplung.1997.273.1.l275
- [68] Dela Paz N.G., D'amore P.A., *Arterial versus venous endothelial cells*, *Cell and tissue research*, 2009, Volume 335, Issue 1, pp. 5-16, DOI: 10.1007/s00441-008-0706-5
- [69] Yartsev A., *Differences between the pulmonary and systemic circulations*, Access date: 21/09/2020, Last updated: 23/05/2020, From: <https://derangedphysiology.com/main/cicm-primary-exam/required-reading/respiratory-system/Chapter%20063/differences-between-pulmonary-and-systemic-circulations>
- [70] Chamarthy M.R., Kandathil A., Kalva S.P., *Pulmonary vascular pathophysiology*, *Cardiovascular diagnosis and therapy*, 2018, Volume 8, Issue 3, pp. 208-213, DOI: 10.21037/cdt.2018.01.08
- [71] Dunham-Snary K.J., Wu D., Sykes E.A., et al., *Hypoxic pulmonary vasoconstriction: From molecular mechanisms to medicine*, *Chest*, 2017, Volume 151, Issue 1, pp. 181-192, DOI: 10.1016/j.chest.2016.09.001
- [72] Peters D.G., Ning W., Chu T.J., et al., *Comparative sage analysis of the response to hypoxia in human pulmonary and aortic endothelial cells*, *Physiological Genomics*, 2006, Volume 26, Issue 2, pp. 99-108, DOI: 10.1152/physiolgenomics.00152.2005
- [73] Sharma S., Hashmi M.F., Rawat D., *Partial pressure of oxygen (po2)*, In: *Statpearls*, 2019, StatPearls Publishing, Treasure Island (FL), Last Update: September 13, 2019.
- [74] Boron W.F., Boulpaep E.L., *Medical physiology: A cellular and molecular approach*, 2012, Saunders Elsevier ISBN: 9781437717532
- [75] Carreau A., El Hafny-Rahbi B., Matejuk A., et al., *Why is the partial oxygen pressure of human tissues a crucial parameter? Small molecules and hypoxia*, *Journal of cellular and molecular medicine*, 2011, Volume 15, Issue 6, pp. 1239-1253, DOI: 10.1111/j.1582-4934.2011.01258.x

- [76] Koh M.Y., Powis G., *Passing the baton: The hif switch*, Trends in biochemical sciences, 2012, Volume 37, Issue 9, pp. 364-372, DOI: 10.1016/j.tibs.2012.06.004
- [77] Larkin B.G., Zimmanck R.J., *Interpreting arterial blood gases successfully*, AORN Journal, 2015, Volume 102, Issue 4, pp. 343-357, DOI: <https://doi.org/10.1016/j.aorn.2015.08.002>
- [78] Saxena K., Jolly M.K., *Acute vs. Chronic vs. Cyclic hypoxia: Their differential dynamics, molecular mechanisms, and effects on tumor progression*, Biomolecules, 2019, Volume 9, Issue 8, p. 339, DOI: 10.3390/biom9080339
- [79] Ibidi, *Why cell culture under flow?*, Access date: 21/04/2021, From: <https://ibidi.com/content/303-why-cell-culture-under-flow>
- [80] Van Der Meer A.D., Poot A.A., Duits M.H.G., et al., *Microfluidic technology in vascular research*, Journal of Biomedicine and Biotechnology, 2009, Volume 2009, p. 823148, DOI: 10.1155/2009/823148
- [81] Van Der Meer A.D., Orlova V.V., Ten Dijke P., et al., *Three-dimensional co-cultures of human endothelial cells and embryonic stem cell-derived pericytes inside a microfluidic device*, Lab on a Chip, 2013, Volume 13, Issue 18, pp. 3562-3568, DOI: 10.1039/C3LC50435B
- [82] Lee H., Chung M., Jeon N.L., *Microvasculature: An essential component for organ-on-chip systems*, MRS Bulletin, 2014, Volume 39, Issue 1, pp. 51-59, DOI: 10.1557/mrs.2013.286
- [83] Ding C., Chen X., Kang Q., et al., *Biomedical application of functional materials in organ-on-a-chip*, Frontiers in bioengineering and biotechnology, 2020, Volume 8, pp. 823-823, DOI: 10.3389/fbioe.2020.00823
- [84] Emulate, *Frequently asked questions*, Access date: 17/03/2021, From: <https://www.emulatebio.com/compound-distribution-faq>
- [85] Zhang B., Montgomery M., Chamberlain M.D., et al., *Biodegradable scaffold with built-in vasculature for organ-on-a-chip engineering and direct surgical anastomosis*, Nature Materials, 2016, Volume 15, Issue 6, pp. 669-678, DOI: 10.1038/nmat4570
- [86] Elveflow, *General guidelines to choose your microfluidic tubing*, Access date, From: <https://www.elveflow.com/microfluidic-reviews/general-microfluidics/how-to-choose-a-microfluidic-tubing/>
- [87] Cole-Palmer, *Tubing selection guide*, Access date: 01/05/2021, Last updated: 01/09/2020, From: <https://www.coleparmer.com/tech-article/tubing-selection-guide>
- [88] Elveflow, *The basics of microfluidic tubings and sleeves*, Access date: 23/04/2021, From: <https://www.elveflow.com/microfluidic-reviews/general-microfluidics/the-basics-of-microfluidic-tubing-sleeves/>
- [89] Vici Jour, *Impermeable polymeric tubing*, Access date: 23/04/2021, From: <https://www.vici-jour.com/tubing/impermeable.php>
- [90] IDEX Health and Science, *Fluidic & optical products and information*, pp. 64-95, Access date: 24/02/2021, From: <https://www.idex-hs.com/wp-content/uploads/2018/07/Fluidics-and-Optics-Catalog.pdf>
- [91] Van Den Driesche S., Lucklum F., Bunge F., et al., *3D printing solutions for microfluidic chip-to-world connections*, Micromachines (Basel), 2018, Volume 9, Issue 2, DOI: 10.3390/mi9020071
- [92] Keller P.E., Kouzes R.T., *Water vapor permeation in plastics*, 2017, United States, DOI: 10.2172/1411940
- [93] Matweb: Online Materials Information Resource, *Oxygen transmission*, Access date: 21/04/2021, From: <http://www.matweb.com/search/PropertySearch.aspx>
- [94] Wang Z., Hu S., Wang H., *Scale-up preparation and characterization of collagen/sodium alginate blend films*, Journal of Food Quality, 2017, Volume 2017, p. 4954259, DOI: 10.1155/2017/4954259
- [95] Jones L., Dumbleton K., *10 - soft contact lens fitting*, pp. 207-222, In: *Contact lenses (sixth edition)*, 2019, Elsevier, London, ISBN: 978-0-7020-7168-3, From: <https://www.sciencedirect.com/science/article/pii/B9780702071683000106>
- [96] Cole-Palmer, *Gas permeability of fluoropolymers*, Access date: 23/04/2021, From: [https://archive-resources.coleparmer.com/Manual\\_pdfs/01410-10Permeability.pdf](https://archive-resources.coleparmer.com/Manual_pdfs/01410-10Permeability.pdf)
- [97] Extrand C.W., Monson L., *Gas permeation resistance of a perfluoroalkoxy-tetrafluoroethylene copolymer*, Journal of Applied Polymer Science, 2006, Volume 100, Issue 3, pp. 2122-2125, DOI: <https://doi.org/10.1002/app.23592>
- [98] Masterflex, *Tubing selection guide*, Access date: 23/04/2021, From: <https://www.masterflex.com/tech-article/tubing-selection-guide>
- [99] Victrex, *Materials properties guide*, Access date: 23/04/2021, From: [https://www.victrex.com/~media/literature/en/material-properties-guide\\_us-4-20.pdf](https://www.victrex.com/~media/literature/en/material-properties-guide_us-4-20.pdf)
- [100] Liu K., Fan Z.H., *Thermoplastic microfluidic devices and their applications in protein and DNA analysis*, The Analyst, 2011, Volume 136, Issue 7, pp. 1288-1297, DOI: 10.1039/c0an00969e
- [101] Wang Z., *Fabrication techniques for production of thermoplastic-based microfluidics devices*, Journal of Molecular and Engineering Materials, 2016, Volume 04, Issue 03, p. 1640016, DOI: 10.1142/S2251237316400165
- [102] Akther F., Yakob S.B., Nguyen N.-T., et al., *Surface modification techniques for endothelial cell seeding in pdms microfluidic devices*, Biosensors, 2020, Volume 10, Issue 11, DOI: 10.3390/bios10110182
- [103] Kuddannaya S., Chuah Y.J., Lee M.H.A., et al., *Surface chemical modification of poly(dimethylsiloxane) for the enhanced adhesion and proliferation of mesenchymal stem cells*, ACS Applied Materials & Interfaces, 2013, Volume 5, Issue 19, pp. 9777-9784, DOI: 10.1021/am402903e
- [104] Riau A.K., Mondal D., Yam G.H.F., et al., *Surface modification of pmma to improve adhesion to corneal substitutes in a synthetic core-skirt keratoprosthesis*, ACS Applied Materials & Interfaces, 2015, Volume 7, Issue 39, pp. 21690-21702, DOI: 10.1021/acsami.5b07621

- [105] Dabaghi M., Shahriari S., Saraei N., et al., *Surface modification of pdms-based microfluidic devices with collagen using polydopamine as a spacer to enhance primary human bronchial epithelial cell adhesion*, *Micromachines* (Basel), 2021, Volume 12, Issue 2, DOI: 10.3390/mi12020132
- [106] Sharma D., Jia W., Long F., et al., *Polydopamine and collagen coated micro-grated polydimethylsiloxane for human mesenchymal stem cell culture*, *Bioactive Materials*, 2019, Volume 4, pp. 142-150, DOI: <https://doi.org/10.1016/j.bioactmat.2019.02.002>
- [107] Koh W., Stratman A.N., Sacharidou A., et al., *Chapter 5 in vitro three dimensional collagen matrix models of endothelial lumen formation during vasculogenesis and angiogenesis*, pp. 83-101, In: *Methods in enzymology*, 2008, Academic Press, ISBN: 0076-6879, From: <https://www.sciencedirect.com/science/article/pii/S0076687908020053>
- [108] ATCC, *Cell lines*, Access date: 28/04/2021, From: [https://www.lgcstandards-atcc.org/en/Products/Cells\\_and\\_Microorganisms/Cell\\_Lines.aspx](https://www.lgcstandards-atcc.org/en/Products/Cells_and_Microorganisms/Cell_Lines.aspx)
- [109] Amsbio, *Cell lines*, Access date: 28/04/2021, From: <https://www.amsbio.com/products/cells-cell-culture/cell-lines>
- [110] Low L.A., Mummery C., Berridge B.R., et al., *Organs-on-chips: Into the next decade*, *Nature Reviews Drug Discovery*, 2020, DOI: 10.1038/s41573-020-0079-3
- [111] Lonza, *Primary and stem cells*, Access date: 27/04/2021, From: <https://bioscience.lonza.com/>
- [112] Promocell, *Human primary cell culture*, Access date: 27/04/2021, From: <https://promocell.com/product-category/human-primary-cell-culture/>
- [113] Takahashi K., Yamanaka S., *Induction of pluripotent stem cells from mouse embryonic and adult fibroblast cultures by defined factors*, *Cell*, 2006, Volume 126, Issue 4, pp. 663-676, DOI: 10.1016/j.cell.2006.07.024
- [114] Orlova V.V., Drabsch Y., Freund C., et al., *Functionality of endothelial cells and pericytes from human pluripotent stem cells demonstrated in cultured vascular plexus and zebrafish xenografts*, *Arteriosclerosis, Thrombosis, and Vascular Biology*, 2014, Volume 34, Issue 1, pp. 177-186, DOI: 10.1161/ATVBAHA.113.302598
- [115] Orlova V.V., Van Den Hil F.E., Petrus-Reurer S., et al., *Generation, expansion and functional analysis of endothelial cells and pericytes derived from human pluripotent stem cells*, *Nature Protocols*, 2014, Volume 9, Issue 6, pp. 1514-1531, DOI: 10.1038/nprot.2014.102
- [116] Halaidych O.V., Cochrane A., Van Den Hil F.E., et al., *Quantitative analysis of intracellular ca(2+) release and contraction in hpsc-derived vascular smooth muscle cells*, *Stem Cell Reports*, 2019, Volume 12, Issue 4, pp. 647-656, DOI: 10.1016/j.stemcr.2019.02.003
- [117] Carter M., Shieh J., *Chapter 15 - biochemical assays and intracellular signaling*, pp. 311-343, In: *Guide to research techniques in neuroscience (second edition)*, 2015, Academic Press, San Diego, ISBN: 978-0-12-800511-8, From: <https://www.sciencedirect.com/science/article/pii/B9780128005118000150>
- [118] Lea T., *Epithelial cell models; general introduction*, pp. 95-102, In: *The impact of food bioactives on health: In vitro and ex vivo models*, 2015, Springer, DOI: 10.1007/978-3-319-16104-4\_9
- [119] Srinivasan B., Kolli A.R., Esch M.B., et al., *Teer measurement techniques for in vitro barrier model systems*, *Journal of Laboratory Automation*, 2015, Volume 20, Issue 2, pp. 107-126, DOI: 10.1177/2211068214561025
- [120] Thomas A., Wang S., Sohrabi S., et al., *Characterization of vascular permeability using a biomimetic microfluidic blood vessel model*, *Biomicrofluidics*, 2017, Volume 11, Issue 2, pp. 024102-024102, DOI: 10.1063/1.4977584
- [121] Wenger R.H., Kurtcuoglu V., Scholz C.C., et al., *Frequently asked questions in hypoxia research*, *Hypoxia* (Auckland, N.Z.), 2015, Volume 3, pp. 35-43, DOI: 10.2147/HP.S92198
- [122] Sander R., *Compilation of henry's law constants (version 4.0) for water as solvent*, *Atmos. Chem. Phys.*, 2015, Volume 15, Issue 8, pp. 4399-4981, DOI: 10.5194/acp-15-4399-2015
- [123] Marieb E.N., Hoehn K.N., Chapter: 17, *The cardiovascular system: Blood*, pp. 631-657, In: *Human anatomy & physiology*, 9th Edition, 2014, Pearson, ISBN: 978-1-292-02649-7
- [124] Anbari K.K., Garino J.P., Mackenzie C.F., *Hemoglobin substitutes*, *European spine journal*, 2004, Volume 13, Issue Suppl 1, pp. S76-S82, DOI: 10.1007/s00586-004-0737-x
- [125] Kobayashi K., Tsuchida E., Horinouchi H., *Artificial oxygen carrier - its front line*, 2005, Springer, Tokyo ISBN: 978-4-431-22074-9
- [126] Oomen P.E., Skolimowski M.D., Verpoorte E., *Implementing oxygen control in chip-based cell and tissue culture systems*, *Lab on a Chip*, 2016, Volume 16, Issue 18, pp. 3394-3414, DOI: 10.1039/C6LC00772D
- [127] Newby D., Marks L., Lyall F., *Dissolved oxygen concentration in culture medium: Assumptions and pitfalls*, *Placenta*, 2005, Volume 26, Issue 4, pp. 353-357, DOI: <https://doi.org/10.1016/j.placenta.2004.07.002>
- [128] Smeller L., *Pressure-temperature phase diagrams of biomolecules*, *Biochimica et Biophysica Acta (BBA) - Protein Structure and Molecular Enzymology*, 2002, Volume 1595, Issue 1, pp. 11-29, DOI: [https://doi.org/10.1016/S0167-4838\(01\)00332-6](https://doi.org/10.1016/S0167-4838(01)00332-6)
- [129] Demicheva M., *Novel oxygen scavenger systems for functional coatings*, 2015, Arcada - Nylands svenska yrkeshögskola, <http://urn.fi/URN:NBN:fi:amk-201502122166>
- [130] Rivera K.R., Yokus M.A., Erb P.D., et al., *Measuring and regulating oxygen levels in microphysiological systems: Design, material, and sensor considerations*, *The Analyst*, 2019, Volume 144, Issue 10, pp. 3190-3215, DOI: 10.1039/C8AN02201A
- [131] Skolimowski M., Nielsen M.W., Emnéus J., et al., *Microfluidic dissolved oxygen gradient generator biochip as a useful tool in bacterial biofilm studies*, *Lab on a Chip*, 2010, Volume 10, Issue 16, pp. 2162-2169, DOI: 10.1039/C003558K

- [132] Mehta G., Mehta K., Sud D., et al., *Quantitative measurement and control of oxygen levels in microfluidic poly(dimethylsiloxane) bioreactors during cell culture*, Biomed Microdevices, 2007, Volume 9, Issue 2, pp. 123-134, DOI: 10.1007/s10544-006-9005-7
- [133] Opegard S.C., Eddington D.T., *A microfabricated platform for establishing oxygen gradients in 3-d constructs*, Biomedical Microdevices, 2013, Volume 15, Issue 3, pp. 407-414, DOI: 10.1007/s10544-013-9737-0
- [134] Place T.L., Domann F.E., Case A.J., *Limitations of oxygen delivery to cells in culture: An underappreciated problem in basic and translational research*, Free Radical Biology and Medicine, 2017, Volume 113, pp. 311-322, DOI: <https://doi.org/10.1016/j.freeradbiomed.2017.10.003>
- [135] Brennan M.D., Rexius-Hall M.L., Elgass L.J., et al., *Oxygen control with microfluidics*, Lab on a Chip, 2014, Volume 14, Issue 22, pp. 4305-4318, DOI: 10.1039/C4LC00853G
- [136] Ramamoorthy R., Dutta P.K., Akbar S.A., *Oxygen sensors: Materials, methods, designs and applications*, Journal of Materials Science, 2003, Volume 38, Issue 21, pp. 4271-4282, DOI: 10.1023/A:1026370729205
- [137] Yoshihara T., Hirakawa Y., Hosaka M., et al., *Oxygen imaging of living cells and tissues using luminescent molecular probes*, Journal of Photochemistry and Photobiology C: Photochemistry Reviews, 2017, Volume 30, pp. 71-95, DOI: <https://doi.org/10.1016/j.jphotochemrev.2017.01.001>
- [138] Grist S.M., Chrostowski L., Cheung K.C., *Optical oxygen sensors for applications in microfluidic cell culture*, Sensors (Basel, Switzerland), 2010, Volume 10, Issue 10, pp. 9286-9316, DOI: 10.3390/s101009286
- [139] Mills A., *Controlling the sensitivity of optical oxygen sensors*, Sensors and Actuators B: Chemical, 1998, Volume 51, Issue 1, pp. 60-68, DOI: [https://doi.org/10.1016/S0925-4005\(98\)00211-1](https://doi.org/10.1016/S0925-4005(98)00211-1)
- [140] Borisov S.M., Nuss G., Klimant I., *Red light-excitable oxygen sensing materials based on platinum(ii) and palladium(ii) benzoporphyrins*, Analytical Chemistry, 2008, Volume 80, Issue 24, pp. 9435-9442, DOI: 10.1021/ac801521v
- [141] Ehgartner J., Sulzer P., Burger T., et al., *Online analysis of oxygen inside silicon-glass microreactors with integrated optical sensors*, Sensors and Actuators B: Chemical, 2016, Volume 228, pp. 748-757, DOI: <https://doi.org/10.1016/j.snb.2016.01.050>
- [142] Koren K., Hutter L., Enko B., et al., *Tuning the dynamic range and sensitivity of optical oxygen-sensors by employing differently substituted PS-derivatives*, Sensors and Actuators B: Chemical, 2013, Volume 176, pp. 344-350, DOI: <https://doi.org/10.1016/j.snb.2012.09.057>
- [143] Zirath H., Rothbauer M., Spitz S., et al., *Every breath you take: Non-invasive real-time oxygen biosensing in two- and three-dimensional microfluidic cell models*, Frontiers in Physiology, 2018, Volume 9, p. 815
- [144] Sun S., Ungerböck B., Mayr T., *Imaging of oxygen in microreactors and microfluidic systems*, Methods and Applications in Fluorescence, 2015, Volume 3, Issue 3, p. 034002, DOI: 10.1088/2050-6120/3/3/034002
- [145] Chen W., Shu Z., Gao D., et al., *Sensing and sensibility: Single-islet-based quality control assay of cryopreserved pancreatic islets with functionalized hydrogel microcapsules*, Advanced Healthcare Materials, 2016, Volume 5, Issue 2, pp. 223-231, DOI: 10.1002/adhm.201500515
- [146] Ehgartner J., Strobl M., Bolivar J.M., et al., *Simultaneous determination of oxygen and ph inside microfluidic devices using core-shell nanosensors*, Analytical Chemistry, 2016, Volume 88, Issue 19, pp. 9796-9804, DOI: 10.1021/acs.analchem.6b02849
- [147] Gruber P., Marques M.P.C., Szita N., et al., *Integration and application of optical chemical sensors in microbioreactors*, Lab on a Chip, 2017, Volume 17, Issue 16, pp. 2693-2712, DOI: 10.1039/C7LC00538E
- [148] Wang L., Acosta M.A., Leach J.B., et al., *Spatially monitoring oxygen level in 3D microfabricated cell culture systems using optical oxygen sensing beads*, Lab on a Chip, 2013, Volume 13, Issue 8, pp. 1586-1592, DOI: 10.1039/C3LC41366G
- [149] Hirvonen L.M., Suhling K., *Wide-field tcspc: Methods and applications*, Measurement Science and Technology, 2016, Volume 28, Issue 1, p. 012003, DOI: 10.1088/1361-6501/28/1/012003
- [150] Sviatlana K., Angelika R., *Fim and plim in biomedical research – an innovative way to combine autofluorescence and oxygen measurements*, Photonics & Lasers in Medicine, 2016, Volume 5, Issue 4, pp. 257-266, DOI: <https://doi.org/10.1515/plm-2016-0026>
- [151] Colibri Photonics, *Optoelectronic sensor devices - opal*, Access date: 03/05/2021, From: <http://colibri-photonics.com/index.php/component/content/article/17>
- [152] Luxcel, *Mitoimage™ - live cell o2 imaging probes*, Access date: 03/05/2021, From: [https://www.sapphire-usa.com/static/images/LUX\\_MitoImage-Brochure.pdf](https://www.sapphire-usa.com/static/images/LUX_MitoImage-Brochure.pdf)
- [153] PyroScience, *Oxygen nanoprobes*, Access date: 03/05/2021, From: <https://www.pyroscience.com/en/products/all-sensors/oxnano>
- [154] Mettler Toledo, *Dissolved oxygen sensors for process and pure water*, Access date: 03/05/2021, From: <https://www.mt.com/nz/en/home/products/Process-Analytcs/DO-CO2-ozone-sensor/dissolved-oxygen-meter.html>
- [155] PyroScience, *Overview fiber optic sensors*, Access date: 03/05/2021, From: <https://www.pyroscience.com/en/products/laboratory-solutions/oxygen-sensors/fiber-optic-oxygen-sensors>
- [156] YSI, *Dissolved oxygen measurement in water with oxygen meters*, Access date: 03/05/2021, From: <https://www.ysi.com/parameters/dissolved-oxygen>
- [157] PreSens, *Oxygen sensor spots*, Access date: 03/05/2021, From: <https://www.presens.de/shop/o2/sensors/oxygen-sensor-spots/?p=1>
- [158] PyroScience, *Contactless oxygen sensors*, Access date: 03/05/2021, From: <https://www.pyroscience.com/en/products/oxygen/contactless-sensors>

- [159] Ibbidi, *Ibbidi opal - optical o2 measurement system*, Access date: 29/10/2020, Last updated: 10/2016, From: [http://www.blossombio.com/pdf/products/FLY\\_74001\\_OPAL\\_150dpi.pdf](http://www.blossombio.com/pdf/products/FLY_74001_OPAL_150dpi.pdf)
- [160] Schmäzlin E., Van Dongen J.T., Klimant I., et al., *An optical multifrequency phase-modulation method using microbeads for measuring intracellular oxygen concentrations in plants*, *Biophysical journal*, 2005, Volume 89, Issue 2, pp. 1339-1345, DOI: 10.1529/biophysj.105.063453
- [161] Batchelor G.K., *An introduction to fluid dynamics*, 2000, Cambridge University Press, Cambridge ISBN: 9780521663960
- [162] Elveflow, *Flow control in microfluidic devices*, Access date: 04/05/2021, From: <https://www.elveflow.com/microfluidic/Flow%20control%20in%20microfluidic%20devices.pdf>
- [163] Harvard Apparatus, *Standard infuse/withdraw pump 11 pico plus elite programmable syringe pump*, Access date: 05/05/2021, From: <https://www.harvardapparatus.com/standard-infuse-withdraw-pump-11-pico-plus-elite-programmable-syringe-pump.html>
- [164] Byun C.K., Abi-Samra K., Cho Y.-K., et al., *Pumps for microfluidic cell culture*, *ELECTROPHORESIS*, 2014, Volume 35, Issue 2-3, pp. 245-257, DOI: <https://doi.org/10.1002/elps.201300205>
- [165] Darwin Microfluidics, *Flow control in microfluidics*, Access date: 05/05/2021, Last updated: 28/11/2017, From: <https://darwin-microfluidics.com/blogs/reviews/flow-control-in-microfluidics>
- [166] Fluigent, *Comparison between peristaltic, syringe and pressure pumps for microfluidic applications*, Access date: 05/05/2021, From: <https://www.fluigent.com/resources/microfluidic-expertise/advantages-of-pressure-based-microfluidic/system-comparison-for-microfluidic-applications/>
- [167] Cochrane A., Albers H.J., Passier R., et al., *Advanced in vitro models of vascular biology: Human induced pluripotent stem cells and organ-on-chip technology*, *Advanced Drug Delivery Reviews*, 2019, Volume 140, pp. 68-77, DOI: <https://doi.org/10.1016/j.addr.2018.06.007>
- [168] Abaci H.E., Devendra R., Soman R., et al., *Microbioreactors to manipulate oxygen tension and shear stress in the microenvironment of vascular stem and progenitor cells*, *Biotechnology and Applied Biochemistry*, 2012, Volume 59, Issue 2, pp. 97-105, DOI: <https://doi.org/10.1002/bab.1010>
- [169] Abaci H.E., Shen Y.-I., Tan S., et al., *Recapitulating physiological and pathological shear stress and oxygen to model vasculature in health and disease*, *Scientific Reports*, 2014, Volume 4, Issue 1, p. 4951, DOI: 10.1038/srep04951
- [170] Wojciak-Stothard B., Ainscough A., Smith T., et al., *A microfluidic chip for pulmonary arterial hypertension*, *Research Square*, 2021, DOI: 10.21203/rs.3.rs-598765/v1, PREPRINT (Version 1)
- [171] Chrobak K.M., Potter D.R., Tien J., *Formation of perfused, functional microvascular tubes in vitro*, *Microvasc Res*, 2006, Volume 71, Issue 3, pp. 185-196, DOI: <https://doi.org/10.1016/j.mvr.2006.02.005>
- [172] Yampolskii Y., *2 - fundamental science of gas and vapour separation in polymeric membranes*, pp. 22-55, In: *Advanced membrane science and technology for sustainable energy and environmental applications*, 2011, Woodhead Publishing, ISBN: 978-1-84569-969-7, From: <https://www.sciencedirect.com/science/article/pii/B9781845699697500023>
- [173] Wagner B.A., Venkataraman S., Buettner G.R., *The rate of oxygen utilization by cells*, *Free radical biology & medicine*, 2011, Volume 51, Issue 3, pp. 700-712, DOI: 10.1016/j.freeradbiomed.2011.05.024
- [174] Poulsen L., Ogilby P.R., *Oxygen diffusion in glassy polymer films: Effects of other gases and changes in pressure*, *The Journal of Physical Chemistry A*, 2000, Volume 104, Issue 12, pp. 2573-2580, DOI: 10.1021/jp993449r
- [175] Markov D.A., Lillie E.M., Garbett S.P., et al., *Variation in diffusion of gases through pdms due to plasma surface treatment and storage conditions*, *Biomedical Microdevices*, 2014, Volume 16, Issue 1, pp. 91-96, DOI: 10.1007/s10544-013-9808-2
- [176] Cox M.E., Dunn B., *Oxygen diffusion in poly(dimethyl siloxane) using fluorescence quenching. I. Measurement technique and analysis*, *Journal of Polymer Science Part A: Polymer Chemistry*, 1986, Volume 24, Issue 4, pp. 621-636, DOI: <https://doi.org/10.1002/pola.1986.080240405>
- [177] Schmitz D., Anlauf R., Rehrmann P., *Effect of air content on the oxygen diffusion coefficient of growing media*, *American Journal of Plant Sciences*, 2013, Volume 4, Issue 5, pp. 955-963, DOI: 10.4236/ajps.2013.45118
- [178] Han P., Bartels D.M., *Temperature dependence of oxygen diffusion in h2o and d2o*, *The Journal of Physical Chemistry*, 1996, Volume 100, Issue 13, pp. 5597-5602, DOI: 10.1021/jp952903y
- [179] Jamnongwong M., Loubiere K., Dietrich N., et al., *Experimental study of oxygen diffusion coefficients in clean water containing salt, glucose or surfactant: Consequences on the liquid-side mass transfer coefficients*, *Chemical Engineering Journal*, 2010, Volume 165, Issue 3, pp. 758-768, DOI: <https://doi.org/10.1016/j.cej.2010.09.040>
- [180] Cheema U., Rong Z., Kirresh O., et al., *Oxygen diffusion through collagen scaffolds at defined densities: Implications for cell survival in tissue models*, *Journal of Tissue Engineering and Regenerative Medicine*, 2012, Volume 6, Issue 1, pp. 77-84, DOI: <https://doi.org/10.1002/term.402>
- [181] Colom A., Galgoczy R., Almendros I., et al., *Oxygen diffusion and consumption in extracellular matrix gels: Implications for designing three-dimensional cultures*, *Journal of Biomedical Materials Research Part A*, 2014, Volume 102, Issue 8, pp. 2776-2784, DOI: <https://doi.org/10.1002/jbm.a.34946>
- [182] Bartoszewski R., Moszyńska A., Serocki M., et al., *Primary endothelial cell-specific regulation of hypoxia-inducible factor (hif)-1 and hif-2 and their target gene expression profiles during hypoxia*, *The FASEB Journal*, 2019, Volume 33, Issue 7, pp. 7929-7941, DOI: <https://doi.org/10.1096/fj.201802650RR>
- [183] Löfstedt T., Fredlund E., Holmquist-Mengelbier L., et al., *Hypoxia inducible factor-2 $\alpha$  in cancer*, *Cell Cycle*, 2007, Volume 6, Issue 8, pp. 919-926, DOI: 10.4161/cc.6.8.4133

- [184] Calderón E., Gómez-Sánchez C.E., Cozza E.N., et al., *Modulation of endothelin-1 production by a pulmonary epithelial cell line: I. Regulation by glucocorticoids*, *Biochemical Pharmacology*, 1994, Volume 48, Issue 11, pp. 2065-2071, DOI: [https://doi.org/10.1016/0006-2952\(94\)90506-1](https://doi.org/10.1016/0006-2952(94)90506-1)
- [185] Chuai Y., Jiang W., Xu X., et al., *Maternal oxygen exposure may not change umbilical cord venous partial pressure of oxygen: Non-random, paired venous and arterial samples from a randomised controlled trial*, *BMC Pregnancy and Childbirth*, 2020, Volume 20, Issue 1, p. 510, DOI: 10.1186/s12884-020-03212-3
- [186] Huxley V.H., Curry F.E., Adamson R.H., *Quantitative fluorescence microscopy on single capillaries: Alpha-lactalbumin transport*, *American Journal of Physiology-Heart and Circulatory Physiology*, 1987, Volume 252, Issue 1, pp. H188-H197, DOI: 10.1152/ajpheart.1987.252.1.H188
- [187] Mayr T., *Database of fluorescent dyes, properties and applications*, Access date: 02/09/2021, From: <http://fluorophores.tugraz.at/substance/750>
- [188] Ogilvie I.R.G., Sieben V.J., Floquet C.F.A., et al., *Reduction of surface roughness for optical quality microfluidic devices in pmma and coc*, *Journal of Micromechanics and Microengineering*, 2010, Volume 20, Issue 6, p. 065016, DOI: 10.1088/0960-1317/20/6/065016
- [189] Lamichhane T.N., Leung C.A., Douti L.Y., et al., *Ethanol induces enhanced vascularization bioactivity of endothelial cell-derived extracellular vesicles via regulation of micromas and long non-coding rnas*, *Scientific Reports*, 2017, Volume 7, Issue 1, pp. 13794-13794, DOI: 10.1038/s41598-017-14356-2
- [190] Inácio Â.S., Mesquita K.A., Baptista M., et al., *In vitro surfactant structure-toxicity relationships: Implications for surfactant use in sexually transmitted infection prophylaxis and contraception*, *PLOS ONE*, 2011, Volume 6, Issue 5, p. e19850, DOI: 10.1371/journal.pone.0019850
- [191] Rho S.-S., Ando K., Fukuhara S., *Dynamic regulation of vascular permeability by vascular endothelial cadherin-mediated endothelial cell-cell junctions*, *Journal of Nippon Medical School*, 2017, Volume 84, Issue 4, pp. 148-159, DOI: 10.1272/jnms.84.148
- [192] Sa S., Gu M., Chappell J., et al., *Induced pluripotent stem cell model of pulmonary arterial hypertension reveals novel gene expression and patient specificity*, *American Journal of Respiratory and Critical Care Medicine*, 2017, Volume 195, Issue 7, pp. 930-941, DOI: 10.1164/rccm.201606-1200OC
- [193] Williams I.M., Wu J.C., *Generation of endothelial cells from human pluripotent stem cells*, *Arteriosclerosis, Thrombosis, and Vascular Biology*, 2019, Volume 39, Issue 7, pp. 1317-1329, DOI: 10.1161/ATVBAHA.119.312265
- [194] Fernandez C.E., Yen R.W., Perez S.M., et al., *Human vascular microphysiological system for in vitro drug screening*, *Scientific Reports*, 2016, Volume 6, pp. 21579-21579, DOI: 10.1038/srep21579
- [195] Tseng H., Gage J.A., Haisler W.L., et al., *A high-throughput in vitro ring assay for vasoactivity using magnetic 3D bioprinting*, *Scientific Reports*, 2016, Volume 6, Issue 1, p. 30640, DOI: 10.1038/srep30640

# LIST OF FIGURES

<b>Figure 1</b> Schematic representation of vascular remodelling as observed in patients with PAH and possible factors that might initiate or aggravate this remodelling. Adapted from [2].	9
<b>Figure 2</b> Various models to study vascular (dys)function, including in vitro models like static culture and OoC systems, as well as computer, animal and human models. Adapted from [14].	10
<b>Figure 3</b> a) Schematic diagram of the PDMS chip used to generate the 3D VoC system. b) Photograph of the 3D VoC system. c) 3D cut-out reconstruction of a 2-photon second harmonic generation image showing the collagen lumen. d-e) Fluorescence confocal micrographs of the engineered vessel made up of ECs viewed in cross-section (d) and from the top (e). From [13] and [17].	12
<b>Figure 4</b> Generalized structure of arteries, veins, and capillaries and their wall structure. From [3].	14
<b>Figure 5</b> Schematic representation of various cell types residing in the vascular wall. Vascular ECs lining the lumen are separated from the SMCs by a basal lamina. Fibroblasts in the tunica adventitia are responsible for the production of ECM proteins.	15
<b>Figure 6</b> Fluorescent images of ECs where nuclei are labelled in blue and VE-cadherin molecules are labelled in green. On the right, the cells are elongated and aligned due to unidirectional flow in the direction as indicated by the arrow. From [12].	15
<b>Figure 7</b> Binding of lectins to hMVECs and hPAECs in vitro. Immunofluorescent HPA (red) binds hPAECs (A) but not hMVECs (C), while immunofluorescent GSL (green) binds hMVECs (D) but not to hPAECs (B). Cell nuclei are stained with DAPI. From [16].	17
<b>Figure 8</b> Schematic overview of a) the cross-sectional area (in $\text{cm}^2$ ), b) the velocity (in $\text{cm}/\text{sec}$ ) and c) the pressure (in $\text{mmHg}$ ) in systemic blood vessels of various types and sizes. From [3].	18
<b>Figure 9</b> Arterial endothelial-like cells showing a low expression of COUP-TFII (a) and a high expression of Ephrin B2 (b), while venous endothelial-like cells show a high expression of COUP-TFII (c) and a low expression of Ephrin B2 (d). From [10].	18
<b>Figure 10</b> Expression of a) NO and b) ET-1 in normoxia (N) or hypoxia (H) (5% $\text{O}_2$ for 24h) in hPAECs. Adapted from [1].	19
<b>Figure 11</b> Physiological oxygen and carbon dioxide concentrations throughout the human body. Adapted from [4].	19
<b>Figure 12</b> (a) Nitric oxide release in flow medium as measured by the total content of nitrite. (b) ET-1 content in the flow medium as measured with ELISA. Medium was collected from the flow circulation after cells were exposed to different shear stresses. From [8].	20
<b>Figure 13</b> Schematic overview of fabrication techniques for the creation of OoC devices. Soft lithography can be used for the fabrication of OoCs from elastomeric materials such as PDMS (a) while for thermoplastics such as PMMA, CNC milling is often employed (b). Surface functionalization can be achieved via APTES + GA coating (c) or using a PDA coating (d) to covalently bind hydrogels such as collagen to the OoC surface. Finally, lumens can be formed via VFP (e).	23
<b>Figure 14</b> Oxygen–haemoglobin dissociation curve showing that only a small percentage of the total oxygen concentration in the blood is dissolved, while most oxygen is bound to hemoglobin. From [7].	27
<b>Figure 15</b> Overview of various techniques for oxygen control, including hypoxic workstations, hypoxic chamber, microenvironmental control systems, nitrogen purging and the use of oxygen scavengers/ generators, oxygen diffusion and mixing, hydrogel diffusion and cellular consumption. Images based on [9] [15] [18] [19] [20] [21] [22].	28
<b>Figure 16</b> Intensity plot of the quenching of luminescence intensity by oxygen, and respective Stern–Volmer plot. From [6].	29
<b>Figure 17</b> Types of commercially available oxygen sensors, including oxygen sensor probes, oxygen sensor spots and oxygen sensitive particles.	30
<b>Figure 18</b> Overview of various flow control systems, including peristaltic pumps, syringe pumps and pressure controllers. Adapted from [5].	32
<b>Figure 19</b> Proposed ideal chip setup consisting of a PMMA chip with two compartments separated by a permeable membrane. The bottom compartment contains gas with 14% oxygen, mimicking the alveoli, while the top compartment mimics the sPA via a 3D collagen lumen lined with hiPSC derived ECs, SMCs and fibroblasts. This lumen is perfused with culture medium containing 5% oxygen at a physiological flow rate.	35
<b>Figure 20</b> a) 3D and 2D velocity profile in a cylindrical channel with a flow rate of 1 $\text{ml}/\text{min}$ as modelled with COMSOL. b) 1D velocity profile and shear stress profile halfway a cylindrical channel for various volumetric flow rates. c) Correlation between the volumetric flow rate and the maximum and mean velocity. d) Correlation between the volumetric flow rate and wall shear stress. In b-d, dots depict results from numerical modelling with COMSOL while lines are analytically calculated with MATLAB.	38
<b>Figure 21</b> 3D representation of the ideal chip design used to model the oxygen concentration within the chip with COMSOL.	40
<b>Figure 22</b> a) Oxygen concentration over time in a PMMA chip (top) and PDMS chip (bottom) as viewed in the x-y plane cross-section. b) Oxygen gradient across the collagen lumen inside a PMMA chip when flushing the lumen with water containing 5% oxygen for various average velocities and the air channel with 14% of oxygen gas. c) Oxygen concentration in a PMMA and PDMS chip as viewed in the y-z plane cross-section. d) Oxygen gradient across the collagen lumen inside a PMMA and PDMS chip at different time points. All data was simulated with COMSOL.	41

<b>Figure 23</b> a) Fluorescent images of hMVECs, hiPSC-ECs and hPAECs stained for VE-cadherin in red, F-actin in green and nuclei in blue. b) Cell count, mean cell area and mean cell eccentricity of hiPSC-ECs, hMVECs and hPAECs as determined with CellProfiler after staining for VE-cadherin, F-actin and DAPI. ....	46
<b>Figure 24</b> Fluorescent images of hiPSC-ECs, hMVECs and hPAECs stained with GSL in green (top) or HPA in red (bottom) and nuclei in blue. ....	47
<b>Figure 25</b> Relative cDNA expression of arterial marker Ephrin B2 and venous marker COUP-TFII in hiPSC-ECs, arterial primary cells (HUAECs) and venous primary cells (HUVECs). Adapted from [11]. ....	48
<b>Figure 26</b> WB images and quantified results of HIF-1 $\alpha$ and HIF-2 $\alpha$ expression in hiPSC-ECs, hPAECs and HUVECs after exposure to 1% or 5% oxygen for 0, 6, 12, 24 or 48 hours. Exposure to 100 $\mu$ M CoCl <sub>2</sub> is used as positive control. Data is normalized to ACTB or GAPDH expression and CoCl <sub>2</sub> exposure in hPAECs is set to 1. ....	49
<b>Figure 27</b> a) ET-1 concentration in culture medium of cells exposed to 5% hypoxia for different lengths of time as analysed with an ELISA assay. b) NO concentration in the same culture medium as determined via a colorimetric assay. ET-1 and NO concentration in culture medium without cells was subtracted and concentration was normalized to residual culture medium volume and protein concentration to accommodate for evaporation and cell number. ....	50
<b>Figure 28</b> Final chip designs and dimensions of a PDMS chip (a) and PMMA chip (b), as well as pictures of a fabricated PDMS chip (c) and PMMA chip (d) and microscopic images of the microfluidic channels inside the PDMS chip (e) and PMMA chip (f). ....	55
<b>Figure 29</b> a) Microscope images and b) surface roughness quantification with MATLAB of microfluidic channels in PMMA chips polished with chloroform vapour for different lengths of time. ....	55
<b>Figure 30</b> a) Process of VFP in PDMS chips as visualized with red food dye. For the top three images, red food dye in PBS was used to create the lumen. For the bottom image, a lumen was formed with PBS and after collagen crosslinking for 24 hours the lumen was perfused with red food dye. b) Collagen lumens formed in PMMA chips without prefilling and after prefilling the channels with ethanol. c) Quantification of bubble formation in PMMA channels prefilled with different liquids immediately after lumen formation and after crosslinking for 2 and 24 hours. d) Collagen lumens in PMMA chips as visualized with PS beads after prefilling with ethanol or 10% SDS in water. Red dotted lines are drawn manually to indicate the edges of the formed lumens. ....	56
<b>Figure 31</b> a) Images of collagen lumens formed in PDMS and PMMA chips and perfused with PS beads. b) Success rates of lumen formation immediately after formation and after crosslinking for 1 day, as well as the percentage of lumens with bubbles before perfusion in PDMS chips (n=24) and PMMA chips (n=20). c) Average lumen diameter of lumens formed in PDMS (n=21) and PMMA chips (n=18). ....	57
<b>Figure 32</b> OCT image of collagen lumen in PMMA chip. ....	57
<b>Figure 33</b> Images of hMVECs cultured in oxygen permeable PDMS VoC system with collagen lumen directly after cell seeding (left) and after 24 hours of culture in normoxic incubator (right). ....	58
<b>Figure 34</b> Results of permeability assay for hiPSC-ECs, hMVECs and hPAECs cultured in oxygen permeable PDMS VoC systems. a) Overlay image of FITC-Dextran perfused through hPAEC lumen. b) Example of measured fluorescence intensity over time. c) Average vessel diameter for each cell type. d) Calculated apparent permeability for each cell type. ....	58
<b>Figure 35</b> Images of hiPSC-ECs, hMVECs and hPAECs cultured in oxygen permeable PDMS VoC systems with collagen lumens stained for VE-cadherin in red, F-actin in green and nuclei in blue. ....	59
<b>Figure 36</b> Images of hiPSC-ECs cultured in oxygen impermeable PMMA VoC system with collagen lumen directly after cell seeding (left) and after 24 hours of culture in normoxic incubator (right). ....	60
<b>Figure 37</b> Oxygen tension measurements over time in PDMS and PMMA chips after injection of oxygen deprived culture medium in a) chips that were stored in ambient air and b) chip that were preconditioned in an hypoxic incubator (0.1%) for 2 days. Oxygen tension in chip as modelled using diffusion coefficients found in literature is shown with dotted lines and oxygen tension as modelled with adjusted diffusion coefficients is shown with dashed lines. c) Overview of initial oxygen tensions and diffusion coefficients used for each model. ....	61

## LIST OF TABLES

---

<b>Table 1</b> Overview of oxygen permeability of various materials commonly used in OoC systems. Data from [92] [93] [94] [95] [96] [97] [98] [99].....	22
<b>Table 2</b> Required volumetric flow rates and corresponding mean and maximum velocities for different desired wall shear stresses in a 3D collagen lumen.....	39
<b>Table 3</b> Overview of oxygen diffusion, permeability and adsorption coefficients for various materials as used to simulate the oxygen transport in the chip with COMSOL. Values from [92] [93] [94] [95] [96] [97] [98] [99] [174] [175] [176] [177] [178] [179] [180] [181].....	41

## LIST OF SUPPLEMENTARY MATERIAL

---

- S1** *Additional background information*
- S1a** *Pulmonary arterial hypertension*
- S1b** *Relevant factors in vascular (dys)function*
- S1c** *Effects of oxygen tension on vascular cells*
- S1d** *Effects of shear stress on vascular cells*
- S1e** *Foetal development of the pulmonary vasculature*
- S1f** *Fluidic connections*
- S1g** *Flow sensing*
- S1h** *Oxygen sensing*
- S2** *Project roadmap*
- S3** *Protocols*
- S3a** *PDMS chip fabrication*
- S3b** *PMMA chip fabrication*
- S3c** *Lectin binding experiment*
- S3d** *Western Blotting*
- S3e** *ET-1 and NO quantification*
- S4** *MATLAB scripts*
- S4a** *Surface roughness quantification*
- S4b** *Bubble quantification*
- S4c** *Lumen diameter quantification*
- S4d** *Flow modelling*
- S4e** *Oxygen sensing and modelling*
- S5** *Flow videos*
- S5a** *Flow in PDMS chip*
- S5b** *Flow in PMMA chip*
- S6** *Societal Embedding*